Karlsruhe Institute of Technology

Institut für Theoretische Festkörperphysik

Wolfgang-Gaede-Str. 1
D-76131 Karlsruhe

Telefon: +49-721-608-43360
Fax: +49-721-608-47040
Web: http://www.tfp.kit.edu

Masterarbeit

Electromagnetic chirality of an isotropic, chiral and spherical scatterer

Elektromagnetische Chiralität eines isotropen, chiralen und sphärischen Streuers

von

B.Sc. Patrizia Stehle

Matrikelnummer 1724587

Abgabe:	16. Oktober 2018
Referent:	Prof. Dr. Carsten Rockstuhl
Koreferent:	Prof. Dr. Martin Wegener
Betreuer:	Dr. Ivan Fernandez-Corbaton

Als Ansichtsexemplar genehmigt von

Karlsruhe, 16. Oktober 2018, ...

(Prof. Dr. C. Rockstuhl)

Eigenständigkeitserklärung

Ich versichere wahrheitsgemäß, die Arbeit selbstständig verfasst, alle benutzten Hilfsmittel vollständig und genau angegeben und alles kenntlich gemacht zu haben, was aus Arbeiten anderer unverändert oder mit Abänderungen entnommen wurde sowie die Satzung des KIT zur Sicherung guter wissenschaftlicher Praxis in der jeweils gültigen Fassung beachtet zu haben.

Karlsruhe, 16. Oktober 2018, ...

(Patrizia Stehle)

Abstract

Chiral media enable the control and manipulation of the different polarization states of light. Maximally em-chiral objects, which are transparent to light of one helicity but not to the other, can be used as non-directional polarizers or in the detection of chiral molecules. Scattering by chiral spheres is well researched in literature. However, most of these works are theoretical and focus on the general scattering behavior. Therein, very large chirality parameters are assumed, for which media are hard to fabricate in the optical regime. In this work we search for intrinsically chiral, isotropic, homogeneous spherical particles, which are maximally em-chiral. We investigate the influence of geometry and material parameters on this quantity. After discussing the theory to describe the scattering by a chiral spherical particle and restricting the parameter space by means of a microscopic model for the chiral scatterers, single chiral spheres and core-shell particles are investigated by means of parameter studies. The chirality of the medium is found to restrict the overall em-chirality of the scatterer, such that for weakly chiral spheres and core-shell particles highly em-chiral configurations are exceptional cases. These exceptions are found in regions where the media meet the refractive index matching condition with the surrounding medium and thus show high em-chirality. High em-chirality is also found for weakly chiral spheres with a thin dielectric coating for specific media and geometries of the core-shell. These objects are appealing for a larger number of applications and seem to be in reach experimentally.

Contents

List of Figures

1 Introduction

Chiral media, which consist of chiral building blocks (e.g. molecules, artificial chiral structures) are of great interest within the field of biology, chemistry, physics, and especially optics. Theoretical studies and the development of highly optically active materials facilitate the control of the polarization states of light and their manipulation: chiral media are used for the detection of enantiomers to enhance their scattered field or emission, for optical traps using chiral nanoparticles, polarizability dependent negative refractive index materials, and broadband, non-directional polarizers/filters.

Optical activity is an effect due to the chirality of the medium and describes the rotation of the plane of polarization of linearly polarized light. Optical activity was first observed by Arago [24] in quartz crystals and was later also found in non-crystalline media, such as solutions of chiral molecules by Biot [18]. The origin of optical rotation was discovered by Pasteur [18] in 1848, who was the first to detect two enantiomers of a chiral substance and connect their geometrical properties to optical activity. In 1904 Lord Kelvin defined "any geometrical figure, or group of points, chiral, and say that it has chirality if its image in a plane mirror, ideally realized, cannot be brought to coincide with itself" [25, p. 619]. The easiest example of a chiral pair are our hands, which motivated the separation of chiral objects/electromagnetic waves into one or the other 'handedness'. It was recognized early that helical structures are one of the basic geometries which posses chirality. In 1898 Bose found the rotation of the polarization plane for twisted jute with the intention of imitating sugar solutions [7]. The possibility of scaling copper helices for the usage in the microwave regime was proposed by Lindmann [32]. Fresnel discovered that linearly polarized light can be described as a superposition of coherent left-handed and right-handed circularly polarized light [1, Ch. 1]. Based on experimental findings and the definition of chirality he proposed that the difference of phase velocity of light (polarization birefringence) within the chiral arrangement causes optical activity. This birefringence is due to the coupling of electric and magnetic fields within chiral media, which means that electric (magnetic) fields result in magnetic (electric) polarization of the medium. This coupling is described by the chirality parameter in an additional term – which relates the electric (magnetic) flux

density to the magnetic (electric) field – in the macroscopic constitutive equations. Since naturally occurring materials show only weak optical activity [34], artificial structures, which possess higher cross-polarizations than natural ones, have become the focus of research in the last decades. Metamaterials consist of periodically arranged – in this context chiral – building blocks, which are typically much smaller than the wavelength. Therefore, homogenization methods can be used to derive effective macroscopic material parameters to describe these media. Examples for chiral components are helical structures out of gold or other metals [20, 44]. These can be tuned in their material properties and geometry such that their (plasmonic) resonances lie within the visible frequency range, which results in strong optical activity and circular dichroism. Several review papers about experimental and theoretical research of such metamaterials (MM) have been published in recent years [10, 35, 49]. Uniaxial chiral MM yield strong optical activity over a broad frequency range [20, 27]. However, the directional dependency renders such structures unsuitable for the control or tuning of the polarization in any direction. On the other hand, 3D isotropic chiral metamaterials are still a mostly theoretical topic with few exceptions: in [23] chiral split ring resonators are arranged on the surface of a cube. A 3D bi-chiral (chiral effects due to the helical components and due to their arrangement within the medium) photonic crystal was proposed by Thiel *et al.* in [44]. Due to its cubic geometry, the MM is approximately isotropic and, theoretically, allows to fabricate chiral media for any desired frequency. Another group of chiral media are self assembled media, which basically consist of self-assembled, metallic nano-particles in a chiral structure by means of templates, such as DNA, or cholesteric liquid crystals [38]. These also allow for electromagnetic chirality in the visible spectrum.

Spheres out of isotropic homogeneous chiral media represent the ideal candidate for non-directional manipulation of light. The scattering problem is analytically solvable by the Mie theory and thus a popular object to explore scattering phenomena. Scattering by chiral spheres [5, 51] in achiral and chiral media [4] and chiral multi-shell particles [41] were theoretically investigated via extensions of the classical Mie theory. These works focus on the basic scattering behavior, chiral nihility and the influence of chiral particles on decay rates of enantiomers [26]. The fabrication of chiral spheres made out of cholesteric liquid crystals in the optical regime and their use as polarization dependent optical trap and for optical manipulation is described in [9].

Kelvin classifies two groups of media: chiral or achiral ones. There are already several quantitative measures of (geometrical) chirality. However, these do not allow for unam-

biguous ordering of the objects with respect to their electromagnetic response. Therefore, Fernandez-Corbaton *et al.* proposed a quantitative measure to order chiral structures and media by means of their interaction with light [14]. This quantity is called *electromagnetic chirality* and is a measure of the difference between the interaction of light of different helicity with the object. Electromagnetic chirality of an object is bounded. Reciprocal objects reaching the upper bound are transparent to light of one helicity.

Motivated by this preliminary work, we aim to find material and geometry combinations for chiral spheres which posses maximal em-chirality and thus are transparent to one helicity.

This work focuses on purely intrinsically chiral, isotropic and homogeneous spherical particles. The geometry itself is achiral, so that there are no effects due to the particle's orientation with respect to the incident light (extrinsic chirality). A quasi-static antenna model for the chiral inclusions allows for a very simple microscopic description of an effectively isotropic metamaterial made of these randomly placed chiral particles. Homogenization yields effective material parameters and their interconnection. This model facilitates a restriction of the parameter space for fixed host media and thus a more realistic approximation of possible material parameter combinations.

The thesis is structured as follows. In chapter 2, the theory of electromagnetic waves and a basis of transverse electromagnetic waves in chiral media is introduced. Thereby, the helicity of the light is used to describe its polarization state. Subsequently, the microscopic description of chiral media comprises a homogenization of the host medium containing sub-wavelength single turn helices, which are described by means of a quasi-static antenna model in chapter 3. Effective material parameters are derived and relations between the inclusion polarizabilities due to the assumed antenna model result in relations between the effective material parameters for chiral media. In chapter 4 an extension of the Mie theory for spherical particles is used to derive the fields from scattering by a chiral (multi-layered) sphere in a (chiral) medium. The theoretical part is completed with the introduction of duality (and its breaking) and electromagnetic chirality in chapter 5. Media/Effective material parameter constraints for dual and maximally electromagnetically chiral media are derived from the surface boundary conditions of arbitrarily shaped particles.

The introduced methods are applied to the problem of a single spherical particle in chapter 6. Electromagnetic chirality of a sphere as a function of the material parameters and the radius is analyzed via parameter studies. The focus is on finding regions of very high electormagnetic chirality, explaining special features and giving an overall impression

of the influence of intrinsic chirality on electromagnetic chirality. In chapter 7, chiral core-shell particles are investigated with the goal of improving electromagnetic chirality in particular in weakly chiral media. The interesting case of thin purely dielectric coatings on chiral spheres is also investigated. Finally, we introduce highly electromagnetically chiral spheres as a possible detector for chiral molecules. The thesis is summarized in chapter 9 and a short outlook is provided.

2 Theory of electromagnetic waves in chiral media

In the following chapter the basic theory is summarized to describe light in chiral media. First of all Maxwell's equations in time and frequency domain are shortly revised. In section 2.2 different formulations of constitutive relations for chiral media are presented and the usage of the Condon-Tellegen constitutive relations in this thesis is motivated. Subsequently, the eigenstates and corresponding wavenumbers, which decouple Maxwell's equations in isotropic and homogeneous chiral media, are derived. It is furthermore shown that these states have well-defined helicity (section 2.3). In section 2.4 a general definition of helicity and its eigenstates are given, as well as a basis of electromagnetic waves in chiral media.

2.1 Maxwell's equations

The description of electromagnetic waves in a source free medium is given by Maxwell's equations [22, Eq. (I.1a)]:

$$\begin{aligned} \boldsymbol{\nabla} \times \boldsymbol{H}(\boldsymbol{r},t) &= \frac{\partial \boldsymbol{D}(\boldsymbol{r},t)}{\partial t} \ , & \vec{\nabla} \cdot \boldsymbol{D}(\boldsymbol{r},t) &= 0 \ , \\ \boldsymbol{\nabla} \times \boldsymbol{E}(\boldsymbol{r},t) &= -\frac{\partial \boldsymbol{B}(\boldsymbol{r},t)}{\partial t} \ , & \vec{\nabla} \cdot \boldsymbol{B}(\boldsymbol{r},t) &= 0 \ . \end{aligned} \tag{2.1}$$

$\boldsymbol{E}(\boldsymbol{r},t)$ and $\boldsymbol{H}(\boldsymbol{r},t)$ are the electric and magnetic fields. $\boldsymbol{D}(\boldsymbol{r},t)$ and $\boldsymbol{B}(\boldsymbol{r},t)$ are the electric flux density (or electric displacement) and the magnetic flux density (or magnetic inductance), which include the electric/magnetic fields in the medium due to electric/ magentic polarization. Under the assumption of linear response only, Maxwell's equations can be transformed from a differential form with respect to time in Eq. (2.1) into algebraic

expressions in the frequency domain. This implicitly assumes that every field can be written as a superposition of time harmonic fields as Fourier transformation [5, Ch. 2.3.1]:

$$\begin{aligned} \boldsymbol{F}(\boldsymbol{r},t) &= \frac{1}{2\pi}\int_{-\infty}^{\infty} \mathrm{d}\omega \boldsymbol{F}(\boldsymbol{r},\omega)e^{-i\omega t} \ , \\ \boldsymbol{F}(\boldsymbol{r},\omega) &= \int_{-\infty}^{\infty} \mathrm{d}t \boldsymbol{F}(\boldsymbol{r},t)e^{i\omega t} \ . \end{aligned} \tag{2.2}$$

The time derivative is transformed accordingly: $\frac{\partial}{\partial t} \longmapsto -i\omega$. Thus, Maxwell's equations in frequency domain are given by

$$\begin{aligned} \boldsymbol{\nabla} \times \boldsymbol{H}(\boldsymbol{r},\omega) &= -i\omega \boldsymbol{D}(\boldsymbol{r},\omega) \ , & \vec{\nabla} \cdot \boldsymbol{D}(\boldsymbol{r},\omega) &= 0 \ , \\ \boldsymbol{\nabla} \times \boldsymbol{E}(\boldsymbol{r},\omega) &= i\omega \boldsymbol{B}(\boldsymbol{r},\omega) \ , & \vec{\nabla} \cdot \boldsymbol{B}(\boldsymbol{r},\omega) &= 0 \ . \end{aligned} \tag{2.3}$$

2.2 Constitutive relations for bi-isotropic media

A macroscopic material is described by its constitutive relations that give a general relationship between the magnetic and electric flux density and the applied fields: $\mathbf{D}[\mathbf{E},\mathbf{B}], \mathbf{H}[\mathbf{E},\mathbf{B}]$ [22]. For a biaxial, anisotropic, linear and non-local medium the constitutive relations take the form

$$\begin{aligned} \boldsymbol{D}(\boldsymbol{r},\omega) &= \int d\boldsymbol{r'} \boldsymbol{\varepsilon}(\boldsymbol{r}-\boldsymbol{r'},\omega) \cdot \boldsymbol{E}(\boldsymbol{r'},\omega) \ , \\ \boldsymbol{H}(\boldsymbol{r},\omega) &= \int d\boldsymbol{r'} \boldsymbol{\mu}(\boldsymbol{r}-\boldsymbol{r'},\omega) \cdot \boldsymbol{B}(\boldsymbol{r'},\omega) \ . \end{aligned} \tag{2.4}$$

Bi-isotropic media are treated in the remainder of this work. These media are isotropic but with an additional magneto-electric coupling [42]. Thus, the material parameters in (2.4) – which are tensors of second rank in general – are scalar quantities below. More specifically, the class of reciprocal chiral media is analyzed. Chiral media show optical activity. For linearly polarized plane waves – these are fundamental solution of Maxwell's equations, with transverse electric and magnetic fields $\propto e^{i(\boldsymbol{kr}-\omega t)}$ and $k = \sqrt{\varepsilon\mu}\omega$ with the electric/magnetic field vectors in constant directions orthogonal to each other [22] – the polarization plane of linearly polarized light is rotated when traveling through the medium. This effect is due to the geometrical properties of the microscopic building blocks (such as molecules or crystal lattices). Depending on the majority of components being either right-handed (RH) or left-handed (LH), the direction of rotation

of the polarization plane changes. A popular example for this effect are solutions of sugar in water. Another phenomenon in chiral media is circular dichroism: light with different polarization handedness is absorbed differently by the medium [32]. There are several different approaches to describe the electromagnetic behavior of such materials. The most common ones are introduced below.

The earliest description of chiral media was established by Fedorov, which was later extended, known as Drude-Born-Fedorov equations [32],[42]

$$\begin{aligned} \boldsymbol{D} &= \varepsilon_{\mathrm{F}}(\boldsymbol{E} + \beta \bigtriangledown \times \boldsymbol{E}) \ , \\ \boldsymbol{B} &= \mu_{\mathrm{F}}(\boldsymbol{H} + \beta \bigtriangledown \times \boldsymbol{H}) \ . \end{aligned} \tag{2.5}$$

The relations are Lorentz-invariant and were derived phenomenologically to describe the effects of optical activity on the fields. Here, and in the following, homogeneity is assumed and the arguments of the material parameters $\varepsilon(\omega), \mu(\omega), \beta(\omega)$ and fields are omitted. β is the chirality parameter. Substituting Maxwell's equations (2.3) into (2.5) yields $\mathbf{D}[\mathbf{E}, \mathbf{B}], \mathbf{H}[\mathbf{E}, \mathbf{B}]$ corresponding to the Post notation [28],[37]

$$\begin{aligned} \boldsymbol{D} &= \varepsilon_{\mathrm{P}}\boldsymbol{E} + \eta\boldsymbol{B} \ , \\ \boldsymbol{H} &= \mu_{\mathrm{P}}\boldsymbol{B} + \eta\boldsymbol{E} \ , \end{aligned} \tag{2.6}$$

with

$$\begin{aligned} \varepsilon_{\mathrm{P}} &= \varepsilon_{\mathrm{F}} \ , \\ \mu_{\mathrm{P}} &= (1 - \omega^2\beta^2\varepsilon_{\mathrm{F}}\mu_{\mathrm{F}})/\mu_{\mathrm{F}} \ , \\ \eta &= i\omega\beta\varepsilon_{\mathrm{F}} \ . \end{aligned} \tag{2.7}$$

Another way to describe bi-isotropic materials is expressing $\mathbf{D}$ and $\mathbf{B}$ as functionals of $\boldsymbol{E}$ and $\boldsymbol{H}$ [32, Ch. 4],[29], called Condon-Tellegen representation:

$$\begin{aligned} \boldsymbol{D} &= \varepsilon\boldsymbol{E} + (\chi + i\kappa)\sqrt{\varepsilon_0\mu_0}\boldsymbol{H} \ , \\ \boldsymbol{B} &= \mu\boldsymbol{H} + (\chi - i\kappa)\sqrt{\varepsilon_0\mu_0}\boldsymbol{E} \ . \end{aligned} \tag{2.8}$$

It is crucial that the material parameters ε, μ are not equivalent to the ones used in the Drude-Born-Fedorov description as indicated by the subscripts. The material parameters ε and μ express the electric and magnetic response of the material. In addition, there is magneto-electric coupling χ and κ caused by electric(magnetic) polarization of the

material by the applied magnetic(electric) field. Reciprocal media, which are examined in this work, require $\chi = 0$ [32, Tab. 1.1]. For chiral media $\kappa \neq 0$ holds due to chirality of the inclusions. The real part of κ gives rise to the optical activity of the medium, whereas the imaginary part is a measure of circular dichroism [35]. κ is a dimensionless quantity normalized by c_0 (vacuum speed of light). The sign of κ reflects the effective handedness of the medium and can either be positive or negative depending on the average response of the object or inclusions. It is important to note that depending on the notation of time harmonic fields – $\propto e^{-i\omega t}$ in Ref. [29] by Lakhtakia and $\propto e^{i\omega t}$ in Ref. [32] by Lindell, Sihvola, Tretyakov and Viitanen – the sign of κ is flipped. In this work, time harmonic fields are $\propto e^{-i\omega t}$. The imaginary number in (2.8) is due to a phase difference of $\pi/2$ between dielectric displacement/polarization and the electric current/applied fields. The parameters

$$\begin{aligned} \varepsilon &= \frac{\varepsilon_\mathrm{F}}{1-\omega^2\beta^2\varepsilon_\mathrm{F}\mu_\mathrm{F}} \,, \\ \mu &= \frac{\mu_\mathrm{F}}{1-\omega^2\beta^2\varepsilon_\mathrm{F}\mu_\mathrm{F}} \,, \\ \kappa\sqrt{\varepsilon_0\mu_0} &= \frac{\omega\beta\varepsilon_\mathrm{F}\mu_\mathrm{F}}{1-\omega^2\beta^2\varepsilon_\mathrm{F}\mu_\mathrm{F}} \end{aligned} \tag{2.9}$$

can be derived from the ones in the Drude-Born-Fedorov notation for $\omega^2\beta^2\varepsilon_\mathrm{F}\mu_\mathrm{F} \neq 1$.

There is no consensus in the field of bi-isotropic material research, which of the constitutive relations are the most convenient. The material parameters have been shown to be transformable into each other in frequency domain. In [17], material parameters that are invariant under the different constitutive relations are found and suggested to be used to avoid complications when comparing results derived with different approaches. The Condon-Tellegen equations (2.8) are employed in this work, as is also done in [32]. These expressions are more convenient to use for scattering problems. They relate the flux densities $\boldsymbol{D}, \boldsymbol{B}$ to the electric and magnetic fields $\boldsymbol{E}, \boldsymbol{H}$ and avoid differential constitutive relations. Thus, wave equations are easily obtained and changed into a basis of well defined helicity. The corresponding wavenumber of states with well defined helicity take an easy form compared to the eigenvalues derived with the relations of Drude, Born and Fedorov, which show a singularity for $\omega = \frac{1}{\beta\sqrt{\varepsilon_F\mu_F}}$. The eigenmodes and wavenumbers of fields in chiral media are discussed in the next section.

2.3 Light propagation in chiral media

Electromagnetic fields at every position in space and time are obtained by solving Maxwell's equations or the wave equations. For a divergence free, homogeneous, isotropic medium without electromagnetic-coupling the constitutive relations $\boldsymbol{D} = \varepsilon \boldsymbol{E}$, $\boldsymbol{B} = \mu \boldsymbol{H}$ are applied, after taking the cross product of the curl Maxwell's equations (2.1) with $\boldsymbol{\nabla} \times \boldsymbol{\nabla} \times = -\boldsymbol{\nabla}^2$. The resulting wave equations with c being the speed of light in the medium, are

$$\begin{aligned} \boldsymbol{\nabla}^2 \boldsymbol{E}(\boldsymbol{r}, t) + \frac{1}{c^2} \frac{\partial^2}{\partial t^2} \boldsymbol{E}(\boldsymbol{r}, t) = 0 \ , \\ \boldsymbol{\nabla}^2 \boldsymbol{H}(\boldsymbol{r}, t) + \frac{1}{c^2} \frac{\partial^2}{\partial t^2} \boldsymbol{H}(\boldsymbol{r}, t) = 0 \ . \end{aligned} \tag{2.10}$$

A more general expression for the wave equations, written in matrix form and transformed into frequency domain, is

$$\boldsymbol{\nabla}^2 \begin{bmatrix} \boldsymbol{E} \\ \boldsymbol{H} \end{bmatrix} - \boldsymbol{K}^2 \begin{bmatrix} \boldsymbol{E} \\ \boldsymbol{H} \end{bmatrix} = 0 \ . \tag{2.11}$$

$\boldsymbol{K}$ is a 6×6 matrix of the form

$$\boldsymbol{K} = \begin{bmatrix} K_{11} \boldsymbol{I}_3 & K_{12} \boldsymbol{I}_3 \\ K_{21} \boldsymbol{I}_3 & K_{22} \boldsymbol{I}_3 \end{bmatrix} \tag{2.12}$$

for isotropic media, which are investigated herein. $\boldsymbol{I}_3$ is the unit matrix in three dimensions, here corresponding to space dimension. For dielectrics $\boldsymbol{K}$ ($\boldsymbol{K}^2$) is a diagonal matrices and the entries are $K_{11}^2 = K_{22}^2 = \omega^2 \varepsilon \mu$.

For chiral media, the off-diagonal elements of $\boldsymbol{K}$ ($\boldsymbol{K}^2$) are non-zero, which leads to coupled equations for the $\boldsymbol{E}$ and $\boldsymbol{H}$. Therefore, $\boldsymbol{E}$ and $\boldsymbol{H}$ are no eigenstates. To determine

the eigenstates and corresponding wave numbers for chiral media Maxwell's curl equations (2.3) and the constitutive equations (2.8) are written in matrix form:

$$\boldsymbol{\nabla} \times \begin{bmatrix} \boldsymbol{E} \\ \boldsymbol{H} \end{bmatrix} = \begin{bmatrix} 0 & i\omega \boldsymbol{I}_3 \\ -i\omega \boldsymbol{I}_3 & 0 \end{bmatrix} \begin{bmatrix} \boldsymbol{D} \\ \boldsymbol{B} \end{bmatrix} , \tag{2.13}$$

$$\begin{bmatrix} \boldsymbol{D} \\ \boldsymbol{B} \end{bmatrix} = \begin{bmatrix} \varepsilon \boldsymbol{I}_3 & i\kappa\sqrt{\varepsilon_0\mu_0}\boldsymbol{I}_3 \\ -i\kappa\sqrt{\varepsilon_0\mu_0}\boldsymbol{I}_3 & \mu \boldsymbol{I}_3 \end{bmatrix} \begin{bmatrix} \boldsymbol{E} \\ \boldsymbol{H} \end{bmatrix} . \tag{2.14}$$

Inserting equation (2.14) into (2.13) yields

$$\boldsymbol{\nabla} \times \begin{bmatrix} \boldsymbol{E} \\ \boldsymbol{H} \end{bmatrix} = \boldsymbol{K} \begin{bmatrix} \boldsymbol{E} \\ \boldsymbol{H} \end{bmatrix} , \tag{2.15}$$

with

$$\boldsymbol{K} = \omega \begin{bmatrix} \kappa\sqrt{\varepsilon_0\mu_0}\boldsymbol{I}_3 & i\mu \boldsymbol{I}_3 \\ -i\varepsilon \boldsymbol{I}_3 & \kappa\sqrt{\varepsilon_0\mu_0}\boldsymbol{I}_3 \end{bmatrix} . \tag{2.16}$$

Another application of the curl operator to the above equations under the additional assumption of a homogeneous material yields the wave equation (2.11), where

$$\boldsymbol{K}^2 = \omega^2 \begin{bmatrix} (\varepsilon\mu + \kappa^2\varepsilon_0\mu_0)\boldsymbol{I}_3 & 2i\mu\kappa\sqrt{\varepsilon_0\mu_0}\boldsymbol{I}_3 \\ -i2\varepsilon\kappa\sqrt{\varepsilon_0\mu_0}\boldsymbol{I}_3 & (\varepsilon\mu + \kappa^2\varepsilon_0\mu_0)\boldsymbol{I}_3 \end{bmatrix} . \tag{2.17}$$

Wavenumbers corresponding to the eigenstates of electromagnetic fields result from the eigenvalue problem (2.15)

$$\begin{aligned} &\det(\boldsymbol{K} - \lambda \boldsymbol{I}_6) = 0 \\ \Rightarrow\ &\lambda_{\pm,j} = \omega(\pm\sqrt{\varepsilon\mu} + \kappa\sqrt{\varepsilon_0\mu_0}) = \pm k_\pm , \quad j = x, y, z . \end{aligned} \tag{2.18}$$

Thus, the wavenumbers are

$$k_\pm = \omega(\sqrt{\varepsilon\mu} \pm \kappa\sqrt{\varepsilon_0\mu_0}) \tag{2.19}$$

and the eigenproblem is solved by

$$\begin{aligned} \boldsymbol{K}\boldsymbol{V}_{\mathrm{l},\pm} &= \pm k_{\pm}\boldsymbol{V}_{\mathrm{l}\pm} \ , \\ \boldsymbol{K}^{\mathrm{T}}\boldsymbol{V}_{\mathrm{r},\pm} &= \pm k_{\pm}\boldsymbol{V}_{\mathrm{r}\pm} \ . \end{aligned} \tag{2.20}$$

The columns of a linear transformation $\boldsymbol{A}$, which diagonalizes $\boldsymbol{K}$, comprise either the left eigenvectors $\boldsymbol{V}_{\mathrm{l},\pm}$ or the right ones $\boldsymbol{V}_{\mathrm{r},\pm}$. The left eigenstates $\boldsymbol{V}_{\mathrm{l},\pm}$ have to fulfill

$$\begin{aligned} &(\boldsymbol{K} - \boldsymbol{I}_6\lambda_{\pm})\,\boldsymbol{V}_{\mathrm{l},\pm} = 0 \\ \Leftrightarrow \quad &\begin{bmatrix} \mp\boldsymbol{I}_3 & i\sqrt{\frac{\mu}{\varepsilon}}\boldsymbol{I}_3 \\ -i\sqrt{\frac{\varepsilon}{\mu}}\boldsymbol{I}_3 & \mp\boldsymbol{I}_3 \end{bmatrix}\boldsymbol{V}_{\mathrm{l},\pm} = 0 \quad \text{with} \quad \kappa \neq 0 \quad . \end{aligned} \tag{2.21}$$

The eigenvectors for each of the triple eigenvalues are given with a conveniently chosen pre-factor and impedance $Z = \sqrt{\frac{\mu}{\varepsilon}}$ of the medium:

$$\begin{aligned} \boldsymbol{V}_{\mathrm{l}+} &= \frac{1}{\sqrt{2}}\begin{bmatrix} \boldsymbol{I}_3 \\ \frac{i}{Z}\boldsymbol{I}_3 \end{bmatrix} \ , \\ \boldsymbol{V}_{\mathrm{l}-} &= \frac{1}{\sqrt{2}}\begin{bmatrix} \boldsymbol{I}_3 \\ -\frac{i}{Z}\boldsymbol{I}_3 \end{bmatrix} \ . \end{aligned} \tag{2.22}$$

Thus, the linear transformation

$$\boldsymbol{U} = \frac{1}{\sqrt{2}}\begin{bmatrix} \boldsymbol{I}_3 & \boldsymbol{I}_3 \\ \frac{i}{Z}\boldsymbol{I}_3 & -\frac{i}{Z}\boldsymbol{I}_3 \end{bmatrix} \tag{2.23}$$

results. Maxwell's equations can now be decoupled by applying the linear transformation $\boldsymbol{U}$ to equation (2.15), which yields

$$\begin{aligned} \boldsymbol{U^{-1}}(\boldsymbol{\nabla}\times)\boldsymbol{U}\boldsymbol{U^{-1}}\begin{bmatrix} \boldsymbol{E} \\ \boldsymbol{H} \end{bmatrix} &= \boldsymbol{U}^{-1}\boldsymbol{K}\boldsymbol{U}\boldsymbol{U}^{-1}\begin{bmatrix} \boldsymbol{E} \\ \boldsymbol{H} \end{bmatrix} \\ \Longleftrightarrow \boldsymbol{\nabla}\times\begin{bmatrix} \boldsymbol{G}_+ \\ \boldsymbol{G}_- \end{bmatrix} &= \begin{bmatrix} k_+\boldsymbol{I}_3 & 0 \\ 0 & -k_-\boldsymbol{I}_3 \end{bmatrix}\begin{bmatrix} \boldsymbol{G}_+ \\ \boldsymbol{G}_- \end{bmatrix} \ . \end{aligned} \tag{2.24}$$

The eigenstates are a superpositions of the electric and magnetic field, which turn out to be states of defined helicity in the Riemann-Silberstein representation in section 2.4.1:

$$\begin{bmatrix} \boldsymbol{G}_+ \\ \boldsymbol{G}_- \end{bmatrix} = \boldsymbol{U}^{-1} \begin{bmatrix} \boldsymbol{E} \\ \boldsymbol{H} \end{bmatrix} = \begin{bmatrix} \boldsymbol{E} + iZ\boldsymbol{H} \\ \boldsymbol{E} - iZ\boldsymbol{H} \end{bmatrix} . \tag{2.25}$$

The modes $\boldsymbol{G}_\pm$ are not coupled and thus propagate independently. Equivalent calculations were done by Bohren [5, Ch. 8.3] for the Drude-Born-Fedorov representation of constitutive relations. Since $\frac{\mu}{\varepsilon} = \frac{\mu_F}{\varepsilon_F}$ the eigenmodes $\boldsymbol{G}_{\pm,\boldsymbol{F}}$ have the same form with $Z \mapsto Z_\mathrm{F}$ and the corresponding wavenumbers are

$$k_{\pm,\mathrm{F}} = \frac{\omega\sqrt{\varepsilon_\mathrm{F}\mu_\mathrm{F}}}{1 \mp \omega\beta\sqrt{\varepsilon_\mathrm{F}\mu_\mathrm{F}}} . \tag{2.26}$$

The singularity at $\omega\beta\sqrt{\varepsilon_\mathrm{F}\mu_\mathrm{F}} = \pm 1$ corresponds to $\kappa\sqrt{\varepsilon_0\mu_0} = \pm\sqrt{\varepsilon\mu}$. In this case one of the eigenvalues $k_\pm$ becomes zero, such that one eigenmode has infinite phase velocity. Such near-zero refractive index materials result in effects like "decoupling of spatial and temporal field variations" [31] and generally in effects independent of geometry. In [8] it is argued, that due to the singularity in the resonance case, the Drude-Born-Fedorov equations can only describe off-resonant systems.

2.4 Polarization and helicity

Eigenstates of electromagnetic waves were derived in the previous section using the Condon-Tellegen relations. In this section, the definition of helicity is given and it is shown that states of well-defined helicity are eigenstates of Maxwell's equations in chiral media. Within subsection 2.4.2, such states are used to built a basis of the Hilbert-space of transverse electromagnetic waves. Finally, polarization and helicity are set into context (section 2.4.3).

2.4.1 Definition of helicity

Helicity is defined as the projection of the total angular momentum operator $\boldsymbol{J}$ on the momentum operator $\boldsymbol{P}$ divided by the norm $|\boldsymbol{P}|$ [12],[48]

$$\boldsymbol{\Lambda} = \frac{\boldsymbol{J}\cdot\boldsymbol{P}}{|\boldsymbol{P}|} = \frac{\boldsymbol{S}_{\mathrm{sp}}\cdot\boldsymbol{P}}{|\boldsymbol{P}|} \ , \tag{2.27}$$

applying $\boldsymbol{J}\cdot\boldsymbol{P} = (\boldsymbol{L}+\boldsymbol{S}_{\mathrm{sp}})\cdot\boldsymbol{P} = (\boldsymbol{r}\times\boldsymbol{P}+\boldsymbol{S}_{\mathrm{sp}})\cdot\boldsymbol{P} = \boldsymbol{S}_{\mathrm{sp}}\cdot\boldsymbol{P}$ ($\boldsymbol{L}$ is the angular momentum operator and $\boldsymbol{S}_{\mathrm{sp}}$ [1] the spin operator). For transversal modes, the spin of a photon can be either parallel (+1) or anti-parallel (-1) to $\boldsymbol{P}$. These states of well-defined helicity $|\Phi_{\pm}\rangle$ fulfill

$$\boldsymbol{\Lambda}\,|\Phi_{\pm}\rangle = \pm 1\,|\Phi_{\pm}\rangle \ . \tag{2.28}$$

To illustrate the states of well defined helicity, the eigenproblem is written in the position space representation. With [11]

$$\boldsymbol{P} = \frac{1}{i}\boldsymbol{\nabla} \ , \tag{2.29}$$

$$(\boldsymbol{S}_{\mathrm{sp},k})_{ij} = -i\varepsilon_{ijk} \tag{2.30}$$

in position space

$$\boldsymbol{\Lambda} = \frac{1}{|\boldsymbol{P}|}\sum_k \varepsilon_{ijk}\frac{\partial}{\partial x_k}\hat{\boldsymbol{x}}_k = \frac{\boldsymbol{\nabla}\times}{|\boldsymbol{P}|} \ . \tag{2.31}$$

Here and in the remainder of this work $\hbar = 1$. For monochromatic plane waves $|\boldsymbol{P}| = k$ holds and the helicity operator becomes [12]

$$\boldsymbol{\Lambda} = \frac{\boldsymbol{\nabla}\times}{k} \ . \tag{2.32}$$

The wavenumber k in this definition refers to the wavenumber in the current medium of the state on which the operator is applied $k = k_0 n$ (in a chiral medium n has different

[1] the subscript is due to $\boldsymbol{S}$ denoting the scattering operator in this work

values for light with different helicity). From (2.24) it is known that $\boldsymbol{G}_\pm$ are eigenstates of the curl operator

$$\boldsymbol{\nabla} \times \boldsymbol{G}_\pm = \pm k_\pm \boldsymbol{G}_\pm \ . \tag{2.33}$$

Dividing this eigenvalue equation by $k_\pm$ yields the helicity operator

$$\boldsymbol{\Lambda} \boldsymbol{G}_\pm = \pm \boldsymbol{G}_\pm \ , \tag{2.34}$$

with the eigenstates in Riemannn-Silberstein notation

$$\boldsymbol{G}_\pm = \frac{1}{\sqrt{2}} (\boldsymbol{E} \pm iZ\boldsymbol{H}) \ . \tag{2.35}$$

Eigenstates in chiral media are of well-defined helicity, that is, they are eigenstates of the helicity operator. Every possible solution of Maxwell's equations is formed by a superposition of these orthogonal eigenstates, which can form a basis. These basis states are defined by their helicity, instead of the polarization defined by the direction of $\boldsymbol{E}$ (next to three more identification numbers, as explained below). A more general way to set a basis for electromagnetic waves is shown in the following subsection.

2.4.2 Helicity basis

In general, the method to find solutions for Maxwell's equations and the vector wave equations [5, Ch. 4.1] for homogeneous, isotropic source free media is to assume time harmonic waves and a scalar function Ψ satisfying the scalar Helmholtz equation [22, Eq. (9.79)]

$$\boldsymbol{\nabla}^2 \Psi(\boldsymbol{r}) - k^2 \Psi(\boldsymbol{r}) = 0 \ . \tag{2.36}$$

The basis vectors are chosen from the common set of eigenstates of commuting operators [48]. The eigenvalues of the independent commuting operators are the three numbers defining the scalar wave solution. Depending on the coordinate system, the set of commuting operators is different. For symmetries in x-, y-, z-direction the Cartesian coordinate

system is chosen. The basis vectors for plane waves are defined by the components of momentum p_x, p_y, p_z

$$|\Psi\rangle = |p_x p_y p_z\rangle \ . \tag{2.37}$$

For systems with rotational symmetry the problem is approached using spherical coordinates and the set of commuting operators $\{\boldsymbol{H}, \boldsymbol{J^2}, \boldsymbol{J_z}\}$ with corresponding eigenvalues ω, l, m and $m = -l, -l+1, ..., l$. The common set of eigenstates are multi-poles with l being the order of the multipole ($l = 1$ dipoles, $l = 2$ quadrupole, and so on). m gives the spatial orientation of the multipoles. In spherical coordinates the basis vectors are

$$\Psi = |\omega\, l\, m\rangle \ . \tag{2.38}$$

We can construct a vector solution to Maxwell's equations from the scalar wave solution using

$$\boldsymbol{M} = \boldsymbol{\nabla} \times \hat{\boldsymbol{c}}\Psi \ , \ \boldsymbol{N} = \frac{\boldsymbol{\nabla} \times \boldsymbol{M}}{k} \ . \tag{2.39}$$

$\hat{\boldsymbol{c}}$ is a fixed unit vector. The fourth quantum number reflects the vectorial character of the fields, i.e. the polarization of the fields. $\boldsymbol{M}$ and $\boldsymbol{N}$ are orthogonal vector wave solutions, which form a suitable basis to expand electromagnetic waves in achiral media. In a reference system, using spherical coordinates the two orthogonal basis vectors are referred to as either magnetic (or TE) $\boldsymbol{M}$ or electric (or TM) multipoles $\boldsymbol{N}$ [43, Sec. 1.11 a. 7.2]. However, the basis vectors are coupled while propagating in a chiral media. In the previous sections it was shown that the eigenstates of the helicity operator decouple Maxwell's equations. Basis vectors are transformed by the helicity operator under the assumption that they both fulfill the wave equation (2.11), as

$$\boldsymbol{N} = \boldsymbol{\Lambda M} \ , \tag{2.40}$$

$$\boldsymbol{M} = \frac{\boldsymbol{\nabla}^2}{k^2}\boldsymbol{M} = \boldsymbol{\Lambda}^2\boldsymbol{M} = \boldsymbol{\Lambda N} \ . \tag{2.41}$$

Orthonormal eigenmodes of well defined helicity are found as a a superposition of $\boldsymbol{M}$, $\boldsymbol{N}$:

$$|\Phi\pm\rangle := \boldsymbol{Q}_{\mathrm{L/R}} = \frac{1}{\sqrt{2}}(\boldsymbol{M} \pm \boldsymbol{N}) \quad . \tag{2.42}$$

$\boldsymbol{Q}_{\mathrm{L/R}}$ form a basis, which is called helicity basis in the frame of this work.

2.4.3 Handedness

In the previous sections it was shown that a basis of electromagnetic fields consists of states of well defined helicity. Now the relation between helicity and polarization of an electromagnetic wave is discussed. For this reason, the basis states are assumed to be plane waves $\{\boldsymbol{M}, \boldsymbol{N}\} \propto e^{i(\boldsymbol{kr}-\omega t)}$. The wavevector is chosen in z-direction $\boldsymbol{k} = k\hat{\boldsymbol{z}}$, and $\boldsymbol{M} = e^{i(\boldsymbol{kr}-\omega t)}\hat{\boldsymbol{x}}$,

$$\boldsymbol{N} \overset{(2.41)}{=} \boldsymbol{\Lambda M} = -ie^{i(\boldsymbol{kr}-\omega t)}\hat{\boldsymbol{y}} \ . \tag{2.43}$$

Thereby, the basis vectors are written as

$$\mathrm{Re}\{\Psi(\boldsymbol{r}, t)_{\pm}\} = \begin{bmatrix} \cos(kz - \omega t) \\ \mp \sin(kz - \omega t) \end{bmatrix} . \tag{2.44}$$

These are circularly polarized waves: for $+1$ helicity the wave is LH circularly polarized and for -1 the light is RH circularly polarized. For plane waves the eigenstates of helicity correspond to the polarization handedness of the light. Thus, in general helicity describes the state of polarization handedness in momentum space [14]. Light of well-defined helicity shows the same circular polarization for every plane wave of its expansion, depicted in Fig. 2.1a. If not all the modes are of the same handedness, the light possesses no defined helicity and the helicity $\Lambda \neq \pm 1$, see Fig. 2.1b.

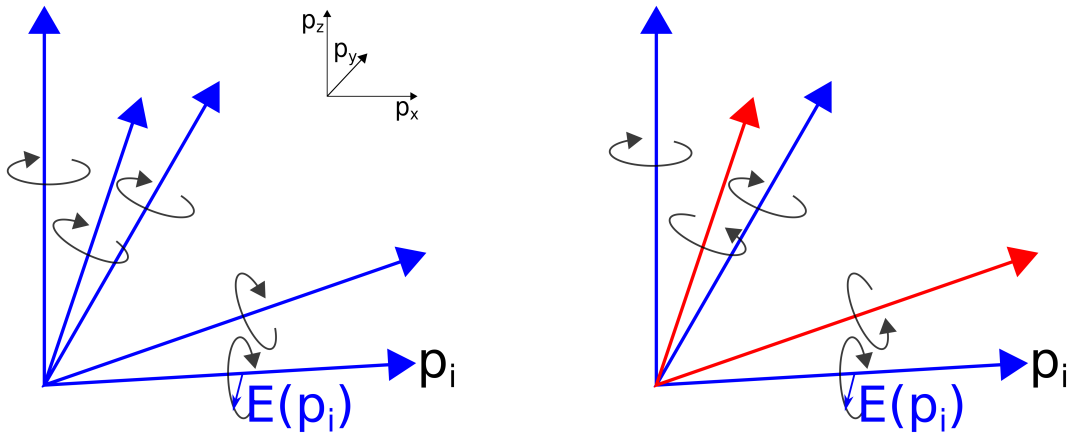

(a) $\Lambda = +1$ (b) $\Lambda \neq \pm 1$

Figure 2.1: Electromagnetic wave represented in momentum space as a superposition of plane waves $\boldsymbol{p}_i$ with electric field amplitudes $\boldsymbol{E}(\boldsymbol{p}_i, \omega)$. The arrows exemplary stand for all modes. In (a), the field vector is left-handed circular and thus the helicity of light is +1. In (b), the handedness is different for each mode. The light possesses no defined helicity.

3 Characterization and modeling of chiral media

This chapter addresses the modeling of chiral media consisting of a homogeneous host medium and chiral inclusions and the restrictions resulting from it. The mixing theory in section 3.1 is a quasi-static approach to calculate the average polarization of the medium, yielding effectively isotropic material parameters as functions of the host medium and the dipole moments of the inclusions. These dipole moments are derived in section 3.2. An antenna model is used to calculate the dipole moments of simple single turn helices and their interconnection. The model assumptions give rise to relations between the effective material constants, examined in the last section (3.3).

3.1 Mixing theory

In the macroscopic constitutive relations in section 2.2, chiral media are assumed to be isotropic and homogeneous. The theory summarized here is valid to describe the effective material response of a dilute solution of chiral particles. It is assumed that these chiral inclusions are placed in a homogeneous isotropic host medium with material parameters $\varepsilon_\mathrm{a}, \mu_\mathrm{a}$. The host medium is achiral and lossless. The inclusions are small enough to assume a homogeneous field across the structure. Thus, a quasi-static approach where the chiral particles can be approximated as electromagnetic dipole scatterers is used, following the approach of [32, Ch. 6] and [47, Ch. 5]. The dipole moments of an inclusion caused by the applied field are

$$\begin{bmatrix} \boldsymbol{p} \\ \boldsymbol{m} \end{bmatrix} = \begin{bmatrix} \boldsymbol{\alpha}_\mathrm{ee} & \boldsymbol{\alpha}_\mathrm{em} \\ \boldsymbol{\alpha}_\mathrm{me} & \boldsymbol{\alpha}_\mathrm{mm} \end{bmatrix} \begin{bmatrix} \boldsymbol{E}_\mathrm{L} \\ \boldsymbol{H}_\mathrm{L} \end{bmatrix} , \tag{3.1}$$

where $\boldsymbol{\alpha}_\mathrm{ee}$ is the electric, $\boldsymbol{\alpha}_\mathrm{em}$ the magnetic polarizability and $\boldsymbol{\alpha}_\mathrm{em}$, $\boldsymbol{\alpha}_\mathrm{me}$ are cross-coupling terms. The polarizabilities become scalar quantities which are equal for every direction in space in the case of an effectively isotropic behavior. This effective isotropy is shown

below. The fields $\boldsymbol{E}_\mathrm{L}$, $\boldsymbol{H}_\mathrm{L}$, so called Lorentz-fields, are the effective local fields at the electromagnetic dipole; including the applied field but also taking into account the additional electromagnetic field by the particles themselves

$$\begin{bmatrix} \boldsymbol{E}_\mathrm{L} \\ \boldsymbol{H}_\mathrm{L} \end{bmatrix} = \begin{bmatrix} \boldsymbol{E} \\ \boldsymbol{H} \end{bmatrix} + \frac{1}{3} \begin{bmatrix} \boldsymbol{I}_3/\varepsilon_\mathrm{a} & 0 \\ 0 & \boldsymbol{I}_3 \end{bmatrix} \begin{bmatrix} < \boldsymbol{P}_\mathbf{e} > \\ < \boldsymbol{P}_\mathbf{m} > \end{bmatrix} . \tag{3.2}$$

A derivation of the interaction term in a quasi-static setting is given in [47, Ch. 5] by Tretyakov *et al.*. For a material built out of cells with one point scatterer each, the main contribution to the local field – besides the external field – is given by the particle in the cell. The contributions of surrounding particles are neglected, since the distances between the center particle and the surrounding particles are assumed to be large. Therefore, the particle-density is required to be low in the material. The material is finite and the particles are randomly distributed. The average field of an electric dipole inside a spherical cell is

$$\begin{aligned} \boldsymbol{E}_\mathrm{cell} &= \boldsymbol{E} - \boldsymbol{E}_\mathrm{L} \\ &= -\frac{1}{3\varepsilon_\mathrm{a} V_\mathrm{cell}} \boldsymbol{p} \\ &= -\frac{\boldsymbol{P_e}}{3\varepsilon_\mathrm{a}} . \end{aligned} \tag{3.3}$$

In general, this proportionality between the average field and the average polarisability $\boldsymbol{P}_\mathbf{e}$ is not true. For arbitrary cell shapes the inclusion density has to be low, which is already implied by the model assumptions, though.

The average flux densities $< \boldsymbol{D} >, < \boldsymbol{B} >$ are composed of the flux density in the host medium and the averaged polarizability of all single dipole scatterers

$$\begin{bmatrix} < \boldsymbol{D} > \\ < \boldsymbol{B} > \end{bmatrix} = \begin{bmatrix} \varepsilon_\mathrm{a} \boldsymbol{I}_3 & 0 \\ 0 & \mu_\mathrm{a} \boldsymbol{I}_3 \end{bmatrix} \begin{bmatrix} \boldsymbol{E} \\ \boldsymbol{H} \end{bmatrix} + \begin{bmatrix} < \boldsymbol{P}_e > \\ \mu_\mathrm{a} < \boldsymbol{P}_m > \end{bmatrix} . \tag{3.4}$$

The effective material parameters relate the average flux density and the applied fields

$$\begin{bmatrix} < \boldsymbol{D} > \\ < \boldsymbol{B} > \end{bmatrix} = \begin{bmatrix} \varepsilon_{eff} \boldsymbol{I}_3 & i\kappa_{eff} \boldsymbol{I}_3 \\ -i\kappa_{eff} \boldsymbol{I}_3 & \mu_{eff} \boldsymbol{I}_3 \end{bmatrix} \begin{bmatrix} \boldsymbol{E} \\ \boldsymbol{H} \end{bmatrix} . \tag{3.5}$$

Using (3.1), (3.2) and $< \boldsymbol{P}_{e/m} >= n\boldsymbol{p}/\boldsymbol{m}$, the average polarizabilities are

$$\begin{bmatrix} < \boldsymbol{P}_e > \\ < \boldsymbol{P}_m > \end{bmatrix} = \boldsymbol{Q} \begin{bmatrix} \boldsymbol{E} \\ \boldsymbol{H} \end{bmatrix} \ , \tag{3.6}$$

with the dyadic $\boldsymbol{Q}$ depending on the number density n of the dipoles and the effective material parameters.

The expression for the average polarization (3.6) is substituted in (3.4) and compared to (3.5). This yields the generalized Lorenz-Lorentz formulas, which relate the inclusion properties $\alpha_{\beta\gamma}$ to effective material properties of the medium

$$\begin{aligned} \varepsilon_{\text{eff}} &= \varepsilon_{\text{a}} + \left(n\alpha_{\text{ee}} - \frac{n^2 \Delta_\alpha}{3\mu_{\text{a}}} \right) / D \ , \\ \mu_{\text{eff}} &= \mu_{\text{a}} + \left(n\alpha_{\text{mm}}\mu_{\text{a}} - \frac{n^2 \Delta_\alpha}{2\varepsilon_{\text{a}}} \right) / D \ , \\ \kappa_{\text{eff}} &= -i \frac{n\alpha_{\text{em}}}{D\sqrt{\varepsilon_{\text{a}}\mu_{\text{a}}}} \ , \end{aligned} \tag{3.7}$$

with

$$D = 1 - \frac{n\alpha_{\text{ee}}}{3\varepsilon_{\text{a}}} - \frac{n\alpha_{\text{mm}}}{3} + \frac{n^2 \Delta_\alpha}{9\varepsilon_{\text{a}}\mu_{\text{a}}} \tag{3.8}$$

and

$$\Delta_\alpha = \alpha_{\text{ee}}\alpha_{\text{mm}} - \alpha_{\text{me}}\alpha_{\text{em}} \ . \tag{3.9}$$

It is important to note that the generalized Lorenz-Lorentz formulas (or generalized Maxwell-Garnett formulas if the inclusions are spheres) are obtained under the following assumptions: firstly, only small inclusions compared to the wavelength are allowed. Secondly, the model holds for dilute mixtures wherein inclusions are so far apart that their interaction can be neglected [33]. Thus, this model cannot describe very dense arrangements of chiral inclusions.

There is a theoretical approach to extend the Maxwell-Garnett formulas to higher inclusion concentrations, discussed in Ref. [33] by Michel, Lakhtakia *et al.*. The homogenization is done stepwise, initialized with a homogeneous material. Subsequently, dilute inclusions are added in N homogenization steps. This is a basis to iteratively

calculate the effective material parameters from the inclusion properties. However, with this approach it is not possible to analytically calculate the polarizabilities from effective material parameters. Therefore, this approach is not used in the present thesis, even though it gives a more realistic model of the medium.

3.2 Analytical modeling of chiral inclusions

One of the simplest analytical descriptions of a chiral inclusion is a helix represented by a split ring connected to two straight wires orthogonal to the loop, depicted in Fig. 3.1a. Since the mixing theory forces the inclusions to be small particles compared to the wavelength, a lumped circuit model can be used to describe the scatterers, where the currents across the inclusion do not vary. This model has been discussed, for example, by Tretyakov *et al.* in [45]. The main findings are summarized below for very small inclusions. Furthermore, the effective material parameters resulting from these model assumptions and their interrelation are presented in subsection 3.2.1 and examined on their physicality (section 3.2.2).

The goal of this section is to derive the polarizability dyadic (3.1) as a function of the surrounding medium and geometrical properties of the inclusions. These are the impedances of the loop Z_l and the wire Z_w, the loop area $S = \pi a^2$ and the effective length $l_{\text{eff}} \approx l/2$ for small antennas. In contrast to the circuit model in [45, Fig. 2], the antenna is described as a series RLC-circuit, neglecting higher order terms of the loop current due to the small object size. The model is shown in Fig. 3.1b. Using Kirchhoff's voltage law [3] on the wire and loop part, the impedances read

$$Z_{\text{w}} = \frac{1}{i\omega C} \ , \tag{3.10}$$

$$Z_{\text{l}} = R_{\text{rad}} + i\omega L \ . \tag{3.11}$$

The material itself from which the helix is made of is assumed to be lossless to simplify the problem. The resulting effective material parameters can still be complex quantities due to scattering losses of the inclusions indicated by R_{rad}.

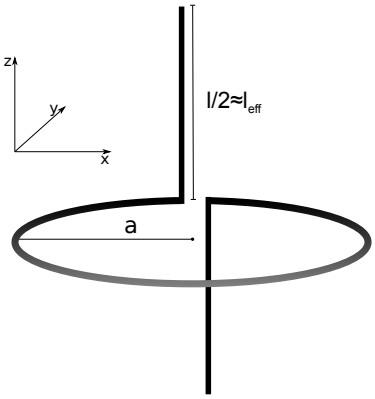

(a) Helix model

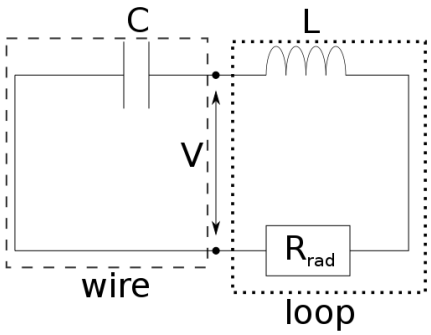

(b) Series circuit

Figure 3.1: Simplified models of a chiral inclusion: (a) shows the helix consisting of two parallel wire parts of equal length and a loop in the plane orthogonal to the wires (b) depicts the corresponding lumped element circuit for a small, lossless helix.

Furthermore, it is assumed that the antenna is excited by a time harmonic electric field along the wire axis, which is w.l.o.g. chosen to be the z-axis, $\boldsymbol{E} = E_z\hat{\boldsymbol{z}}$. This field produces a homogeneous current

$$I_E(\boldsymbol{r}, t) = I(t) = \frac{E_z l_{\text{eff}}}{Z_{\text{l}} + Z_{\text{w}}} = Ie^{-i\omega t} \tag{3.12}$$

which generates an electric dipole moment

$$\begin{aligned} p_z &= l_{\text{eff}} \int \mathrm{d}t\, I(t) \\ &= \frac{l_{\text{eff}}^2}{i\omega(Z_{\text{l}} + Z_{\text{w}})} E_z \\ &= \alpha_{\text{ee}}^{zz} E_z \ . \end{aligned} \tag{3.13}$$

The current (3.12) which flows through the loop creates a magnetic moment in z-direction

$$\begin{aligned} m_z &= \mp\pi a^2 I(t) \overset{(3.12)}{=} \mp\frac{S l_{\text{eff}}}{Z_{\text{l}} + Z_{\text{w}}} E_z \\ &= \mp\alpha_{\text{me}}^{zz} E_z \ . \end{aligned} \tag{3.14}$$

Depending on the handedness of the helix, the current can either flow clockwise or counter-clockwise expressed by either plus or minus sign. A time harmonic magnetic field $\boldsymbol{H} = H_z\hat{\boldsymbol{z}}$ along the wire axis induces a current in the loop in the x-y plane

$$I_H = -2a\frac{J_1(ka)}{A_0}\frac{Z_\mathrm{l}}{Z_\mathrm{l}+Z_\mathrm{w}}H_z \ . \tag{3.15}$$

$A_0 = \frac{iZ_\mathrm{l}}{\pi\sqrt{\frac{\mu_\mathrm{a}}{\varepsilon_\mathrm{a}}}}$ if higher order terms of the current are neglected and $J_1(ka)$ is a Bessel-function of the first kind. For small loops, it holds $J_1(ka) \approx ka/2$. Using (3.14), the magnetic polarizability of the helix caused by the applied magnetic field is

$$\alpha_{mm}^{zz} = -\mu_\mathrm{a}\frac{i\omega S^2}{Z_\mathrm{l}+Z_\mathrm{w}} \ . \tag{3.16}$$

The current (3.15) through the wire also creates an electric dipole moment

$$\begin{aligned} p_z &= \pm\frac{\mu_a S l_\mathrm{eff}}{Z_\mathrm{l}+Z_\mathrm{w}}H_z \\ &= \pm\alpha_\mathrm{em}^{zz}H_z \ . \end{aligned} \tag{3.17}$$

The derived entries of the polarizability tensors (3.13),(3.16) and (3.17):

$$\begin{aligned} \alpha_\mathrm{ee}^{zz} &= \frac{Cl_\mathrm{eff}^2}{1-\omega^2LC+i\omega CR_\mathrm{rad}} \ , \\ \alpha_\mathrm{mm}^{zz} &= \frac{\mu_\mathrm{a}\omega^2CS^2}{1-\omega^2LC+i\omega CR_\mathrm{rad}} \ , \\ \alpha_\mathrm{em}^{zz} &= \pm\frac{i\mu\omega CSl_\mathrm{eff}}{1-\omega^2LC+i\omega CR_\mathrm{rad}} = -\mu_\mathrm{a}\alpha_\mathrm{me}^{zz} \end{aligned} \tag{3.18}$$

fulfill the relation

$$\alpha_\mathrm{ee}^{zz}\alpha_\mathrm{mm}^{zz} = -(\alpha_\mathrm{em}^{zz})^2/\mu_\mathrm{a} \ . \tag{3.19}$$

Unlike in Ref. [45], the current is assumed to be uniform meaning that all higher order Fourier expansion coefficients are neglected. Only moments which are parallel to the axis of the helix caused by fields parallel to the polarization are considered. The average

polarizabilities of the medium which consists of randomly orientated helices result in effective isotropic behavior [45]

$$\begin{aligned} \alpha_{\mathrm{ee}} &= \frac{\alpha_{\mathrm{ee}}^{zz}}{3} \ , \\ \alpha_{\mathrm{mm}} &= \frac{\alpha_{\mathrm{mm}}^{zz}}{3} \ , \\ \alpha_{\mathrm{em}} &= \frac{\alpha_{\mathrm{em}}^{zz}}{3} \ . \end{aligned} \tag{3.20}$$

3.2.1 Effective material parameters

Applying relation (3.19) $\Delta_\alpha = 0$ in (3.9) and with (3.20) the effective material parameters become [32, Ch. 6.6]

$$\begin{aligned} \varepsilon_{eff} &= \varepsilon_a + \frac{n\alpha_{ee}}{3D} \ , \\ \mu_{eff} &= \mu_a + \frac{n\alpha_{mm}}{3D}\mu_a \ , \\ \kappa_{eff} &= \frac{in\alpha_{em}}{3D\sqrt{\varepsilon_0\mu_0}} \ , \end{aligned} \tag{3.21}$$

with

$$D = 1 - \frac{n\alpha_{ee}}{3\varepsilon_a} - \frac{n\alpha_{mm}}{3} \ . \tag{3.22}$$

We substitute these expressions into (3.19) to obtain an interrelation between the effective material parameters:

$$\begin{aligned} \frac{(\varepsilon_{\mathrm{eff}} - \varepsilon_{\mathrm{a}})3D}{n}\frac{(\mu_{\mathrm{eff}} - \mu_{\mathrm{a}})3D}{n} &= \left(\frac{(3\kappa_{\mathrm{eff}}D\sqrt{\varepsilon_0\mu_0}}{n}\right)^2 \\ \Leftrightarrow (\varepsilon_{\mathrm{eff}} - \varepsilon_{\mathrm{a}})(\mu_{\mathrm{eff}} - \mu_{\mathrm{a}}) &= \kappa_{\mathrm{eff}}^2\varepsilon_0\mu_0 \ . \end{aligned} \tag{3.23}$$

Hence, there is no effective chirality if the chiral inclusions do not show both electric and magnetic polarization. Isotropic, chiral, reciprocal media have to be magnetic $\mu_{\mathrm{eff}} \neq \mu_0$. Furthermore, the chirality is dictated by the electric and magnetic response of the inclusions. For very high values of κ_{eff}, the difference between the effective parameters and the host medium is maximal when both electric and magnetic response are very large (see (3.19)).

3.2.2 Onsager's reciprocal theorem and energy preservation

To conclude this subsection about the analytical antenna model, it is shown that the derived polarizabilities fulfill necessary conditions to be physical. The model fulfills Onsager's reciprocal theorem (even for higher order current effects, see Ref. [45]):

$$\alpha_{\mathrm{em}}^{zz} = -\mu_{\mathrm{a}} \alpha_{\mathrm{me}}^{zz} \ . \tag{3.24}$$

Furthermore, the antenna model has to preserve energy. This means that for a lossless medium the extinction equals the scattered power. These considerations lead to a restriction on the polarizability dyadic [40]

$$\boldsymbol{\alpha} = \begin{bmatrix} \alpha_{\mathrm{ee}} & \alpha_{\mathrm{em}} \\ -\alpha_{\mathrm{em}}/\mu_{\mathrm{a}} & \alpha_{\mathrm{mm}} \end{bmatrix} \ , \tag{3.25}$$

which reads [2][1]

$$\frac{1}{2i}(\boldsymbol{\alpha} - \boldsymbol{\alpha}^{\dagger}) = -\frac{k^3}{6\pi} \boldsymbol{\alpha}^{\dagger} \begin{bmatrix} 1/\varepsilon_{\mathrm{a}} & 0 \\ 0 & \mu_{\mathrm{a}} \end{bmatrix} \boldsymbol{\alpha} \ . \tag{3.26}$$

There are four equations relating the polarizabilities of which the two cross equations are identical due to reciprocity:

$$\begin{aligned} \frac{1}{2i}(\alpha_{ee} - \alpha_{ee}^*) &= -\frac{k^3}{6\pi\varepsilon_a} \left(\alpha_{ee}^* \alpha_{ee} + \alpha_{em}^* \alpha_{em}/Z_a^2\right) \ , \\ \frac{1}{2i}(\alpha_{mm} - \alpha_{mm}^*) &= -\frac{k^3}{6\pi} \left(\alpha_{mm}^* \alpha_{mm} + \alpha_{em}^* \alpha_{em} c_a^2\right) \ , \\ \frac{1}{2i}(\alpha_{em} + \alpha_{em}^*) &= -\frac{k^3}{6\pi\varepsilon_a} \left(\alpha_{ee}^* \alpha_{em} - \alpha_{em}^* \alpha_{mm} \varepsilon_a\right) \ . \end{aligned} \tag{3.27}$$

[1] In general, $\boldsymbol{\alpha}$ is a 6×6 matrix with $\boldsymbol{\alpha}_{\beta\gamma}$ are 3×3 matrices, but with the antenna model $\boldsymbol{\alpha}_{\beta\gamma}^{ij} = 0 \ \forall (ij) \neq (zz)$. Thus, the equation also holds for $\boldsymbol{\alpha}^{zz}$ and the super-index is omitted.

$Z_\mathrm{a} = \sqrt{\frac{\mu_\mathrm{a}}{\varepsilon_\mathrm{a}}}$ is the impedance of the host medium, c_a is the speed of light in the host medium and * denotes the complex conjugate of a quantity. If the polarizabilities (3.18) are substituted, the energy is preserved for

$$R_\mathrm{rad} = \frac{1}{6\pi\varepsilon_\mathrm{a} c_\mathrm{a}}(l_\mathrm{eff}^2 k^2 + S^2 k^4) \ . \tag{3.28}$$

The first summand is due to the radiation resistance of the wire with $R_\mathrm{rad,w} = \frac{2P}{I_0^2}$ [22, Ch. 9.2]. P is the radiated power of the electric dipole and I_0 is the current over the helix. The second summand corresponds to the radiation losses of the loop.

3.3 Constraints on material parameters

Knowledge of the polarizabilities of the single scatterer yields the effective behavior of the material. For simulation purposes it is important to know how the single material parameters are connected to each other while meeting energy preservation constraints. In this section, general relations between the polarizabilities are derived for which energy is preserved using the Sipe-Kranendonk conditions. It is shown, that

$$\alpha_\mathrm{ee}\alpha_\mathrm{mm} = -\alpha_\mathrm{em}^2/\mu_\mathrm{a} \tag{3.29}$$

and therefore,

$$(\varepsilon_\mathrm{eff} - \varepsilon_\mathrm{a})(\mu_\mathrm{eff} - \mu_\mathrm{a}) = \kappa_\mathrm{eff}^2 \varepsilon_0 \mu_0 \tag{3.30}$$

are not sufficient conditions to preserve energy, although the polarizabilities (3.18), by themselves, preserve energy as shown in the previous section. The first two conditions in (3.27) are transformed into

$$\begin{aligned} \alpha_\mathrm{em}^* \alpha_\mathrm{em}/Z_\mathrm{a}^2 &= \frac{\mathrm{Im}(\alpha_\mathrm{ee})6\pi\varepsilon_\mathrm{a}}{k^3} - \alpha_\mathrm{ee}^*\alpha_\mathrm{ee} \ , \\ \alpha_\mathrm{em}^* \alpha_\mathrm{em} c_\mathrm{a}^2 &= \frac{\mathrm{Im}(\alpha_\mathrm{mm})6\pi}{k^3} - \alpha_\mathrm{mm}^*\alpha_\mathrm{mm}/Z^2 \ . \end{aligned} \tag{3.31}$$

Multiplying both equations yields

$$\frac{c_\mathrm{a}^2}{Z_\mathrm{a}^2}(\alpha_{em}^*)^2\alpha_\mathrm{em}^2 = \left(\frac{\mathrm{Im}(\alpha_\mathrm{ee})6\pi\varepsilon_\mathrm{a}}{k^3} - \alpha_\mathrm{ee}^*\alpha_\mathrm{ee}\right)\left(\frac{\mathrm{Im}(\alpha_\mathrm{mm})6\pi}{k^3} - \alpha_\mathrm{mm}^*\alpha_\mathrm{mm}\right)$$

$$\begin{aligned}\Leftrightarrow\ (\alpha_\mathrm{em}^2)^*\alpha_\mathrm{em}^2/\mu_a^2 = (\alpha_\mathrm{ee}\alpha_\mathrm{mm})^*(\alpha_\mathrm{ee}\alpha_\mathrm{mm}) &+ \frac{\mathrm{Im}(\alpha_\mathrm{ee})\,\mathrm{Im}(\alpha_\mathrm{mm})(6\pi)^2\varepsilon_\mathrm{a}}{k^6} \\ &- \frac{\mathrm{Im}(\alpha_\mathrm{ee})6\pi\varepsilon_\mathrm{a}}{k^3}\alpha_\mathrm{mm}^*\alpha_\mathrm{mm} - \frac{\mathrm{Im}(\alpha_\mathrm{mm})6\pi}{k^3}\alpha_\mathrm{ee}^*\alpha_\mathrm{ee}\ .\end{aligned}$$

The left hand side and the first term on the right hand side in the previous equation are identified as condition (3.29) multiplied with its complex conjugate. Thus, these terms vanish if the condition is fulfilled. The polarizabilities then have to meet additionally

$$\frac{\alpha_\mathrm{mm}^*\alpha_\mathrm{mm}}{\mathrm{Im}(\alpha_\mathrm{mm})}\varepsilon_a + \frac{\alpha_\mathrm{ee}^*\alpha_\mathrm{ee}}{\mathrm{Im}(\alpha_\mathrm{ee})} = \frac{6\pi\varepsilon_a}{k^3}\ . \tag{3.32}$$

From the third constraint in (3.27), the same conditions can be derived, so they comprise no additional information. Due to the non-linear dependence of the effective material parameters on the polarizabilities, this additional constraint on the imaginary and real parts yields no explicit analytic relation between the permeability, permittivity and the chirality parameter.

To solve the problem, by means of (3.18) geneneral relations between the polarizabilities are derived, which read

$$\begin{aligned}\alpha_\mathrm{ee} &= \pm iA\alpha_\mathrm{em}\ , \\ \alpha_\mathrm{mm} &= A^{-2}\mu_a^{-1}\alpha_\mathrm{ee} \text{ with } A \in \mathbb{R}\ .\end{aligned} \tag{3.33}$$

$A = \frac{l_\mathrm{eff}}{\omega S\mu_a}$ is a function of the geometrical parameters S and l_eff, the host medium and the frequency. It can be seen that (3.29) is a necessary but not sufficient condition for (3.33). These are not new relations. While Tretyakov *et al.* used the relations between the polarizabilities (3.33), cf. [46, Eq. (24)], to propose a dispersion relation for the polarizabilities, we derive relations between the effective material parameters from them in this thesis. Thereby, energy preservation is ensured when alternating material parameters

during simulations. Thus, for fixed α_{ee} and imaginary part $\mathrm{Im}(\alpha_{\mathrm{em}})$ (which relates to the real part of the chiral parameter) relations (3.33) can be used to derive α_{mm}:

$$\begin{aligned} \alpha_{\mathrm{ee}} &= \mathrm{Re}\{\alpha_{\mathrm{ee}}\} + i\,\mathrm{Im}(\alpha_{\mathrm{ee}}) \ , \\ \alpha_{\mathrm{mm}} &= \frac{\mathrm{Im}(\alpha_{\mathrm{em}})^2}{\mathrm{Re}(\alpha_{\mathrm{ee}})^2 \mu_a} \left(\mathrm{Re}(\alpha_{\mathrm{ee}}) + i\,\mathrm{Im}(\alpha_{\mathrm{ee}})\right) \ , \\ \alpha_{\mathrm{em}} &= \mathrm{Im}(\alpha_{\mathrm{em}}) \left(-\frac{\mathrm{Im}(\alpha_{\mathrm{ee}})}{\mathrm{Re}(\alpha_{\mathrm{ee}})} + i\right) \ . \end{aligned} \tag{3.34}$$

The $\alpha_{\beta\gamma}$ related by equation (3.34) fulfill the generalized Sipe-Kranendonk relations (3.27) and thus preserve energy. Now, (3.34) is used to derive relations between the effective material parameters defined in equation (3.21). Given the effective permittivity $\varepsilon_{\mathrm{eff}}$ and the real part of the chiral parameter κ_1, the magnetic material properties and the imaginary part of the chirality parameter are derived

$$\begin{aligned} \varepsilon_{\mathrm{eff}} &= \mathrm{Re}(\varepsilon) + i\,\mathrm{Im}(\varepsilon) \ , \\ \mu_{\mathrm{eff}} &= \mu_a + \frac{\mathrm{Re}(\kappa)^2 \varepsilon_0 \mu_0}{(\mathrm{Re}(\varepsilon) - \varepsilon_a)^2} \left(\mathrm{Re}(\varepsilon) + i\,\mathrm{Im}(\varepsilon) - \varepsilon_a\right) \ , \\ \kappa_{\mathrm{eff}} &= \mathrm{Re}(\kappa) + i\,\mathrm{Re}(\kappa) \frac{\mathrm{Im}(\varepsilon)}{\mathrm{Re}(\varepsilon) - \varepsilon_a} \ . \end{aligned} \tag{3.35}$$

Relation (3.35) is used to calculate α_{mm} or μ_{eff} for fixed electric response and coupling in simulations. For very small object sizes $S \ll k^{-4}, l_{\mathrm{eff}} \ll k^{-2}$, the material parameters are nearly lossless and sufficiently described by equations (3.30):

$$\mu_{\mathrm{eff}} = \mu_a + \frac{\kappa_{\mathrm{eff}}^2 \varepsilon_0 \mu_0}{\varepsilon_{\mathrm{eff}} - \varepsilon_a} \ . \tag{3.36}$$

The subscripts indicating that the parameters are effective ones are omitted from here on.

4 Scattering theory

In this chapter we deal with scattering by isotropic chiral spherical particles. The chapter aims at finding expressions for the field inside and outside the sphere at every position in space and time. Electromagnetic waves in achiral and chiral media were found as solutions of Maxwell's equations in section 2.3. The only region where the behavior of the field is not yet defined is at the boundary of the scatterer. The boundary problem has to be solved. Therefore, boundary conditions for arbitrary interfaces are set up and expressed in the helicity basis, as introduced in section 4.1. The solution of the boundary problem in case of scatterers with spherical symmetry is found by using the theory of Mie in section 4.2, which is then extended to chiral media in section 4.3. At the end of this chapter, quantities such as the scattering matrix and cross section, which are needed in the remainder of this work to describe scattering, are introduced.

4.1 Boundary conditions for arbitrary chiral scatterers

It is well known that electromagnetic fields at an interface with the surface normal vector $\hat{\boldsymbol{n}}$ have to meet the boundary conditions (see Fig. 4.1) [22, Ch. 1.5]

$$\begin{aligned} (\boldsymbol{D}_2 - \boldsymbol{D}_1) \cdot \hat{\boldsymbol{n}} &= 0 \ , \\ (\boldsymbol{B}_2 - \boldsymbol{B}_1) \cdot \hat{\boldsymbol{n}} &= 0 \ , \\ \hat{\boldsymbol{n}} \times (\boldsymbol{E}_2 - \boldsymbol{E}_1) &= \boldsymbol{0} \ , \\ \hat{\boldsymbol{n}} \times (\boldsymbol{H}_2 - \boldsymbol{H}_1) &= \boldsymbol{0} \ , \end{aligned} \qquad \forall \boldsymbol{r} \in A \ . \tag{4.1}$$

The bold $\boldsymbol{0}$ in the tangential field equations has a vectorial character. These conditions are valid for all divergence free media and arbitrarily shaped boundaries A. The subscripts stand for the fields inside (subscript 1) and outside (subscript 2) of the object. The field in the outer region is composed of the incident field $\boldsymbol{E}_\mathrm{i}, \boldsymbol{H}_\mathrm{i}$ and the scattered field $\boldsymbol{E}_\mathrm{S}, \boldsymbol{H}_\mathrm{S}$.

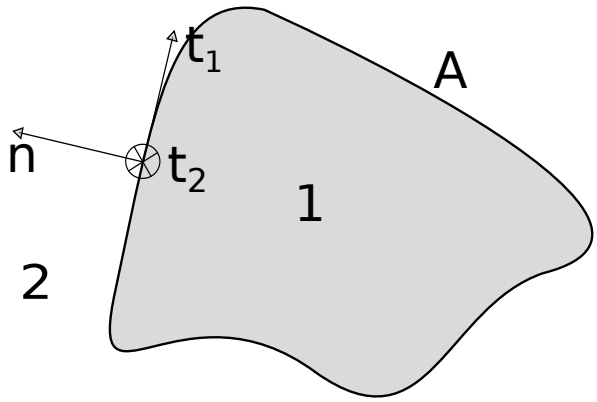

Figure 4.1: Arbitrarily shaped object with local coordinate system $(\hat{\boldsymbol{t}}_k, \hat{\boldsymbol{t}}_l, \hat{\boldsymbol{n}})$, where $\hat{\boldsymbol{n}}$ is always the surface normal at this point on the boundary A and the $\hat{\boldsymbol{t}}_i$ lie in the tangential plane.

The spatial and frequency dependency of the fields and material constants are omitted to simplify the representation. The local coordinate system is formed by the surface normal vector $\hat{\boldsymbol{n}}$ and the tangential vectors $\hat{\boldsymbol{t}}_k$, $\hat{\boldsymbol{t}}_l$. The constitutive relations (2.8) and boundary conditions are written in matrix form (where $t = t_k/t_l$ are the tangential and n are the normal components of the fields)

$$\begin{bmatrix} E_t \\ H_t \end{bmatrix}_2 - \begin{bmatrix} E_t \\ H_t \end{bmatrix}_1 = \begin{bmatrix} 0 \\ 0 \end{bmatrix} , \tag{4.2}$$

$$\begin{bmatrix} D_n \\ B_n \end{bmatrix}_2 - \begin{bmatrix} D_z \\ B_z \end{bmatrix}_1 = \begin{bmatrix} 0 \\ 0 \end{bmatrix} , \tag{4.3}$$

$$\begin{bmatrix} D_n \\ B_n \end{bmatrix} = \begin{bmatrix} \varepsilon & i\kappa/c_0 \\ -i\kappa/c_0 & \mu \end{bmatrix} \begin{bmatrix} E_n \\ H_n \end{bmatrix} . \tag{4.4}$$

Substituting (4.4) into (4.3), yields a relation between the normal components of the E- and H-field inside and outside of the object

$$\begin{aligned} \boldsymbol{A}_{n,1}\begin{bmatrix} E_n \\ H_n \end{bmatrix}_1 &= \boldsymbol{A}_{n,2}\begin{bmatrix} E_n \\ H_n \end{bmatrix}_2 , \\ \begin{bmatrix} E_n \\ H_n \end{bmatrix}_1 &= \boldsymbol{A}_{n,1}^{-1}\boldsymbol{A}_{n,2}\begin{bmatrix} E_n \\ H_n \end{bmatrix}_2 = \boldsymbol{A}_n\begin{bmatrix} E_n \\ H_n \end{bmatrix}_2 , \end{aligned} \tag{4.5}$$

where

$$\boldsymbol{A}_n = \frac{1}{\varepsilon_1\mu_1 - \kappa_1^2/c_0^2}\begin{bmatrix} \varepsilon_2\mu_1 - \kappa_1\kappa_2/c_0^2 & i(\mu_1\kappa_2/c_0 - \mu_2\kappa_1/c_0) \\ i(\varepsilon_2\kappa_1/c_0 - \varepsilon_1\kappa_2/c_0) & \varepsilon_1\mu_2 - \kappa_1\kappa_2/c_0^2 \end{bmatrix} . \tag{4.6}$$

$\boldsymbol{A}_{\mathrm{n},1/2}$ are singular matrices for $\varepsilon_{1/2}\mu_{1/2} = \kappa_{1/2}^2/c_0^2$. In this case, one of the wavenumbers $k_\pm = 0$. The resulting effects are mentioned in section 2.3. Although the Condon-Tellegen constitutive relations allow for the resonance case – as opposed to the Drude-Born-Fedorov equations – it is excluded from further analysis. Combining (4.5) and (4.2) yields

$$\begin{bmatrix} \boldsymbol{E} \\ \boldsymbol{H} \end{bmatrix}_1 = \boldsymbol{A}\begin{bmatrix} \boldsymbol{E} \\ \boldsymbol{H} \end{bmatrix}_2 , \tag{4.7}$$

with

$$\boldsymbol{A} = \begin{bmatrix} 1 & 0 & 0 & 0 & 0 & 0 \\ 0 & 1 & 0 & 0 & 0 & 0 \\ 0 & 0 & (\boldsymbol{A}_n)_{11} & 0 & 0 & (\boldsymbol{A}_n)_{12} \\ 0 & 0 & 0 & 1 & 0 & 0 \\ 0 & 0 & 0 & 0 & 1 & 0 \\ 0 & 0 & (\boldsymbol{A}_n)_{21} & 0 & 0 & (\boldsymbol{A}_n)_{22} \end{bmatrix} .$$

With regard to chapter 5, the constitutive relations are written in the basis of helicity eigenstates in the Riemann-Silberstein representation introduced in (2.35). Equivalently, the electric and magnetic flux densities are transformed into helicity preserving states

$$\boldsymbol{F}_\pm = \frac{1}{\sqrt{2}}(Z\boldsymbol{D} \pm i\boldsymbol{B}) . \tag{4.8}$$

$$\boldsymbol{U} = \frac{1}{\sqrt{2}} \begin{bmatrix} \boldsymbol{I}_3 & iZ\boldsymbol{I}_3 \\ \boldsymbol{I}_3 & -iZ\boldsymbol{I}_3 \end{bmatrix} , \tag{4.9}$$

cf. (2.23), transforms the fields into the basis of helicity eigenstates:

$$\begin{bmatrix} \boldsymbol{G}_+ \\ \boldsymbol{G}_- \end{bmatrix} = \boldsymbol{U} \begin{bmatrix} \boldsymbol{E} \\ \boldsymbol{H} \end{bmatrix} . \tag{4.10}$$

Applying the above transformations to the boundary conditions (4.7) results in

$$\begin{bmatrix} \boldsymbol{E} \\ \boldsymbol{H} \end{bmatrix}_1 = \boldsymbol{U}_1^{-1} \begin{bmatrix} \boldsymbol{G}_+ \\ \boldsymbol{G}_- \end{bmatrix}_1 = \boldsymbol{A} \begin{bmatrix} \boldsymbol{E} \\ \boldsymbol{H} \end{bmatrix}_2 = \boldsymbol{A}\boldsymbol{U}_1^{-1} \begin{bmatrix} \boldsymbol{G}_+ \\ \boldsymbol{G}_- \end{bmatrix}_2 . \tag{4.11}$$

Thus, the boundary conditions in the Riemann-Silberstein representation are written in the form of a transfer matrix, relating the field inside to the field outside the scatter:

$$\begin{aligned} \begin{bmatrix} \boldsymbol{G}_+ \\ \boldsymbol{G}_- \end{bmatrix}_1 &= \boldsymbol{U}_1 \boldsymbol{A} \boldsymbol{U}_2^{-1} \begin{bmatrix} \boldsymbol{G}_+ \\ \boldsymbol{G}_- \end{bmatrix}_2 \\ &= \begin{bmatrix} \boldsymbol{M}_{++} & \boldsymbol{M}_{+-} \\ \boldsymbol{M}_{-+} & \boldsymbol{M}_{--} \end{bmatrix} \begin{bmatrix} \boldsymbol{G}_+ \\ \boldsymbol{G}_- \end{bmatrix}_2 . \end{aligned} \tag{4.12}$$

The full expressions for the diagonal matrices $\boldsymbol{M}_{\alpha\beta}$ are given in appendix A.

4.2 Scattering by a sphere: Mie theory

The theory describing the scattering by a small isotropic homogeneous sphere is called Mie theory [6, Ch. 14.5]. This theory was extended by Bohren, among others, to the treatment of absorbing and chiral spheres. The basic approach for solving the scattering problem is summarized following Bohren and Huffmann's description in [5, Ch. 4] by means of an achiral sphere. Firstly, the fields are expanded in vector spherical harmonics (VSH) in section 4.2.1 and then used to solve the boundary problem yielding the Mie coefficients in section 4.2.2.

4.2.1 Field expansion

Expressions for the fields inside and outside of the sphere are derived by expanding the fields in VSH. The basis of Maxwell's equations for achiral media was derived in section 2.4.2. For rotational symmetry $\hat{\boldsymbol{c}} = \hat{\boldsymbol{r}}$ in (2.39) and

$$\begin{aligned} \boldsymbol{M} &= \boldsymbol{\nabla} \times \hat{\boldsymbol{r}}\Psi \ , \\ \boldsymbol{N} &= \frac{\boldsymbol{\nabla} \times \boldsymbol{M}}{k} \ . \end{aligned} \tag{4.13}$$

The explicit solution of the scalar wave equation in spherical coordinates [5, Eq. (4.2)]

$$\frac{1}{r^2}\frac{\partial}{\partial r}\left(r^2\frac{\partial \Psi}{\partial r}\right) + \frac{1}{r^2\sin(\Theta)}\frac{\partial}{\partial \Theta}\left(\sin(\Theta)\frac{\partial \Psi}{\partial \Theta}\right) + \frac{1}{r^2\sin(\Theta)}\frac{\partial^2 \Psi}{\partial \phi^2} + k^2\Psi = 0$$

is given by a product ansatz

$$\Psi = A(\Theta)B(\phi)C(r) \ , \tag{4.14}$$

for $r \in \mathbb{R}_{0+}$, $\Theta \in [0, \pi]$ and $\phi \in [0, 2\pi)$. Hence, the scalar solutions in position space representation are

$$\Psi_{l,m}(r, \Theta, \phi) = Y_{l,m}(\Theta, \phi) z_l(kr) \ . \tag{4.15}$$

The harmonic time dependency is not explicitly written in the following for the sake of clarity. z_l stands for one of the spherical Bessel function: spherical Bessel functions of the first kind j_n, of the second kind y_l (Neumann functions) or of the third kind $h_l^{1/2} = j_l \pm i y_l$ (Hankel functions). The spherical harmonics [22, Eq. (3.53)]

$$Y_{l,m}(\Theta, \phi) = \sqrt{\frac{2l+1}{4\pi}\frac{(l-m)!}{(l+m)!}} P_l^m(\cos\Theta) e^{im\phi} \tag{4.16}$$

have a harmonic dependence on ϕ and the Θ dependency is expressed by associated Legendre functions of the first kind

$$P_l^m(x) = \frac{(-1)^m}{2^l l!}(1-x^2)^{m/2}\frac{\mathrm{d}^{l+m}}{\mathrm{d}x^{l+m}}\left(x^2-1\right)^l \ . \tag{4.17}$$

Bohren's representation of the spherical harmonics in [5] deviates from (4.16): two real linearly independent solutions $\cos(m\phi)$ and $\sin(m\phi)$ instead of a complex one $e^{im\Phi}$ and in contrast to $m = -l, ..., l$ the m is defined as positive, real number. Bohren shows that due to orthogonality of the vector spherical harmonics the expansion consists only of one of the two functions for each polarization. Eventually, the resulting expansions of the fields are identical in both vector bases. The fields inside and outside of the scatterer are expanded in VSHs. The surrounding field is composed of the incident field and the scattered field

$$\boldsymbol{E}_2 = \boldsymbol{E}_\mathrm{i} + \boldsymbol{E}_\mathrm{S} \ , \tag{4.18}$$

$$\boldsymbol{H}_2 = \boldsymbol{H}_\mathrm{i} + \boldsymbol{H}_\mathrm{S} \ . \tag{4.19}$$

The incident field is finite at the origin, which is why expansion terms $\propto y_l$ are neglected (Neumann functions are infinite at the origin). Hence,

$$\boldsymbol{E}_\mathrm{i} = E_0 \sum_{l=1}^{\infty} \sum_{m=-l}^{l} A^\mathrm{i}_{lm} \boldsymbol{N}^{(1)}_{lm}(\boldsymbol{r}, k_2) + B^\mathrm{i}_{lm} \boldsymbol{M}^{(1)}_{lm}(\boldsymbol{r}, k_2) \tag{4.20}$$

and using Maxwell's equations and relations (2.39) between the basis vectors

$$\boldsymbol{H}_\mathrm{i} = \frac{k_2}{i\omega\mu_2} E_0 \sum_{l=1}^{\infty} \sum_{m=-l}^{l} A^\mathrm{i}_{lm} \boldsymbol{M}^{(1)}_{lm}(\boldsymbol{r}, k_2) + B^\mathrm{i}_{lm} \boldsymbol{N}^{(1)}_{lm}(\boldsymbol{r}, k_2) \ .$$

The superscripts at $\boldsymbol{M}$, $\boldsymbol{N}$ stand for the kind (first – (1), second – (2), third – (3)/(4)) of Bessel functions, which are used. The expansion coefficients of the incident field $A^\mathrm{i}_{lm}, B^\mathrm{i}_{lm}$ are known. For the scattered field both spherical Bessel functions are valid and their superposition in form of the Hankel functions appropriate. The Hankel functions are shown to represent outward and inward traveling waves in the asymptotic limit $kr \gg l^2$ [5, Eq. (4.42) and (4.43)]:

$$\begin{aligned} h^{(1)}_l &\propto \frac{(-i)^l e^{ikr}}{ikr} \ , \\ h^{(2)}_l &\propto \frac{-i^l e^{-ikr}}{ikr} \ . \end{aligned} \tag{4.21}$$

The scattered field is outward going and thus expanded in $h^{(1)}$. The corresponding VSH is labeled with superscript (3) and the scattered fields read

$$\begin{aligned} \boldsymbol{E}_{\mathrm{S}} &= E_0 \sum_{l=1}^{\infty} \sum_{m=-l}^{l} A_{lm}^{\mathrm{S}} \boldsymbol{N}_{lm}^{(3)}(\boldsymbol{r}, k_2) + B_{lm}^{\mathrm{S}} \boldsymbol{M}_{lm}^{(3)}(\boldsymbol{r}, k_2) \ , \\ \boldsymbol{H}_{\mathrm{S}} &= \frac{k_2}{i\omega\mu_2} E_0 \sum_{l=1}^{\infty} \sum_{m=-l}^{l} A_{lm}^{\mathrm{S}} \boldsymbol{M}_{lm}^{(3)}(\boldsymbol{r}, k_2) + B_{lm}^{\mathrm{S}} \boldsymbol{N}_{lm}^{(3)}(\boldsymbol{r}, k_2) \ . \end{aligned} \tag{4.22}$$

The fields inside of the sphere are treated equivalently and again Bessel functions of the first kind are chosen to avoid singularities at the origin,

$$\begin{aligned} \boldsymbol{E}_{1} &= E_0 \sum_{l=1}^{\infty} \sum_{m=-l}^{l} A_{lm}^{1} \boldsymbol{N}_{lm}^{(1)}(\boldsymbol{r}, k_1) + B_{lm}^{1} \boldsymbol{M}_{lm}^{(1)}(\boldsymbol{r}, k_1) \ , \\ \boldsymbol{H}_{1} &= \frac{k_1}{i\omega\mu_1} E_0 \sum_{l=1}^{\infty} \sum_{m=-l}^{l} A_{lm}^{1} \boldsymbol{M}_{lm}^{(1)}(\boldsymbol{r}, k_1) + B_{lm}^{1} \boldsymbol{N}_{lm}^{(1)}(\boldsymbol{r}, k_1) \ . \end{aligned} \tag{4.23}$$

The arguments are omitted from here on.

4.2.2 Mie coefficients

The unknown coefficients A_{lm}^{S}, B_{lm}^{S}, A_{lm}^{1}, B_{lm}^{1} are determined by the boundary conditions at $r = a$. The equations for the tangential field components (4.2) orthogonal to $\hat{\boldsymbol{r}}$, yield four equations for the four unknown quantities:

$$\begin{aligned} (\boldsymbol{E}_{\mathrm{i}} + \boldsymbol{E}_{\mathrm{S}} - \boldsymbol{E}_{1}) \cdot \hat{\boldsymbol{e}}_{\Theta} = 0 \ , \qquad & (\boldsymbol{E}_{\mathrm{i}} + \boldsymbol{E}_{\mathrm{S}} - \boldsymbol{E}_{1}) \cdot \hat{\boldsymbol{e}}_{\phi} = 0 \ , \\ (\boldsymbol{H}_{\mathrm{i}} + \boldsymbol{H}_{\mathrm{S}} - \boldsymbol{H}_{1}) \cdot \hat{\boldsymbol{e}}_{\Theta} = 0 \ , \qquad & (\boldsymbol{H}_{\mathrm{i}} + \boldsymbol{H}_{\mathrm{S}} - \boldsymbol{H}_{1}) \cdot \hat{\boldsymbol{e}}_{\phi} = 0 \ , \end{aligned} \tag{4.24}$$

at $r = a$. Solving the equations for the unknown parameters yields the expansion coefficients of the scattered field as functions of the expansion coefficients of the incident field

$$A_{lm}^{\mathrm{S}} = a_l A_{lm}^{\mathrm{i}} \ , \tag{4.25}$$

$$B_{lm}^{\mathrm{S}} = b_l B_{lm}^{\mathrm{i}} \ . \tag{4.26}$$

The Mie coefficients a_l, b_l are the ratios between the scattered and incident field coefficients for each polarization. Due to the rotational symmetry of the object they are independent of the angle, i.e. of m, and thus only depend on the radius and the defining number l.

4.3 Scattering by and in chiral media

In this section the Mie theory is extended to chiral multi-layered spheres in chiral media. Therefore, several changes of the model have to be made. First, chirality of the sphere is taken into account by using the Condon-Tellegen constitutive relations. This extension was already proposed by Bohren in [5, Ch. 8.3.] (a different notation is used in this reference) and by Wu *et al.* in [51]. The formalism to expand the fields is maintained. However, since the basis vectors are no eigenstates in chiral media the basis vectors for chiral Maxwell's equations are used. The helicity basis was introduced in section 2.4.2 and reads

$$\boldsymbol{Q}_{\mathrm{L/R}} = \frac{1}{\sqrt{2}}(\boldsymbol{M} \pm \boldsymbol{N}) \ . \tag{4.27}$$

These states of well defined helicity are not mixed while propagating in the medium, but at the interface there is the possibility of helicity change. This mixing is also seen in the non-diagonal form of the boundary conditions (4.12) in the Riemann-Silberstein representation.

In the case of a chiral sphere in an achiral host medium, the fields are expanded in a linear combination of VSH

$$\begin{aligned} \boldsymbol{E}_1 &= E_0 \sum_{l=1}^{\infty} \sum_{m=-l}^{l} L^1_{lm} \boldsymbol{Q}^{(1)}_{\mathrm{L},lm}(\boldsymbol{r}, k_{\mathrm{L}}) + R^1_{lm} \boldsymbol{Q}^{(1)}_{\mathrm{R},lm}(\boldsymbol{r}, k_{\mathrm{R}}) \ , \\ \boldsymbol{H}_1 &= \frac{k_1}{i\omega\mu_1} E_0 \sum_{l=1}^{\infty} \sum_{m=-l}^{l} L^1_{lm} \boldsymbol{Q}^{(1)}_{\mathrm{L},lm}(\boldsymbol{r}, k_{\mathrm{L}}) + R^1_{lm} \boldsymbol{Q}^{(1)}_{\mathrm{R},lm}(\boldsymbol{r}, k_{\mathrm{R}}) \end{aligned} \tag{4.28}$$

such that the boundary conditions for the E- and H-fields can be used again. Solving the boundary problem leads to the well-known Mie coefficients and additional cross-coupling coefficients. These off-diagonal elements c_l, d_l express the amount of incoming light of

one polarization which is scattered into light of the opposite one and vice versa. The expansion coefficients are hence related by

$$\begin{bmatrix} A_{lm}^{\mathrm{S}} \\ B_{lm}^{\mathrm{S}} \end{bmatrix} = \begin{bmatrix} a_l & c_l \\ d_l & b_l \end{bmatrix} \begin{bmatrix} A_{lm}^{\mathrm{i}} \\ B_{lm}^{\mathrm{i}} \end{bmatrix} . \tag{4.29}$$

It is important to note that the coefficients correspond to the $\boldsymbol{M}$, $\boldsymbol{N}$.

Scattering by a chiral sphere inside a chiral host medium was treated by Hinders and Rhodes in [21]. An equivalent expansion as in (4.28) is also used for the surrounding fields and substituted into the boundary conditions for the tangential fields. This yields relations between the scattering coefficients for light of well defined helicity as functions of the incident field. The subsequent relation is, therefore, written in the helicity basis

$$\begin{bmatrix} L_{lm}^{\mathrm{S}} \\ R_{lm}^{\mathrm{S}} \end{bmatrix} = \begin{bmatrix} l_l^{\mathrm{L}} & l_l^{\mathrm{R}} \\ r_l^{\mathrm{L}} & r_l^{\mathrm{R}} \end{bmatrix} \begin{bmatrix} L_{lm}^{\mathrm{i}} \\ R_{lm}^{\mathrm{i}} \end{bmatrix} , \tag{4.30}$$

in which the L/R are expansion coefficients of the helicity basis vectors $\boldsymbol{Q}_{\mathrm{L/R}}$. The Mie-coefficients result from a transformation with the unitary transformation matrix following from relation (2.42):

$$\begin{bmatrix} a_l & c_l \\ d_l & b_l \end{bmatrix} = \frac{1}{2} \begin{bmatrix} 1 & 1 \\ 1 & -1 \end{bmatrix} \begin{bmatrix} l_l^{\mathrm{L}} & l_l^{\mathrm{R}} \\ r_l^{\mathrm{L}} & r_l^{\mathrm{R}} \end{bmatrix} \begin{bmatrix} 1 & 1 \\ 1 & -1 \end{bmatrix} . \tag{4.31}$$

After presenting the basic approach to the treatment of scattering in chiral media, a multi-layered chiral sphere in a chiral host medium is examined in more detail. Scattering by a multi-layered chiral sphere is described by Shang, Wu *et al.* in [41]. A recursive algorithm is used to iteratively calculate the relations between the field coefficients between adjacant layers from inside to outside. This yields a recursive formulation for the expansion coefficients for the surrounding field that depends on the material and radius of each layer and on the incident field. In the paper by Wu *et al.* [41] only the application to multi-layered chiral spheres in an achiral host medium is shown. It is shown below that the approach is applicable to chiral host media as well. A sphere with t layers, where the first layer is the core of the sphere, is depicted in Fig. 4.2. The different material parameters $\varepsilon_j, \mu_j, \kappa_j$ have subscript $j = 1, ..., t$ corresponding to each layer. The host medium is indicated by subscript $t + 1$. a_j is the radius of the j-th layer. For a single

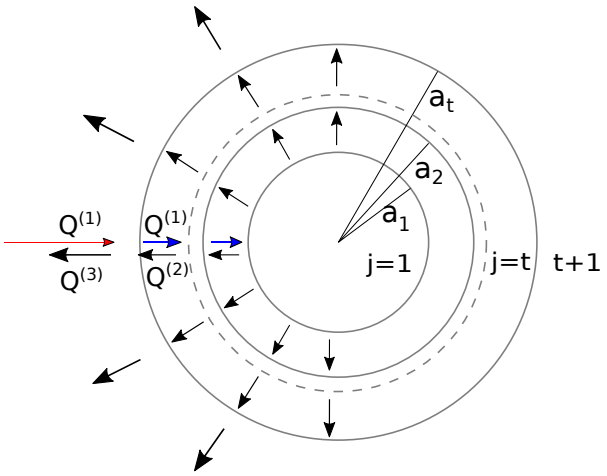

Figure 4.2: Multi-layered chiral sphere with t layers and radius a_j of the j-th layer. The incident field is depicted in red and is expanded in $\boldsymbol{Q}^{(1)}_{\mathrm{L/R}}$ with Bessel functions of the first kind. The scattered field is expanded with Hankel functions of the first kind $\boldsymbol{Q}^{(3)}_{\mathrm{L/R}}$. In each layer the incoming and outgoing waves are expanded with Bessel functions of the first and second kind.

layer there are four equations to solve for the four unknown parameters. Thus, for the t-layered sphere, $4t$ equations have to be solved for the $4t$ unknown scattering coefficients. To avoid this potentially large set of linear equations, the paper suggests a recursive approach. At the end, the scattered field shall be described depending on the incident field coefficients. Therefore, the field at layer t has to be known. Since there is another boundary between layer t and $t-1$ the field is also scattered at this boundary, and so on. Hence, fields in every layer are composed of incoming and scattered fields and expanded in vector spherical harmonics in the helicity basis, see [41, Eq. 1-4]

$$\begin{aligned}
\boldsymbol{E}_j = E_0 \sum_{l=1}^{\infty} \sum_{m=-l}^{l} & L^j_{lm} \boldsymbol{Q}^{(1)}_{\mathrm{L},lm}(\boldsymbol{r}, k^j_{\mathrm{L}}) + R^j_{lm} \boldsymbol{Q}^{(1)}_{\mathrm{R},lm}(\boldsymbol{r}, k^j_{\mathrm{R}}) \\
& + L'^j_{lm} \boldsymbol{Q}^{(2)}_{\mathrm{L},lm}(\boldsymbol{r}, k^j_{\mathrm{L}}) + R'^j_{lm} \boldsymbol{Q}^{(2)}_{\mathrm{R},lm}(\boldsymbol{r}, k^j_{\mathrm{R}}) \ , \\
\boldsymbol{H}_j = \frac{-i}{Z_j} E_0 \sum_{l=1}^{\infty} \sum_{m=-l}^{l} & L^j_{lm} \boldsymbol{Q}^{(1)}_{\mathrm{L},lm}(\boldsymbol{r}, k^j_{\mathrm{L}}) + R^j_{lm} \boldsymbol{Q}^{(1)}_{\mathrm{R},lm}(\boldsymbol{r}, k^j_{\mathrm{R}}) \\
& + L'^j_{lm} \boldsymbol{Q}^{(2)}_{\mathrm{L},lm}(\boldsymbol{r}, k^j_{\mathrm{L}}) + R'^j_{lm} \boldsymbol{Q}^{(2)}_{\mathrm{R},lm}(\boldsymbol{r}, k^j_{\mathrm{R}}) \ ,
\end{aligned} \tag{4.32}$$

with the superscripts (1) and (2) corresponding to the kind of Bessel function used in the VSHs. $k_{\mathrm{L/R}}$ are identical to the wavenumbers of the helicity eigenstates in (2.19). Both kinds of Bessel functions are allowed except for the first layer, where the fields have to be finite in the origin and thus

$$L'^{1}_{lm} = R'^{1}_{lm} = 0 \ . \tag{4.33}$$

The field expansion in the host medium is done as is for simple spheres

$$\begin{aligned}
\boldsymbol{E}_{t+1} = E_0 \sum_{l=1}^{\infty} \sum_{m=-l}^{l} & L^{t+1}_{lm} \boldsymbol{Q}^{(1)}_{\mathrm{L},lm}(\boldsymbol{r}, k^{t+1}_{\mathrm{L}}) + R^{t+1}_{lm} \boldsymbol{Q}^{(1)}_{\mathrm{R},lm}(\boldsymbol{r}, k^{t+1}_{\mathrm{R}}) \\
& + L'^{t+1}_{lm} \boldsymbol{Q}^{(3)}_{\mathrm{L},lm}(\boldsymbol{r}, k^{t+1}_{\mathrm{L}}) + R'^{j}_{lm} \boldsymbol{Q}^{(3)}_{\mathrm{R},lm}(\boldsymbol{r}, k^{t+1}_{\mathrm{R}}) \ , \\
\boldsymbol{H}_{t+1} = E_0 Q_{t+1} \sum_{l=1}^{\infty} \sum_{m=-l}^{l} & L^{t+1}_{lm} \boldsymbol{Q}^{(1)}_{\mathrm{L},lm}(\boldsymbol{r}, k^{t+1}_{\mathrm{L}}) + R^{t+1}_{lm} \boldsymbol{Q}^{(1)}_{\mathrm{R},lm}(\boldsymbol{r}, k^{t+1}_{\mathrm{R}}) \\
& + L'^{t+1}_{lm} \boldsymbol{Q}^{(3)}_{\mathrm{L},lm}(\boldsymbol{r}, k^{t+1}_{\mathrm{L}}) + R'^{t+1}_{lm} \boldsymbol{Q}^{(3)}_{\mathrm{R},lm}(\boldsymbol{r}, k^{t+1}_{\mathrm{R}}) \ .
\end{aligned} \tag{4.34}$$

Instead of Bessel functions of first and second kind, Bessel functions of first and third kind are used representing the incident and scattered field. The fields from layer j and $j+1$ have to satisfy the boundary conditions, which is equal to the boundary problem of a sphere in a host medium

$$\begin{aligned}
(\boldsymbol{E}_{j+1} - \boldsymbol{E}_j) \times \hat{\boldsymbol{r}} = 0 \ , \\
(\boldsymbol{H}_{j+1} - \boldsymbol{H}_j) \times \hat{\boldsymbol{r}} = 0 \ ,
\end{aligned} \qquad r = a_j \ , \ j = 1, ..., t \ . \tag{4.35}$$

The expressions for the fields (4.32) are substituted into (4.35). An explicit form is given in [41, Eq. (6-9)]. Since the media are chiral, the same Bessel functions have different arguments for the light of different helicity, $k^j_{\mathrm{L}} a_j$ or $k^j_{\mathrm{R}} a_j$, as is apparent in (4.32). For simpler expressions of equations, four new variables $r^{\mathrm{R},j}_{lm}, \tilde{r}^{\mathrm{L},j}_{lm}, \tilde{l}^{\mathrm{R},j}_{lm}, l^{\mathrm{L},j}_{lm}$ are introduced. These variables relate the expansion coefficients of VSHs of different kind in the following way:

$$\begin{aligned}
L'^{j}_{lm} &= l^{\mathrm{L},j}_{l} L^{j}_{lm} + \tilde{l}^{\mathrm{R},j}_{l} m^j R^{j}_{lm} \ , \\
R'^{j}_{lm} &= \tilde{r}^{\mathrm{L},j}_{l} / m^j L^{j}_{lm} + r^{\mathrm{R},j}_{l} R^{j}_{lm} \ ,
\end{aligned} \tag{4.36}$$

with $m^j = \frac{n_l^j}{n_r^j}$ ($n_{l/r}^j = \sqrt{\varepsilon_{\mathrm{r},j}\mu_{\mathrm{r},j}} \pm \kappa_j$). Comparison with (4.30) shows that the primed coefficients for $j = t+1$ are equivalent to the scattering coefficients for the surrounding field and the unprimed ones correspond to the incident field. From this it is already clear that calculating the r^{t+1}, l^{t+1} results in the scattering coefficients in the case of a chiral host medium in the helicity basis, except for a prefactor in the cross coupling terms

$$l_l^{\mathrm{R},j} = \tilde{l}_l^{\mathrm{R},j} m^j \ , \tag{4.37}$$

$$r_l^{\mathrm{R},j} = \tilde{r}_l^{\mathrm{R},j} \frac{1}{m^j} \ . \tag{4.38}$$

The introduction of the new variables, therefore, corresponds to a basis change into the helicity basis. Using transformation (4.31) yields the Mie coefficients

$$\begin{bmatrix} A_{lm}^{\mathrm{S}} \\ B_{lm}^{\mathrm{S}} \end{bmatrix} = \frac{1}{2} \begin{bmatrix} l_l^{t+1,\mathrm{L}} + r_l^{t+1,\mathrm{R}} + m^{t+1} l_l^{t+1,\mathrm{R}} + 1/m^{t+1} r_l^{t+1,\mathrm{L}} \\ l_l^{t+1,\mathrm{L}} - r_l^{t+1,\mathrm{R}} + m^{t+1} l_l^{t+1,\mathrm{R}} - 1/m^{t+1} r_l^{t+1,\mathrm{L}} \end{bmatrix}$$
$$\begin{bmatrix} l_l^{t+1,\mathrm{L}} - r_l^{t+1,\mathrm{R}} - m^{t+1} l_l^{t+1,\mathrm{R}} + 1/m^{t+1} r_l^{t+1,\mathrm{L}} \\ l_l^{t+1,\mathrm{L}} + r_l^{t+1,\mathrm{R}} - m^{t+1} l_l^{t+1,\mathrm{R}} - 1/m^{t+1} r_l^{t+1,\mathrm{L}} \end{bmatrix} \begin{bmatrix} A_l^{\mathrm{i}} \\ B_l^{\mathrm{i}} \end{bmatrix} . \tag{4.39}$$

For an achiral host medium, the fraction $m^{t+1} = 1$ and the expressions for the Mie coefficients equal the ones derived for an isotropic achiral medium in [41, Eq. (33+34)].

Equations (4.36) are substituted into the boundary conditions and after many simple but extensive transformations, relations between the coefficients r^{R}, l^{L}, r^{L}, l^{R} in adjacent layers j, $j+1$ read

$$\begin{aligned} r_l^{j+1,\mathrm{R}} &= f_1(r_l^{j,\mathrm{R}}, l_l^{j,\mathrm{L}}, r_l^{j,\mathrm{L}}, l_l^{j,\mathrm{R}}) \ , \\ l_l^{j+1,\mathrm{L}} &= f_2(r_l^{j,\mathrm{R}}, l_l^{j,\mathrm{L}}, r_l^{j,\mathrm{L}}, l_l^{j,\mathrm{R}}) \ , \\ r_l^{j+1,\mathrm{L}} &= f_3(r_l^{j,\mathrm{R}}, l_l^{j,\mathrm{L}}, r_l^{j,\mathrm{L}}, l_l^{j,\mathrm{R}}) \ , \\ l_l^{j+1,\mathrm{R}} &= f_4(r_l^{j,\mathrm{R}}, l_l^{j,\mathrm{L}}, r_l^{j,\mathrm{L}}, l_l^{j,\mathrm{R}}) \ . \end{aligned} \tag{4.40}$$

Since the explicit expressions are lengthy and provide little additional value, we refer to [41, Eq. 16-19, B1-B4], where the explicit functional dependencies are represented. The initial values in (4.33) imply

$$r_l^{1,\mathrm{R}} = r_l^{1,\mathrm{L}} = l_l^{1,\mathrm{R}} = l_l^{1,\mathrm{L}} = 0 \tag{4.41}$$

for the core. Taking that as starting point, the coefficients for every following layer can be calculated recursively.

4.4 T-matrix and total scattering cross section

One method to describe the scattering by an arbitrary particle is to calculate the transfer matrix or T-matrix, first introduced by Waterman [50]. The T-matrix relates the scattered field coefficients of a multipole expansion to the ones of the incident field:

$$\begin{bmatrix} A^{\mathrm{S}} \\ B^{\mathrm{S}} \end{bmatrix} = \boldsymbol{T} \begin{bmatrix} A^{\mathrm{i}} \\ B^{\mathrm{i}} \end{bmatrix} . \tag{4.42}$$

From (4.29) the entries of the T-matrix for a spherical particle are identified as the Mie coefficients. $\boldsymbol{T}$ possess the form of a block matrix

$$\boldsymbol{T} = \begin{bmatrix} \boldsymbol{T}_{ee} & \boldsymbol{T}_{em} \\ \boldsymbol{T}_{me} & \boldsymbol{T}_{mm} \end{bmatrix} \tag{4.43}$$

in which the columns represent the scattering of either electric (subscript e) or magnetic (subscript m) multipoles into light of either electric or magnetic character. $\boldsymbol{T}_{\alpha\beta}$ are diagonal matrices. The first three diagonal elements correspond to $l = 1$ with the three possible m values. Due to the rotational symmetry of the problem, the diagonal elements are equal. The next $2 \cdot 2 + 1$ diagonal elements are due to scattering of quadrupoles $l = 2$ and so on, which yields

$$\boldsymbol{T}_{ee} = \begin{bmatrix} a_1 \boldsymbol{I}_3 & & \\ & a_2 \boldsymbol{I}_5 & \\ & & \cdots \end{bmatrix} \tag{4.44}$$

and equivalently $\boldsymbol{T}_{em/me}$ with c_l/d_l and $\boldsymbol{T}_{mm}$ with b_l. The scattering matrix $\boldsymbol{S}$ (or scattering operator) provides another complete description of the scatterer, which relates the incoming to the outgoing waves, or rather their expansion coefficients

$$\begin{bmatrix} A^{\mathrm{out}} \\ B^{\mathrm{out}} \end{bmatrix} = \boldsymbol{S} \begin{bmatrix} A^{\mathrm{in}} \\ B^{\mathrm{in}} \end{bmatrix} . \tag{4.45}$$

The S- and T-matrices are related by [15, Eq. (32)], [50]

$$\boldsymbol{S} = \boldsymbol{I} + 2\boldsymbol{T} \ . \tag{4.46}$$

A derivation for chiral media is given below. Inward and outward going waves are described by the Hankel functions in the asymptotic limit, shown in (4.21). The scattered field, as described in (4.22), only comprises outgoing spherical waves. However, the incident field is a superposition of incoming and outgoing waves with respect to the origin of the scatterer. This fact is inherent in the defintion of the spherical Bessel functions [15]

$$j_l(x) = \frac{1}{2}\left(h_l^{(1)}(x) + h_l^{(2)}(x)\right) \ . \tag{4.47}$$

Thereby, the incident field is decomposed into incoming ($\propto (\boldsymbol{M}/\boldsymbol{N})^{(4)}(\boldsymbol{r}, k)$) and outgoing fields ($\propto (\boldsymbol{M}/\boldsymbol{N})^{(3)}(\boldsymbol{r}, k)$), yielding

$$\begin{aligned}
\boldsymbol{E}_{\text{in}} &= E_0 \sum_{l=1}^{\infty} \sum_{m=-l}^{l} \frac{A_{lm}^i}{2} \boldsymbol{N}_{lm}^{(4)}(\boldsymbol{r}, k) + \frac{B_{lm}^i}{2} \boldsymbol{M}_{lm}^{(4)}(\boldsymbol{r}, k) \ , \\
\boldsymbol{E}_{\text{out}} &= E_0 \sum_{l=1}^{\infty} \sum_{m=-l}^{l} \left(\frac{A_{lm}^i}{2} + A_{lm}^S\right) \boldsymbol{N}_{lm}^{(3)}(\boldsymbol{r}, k) + \left(\frac{B_{lm}^i}{2} + B_{lm}^S\right) \boldsymbol{M}_{lm}^{(3)}(\boldsymbol{r}, k)
\end{aligned}$$

and the H-fields accordingly. The expansion coefficients of the outgoing field are

$$\begin{aligned}
\begin{bmatrix} A_{lm}^{\text{out}} \\ B_{lm}^{\text{out}} \end{bmatrix} &= \begin{bmatrix} 1 & 0 \\ 0 & 1 \end{bmatrix} \begin{bmatrix} A_{lm}^{\text{S}} \\ B_{lm}^{\text{S}} \end{bmatrix} + \begin{bmatrix} \frac{1}{2} & 0 \\ 0 & \frac{1}{2} \end{bmatrix} \begin{bmatrix} A_{lm}^{\text{i}} \\ B_{lm}^{\text{i}} \end{bmatrix} \\
&= \begin{bmatrix} a_l & c_l \\ d_l & b_l \end{bmatrix} \begin{bmatrix} A_{lm}^{\text{i}} \\ B_{lm}^{\text{i}} \end{bmatrix} + \begin{bmatrix} A_{lm}^{\text{in}} \\ B_{lm}^{\text{in}} \end{bmatrix} \\
&= 2 \begin{bmatrix} a_l & c_l \\ d_l & b_l \end{bmatrix} \begin{bmatrix} A_{lm}^{\text{in}} \\ B_{lm}^{\text{in}} \end{bmatrix} + \begin{bmatrix} A_{lm}^{\text{in}} \\ B_{lm}^{\text{in}} \end{bmatrix}
\end{aligned} \tag{4.48}$$

and thus,

$$\boldsymbol{S} = \boldsymbol{I} + 2\boldsymbol{T} \ .$$

So far, the reciprocity of the object is not explicitly considered in the Mie coefficients. However, with the assumption of reciprocal media in the constitutive relations, calculating the Mie coefficients results in [51, Eq. (18)][5, Ch. 8.3]

$$d_l = c_l \ , \tag{4.49}$$

or in the helicity basis

$$l_l^{\mathrm{R}} = r_l^{\mathrm{L}} \ . \tag{4.50}$$

Now that the scatterer is fully described by its T-matrix (or S-matrix), expressions for the total scattering cross section as a function of the T-matrix are derived. The total scattering cross section is a measure for the total power which is scattered by the object in every direction and for every polarization normalized to the intensity of the incident field

$$C_{\mathrm{sca}} = \frac{W_{\mathrm{S}}}{I_{\mathrm{i}}} \ . \tag{4.51}$$

The scattered power is given by the integral over a surface A of a sphere surrounding the scatterer of the time-averaged Poynting-vector for the scattered field $\boldsymbol{S}_{\mathrm{S}} = \frac{1}{2}\,\mathrm{Re}(\boldsymbol{E}_{\mathrm{S}} \times \boldsymbol{H}_{\mathrm{S}}^{*})$ [5, p. 3.19]

$$W_{\mathrm{S}} = \int_A \mathrm{d}A\, \boldsymbol{S}_{\mathrm{S}} \cdot \hat{\boldsymbol{r}} \tag{4.52}$$

and $I_{\mathrm{i}} = \boldsymbol{S}_{\mathrm{i}} \cdot \hat{\boldsymbol{r}}$ is the incident irradiance. The cross section has the unit of area. An exact derivation using the expansion of the fields in VSH in (4.20), (4.22) is given in [5, Ch. 4.4.1]. These calculations result in an expression for the total scattering cross section of an achiral sphere as a function of its Mie coefficients

$$C_{\mathrm{sca}} = \frac{2\pi}{k^2} \sum_{l=1} (2l+1) \left(|a_l|^2 + |b_l|^2 \right) \ . \tag{4.53}$$

The $2l+1$ is due to the summation over m from $m=-l$ to $m=l$. For chiral media there are additional cross-coupling coefficients in the scattering cross section [5, Ch. 8.3.1]

$$C_{\mathrm{sca}} = \frac{2\pi}{k^2}\sum_{l=1}(2l+1)\left(|a_l|^2+|b_l|^2+2|c_l|^2\right) \ . \tag{4.54}$$

This expression of the scattering cross section is composed of the total scattering cross section for incident light of $+1$ and -1 helicity

$$C_{\mathrm{sca}} = C_{\mathrm{sca,L}} + C_{\mathrm{sca,R}} \ , \tag{4.55}$$

with [5, Eq. (8.17)]

$$\begin{aligned} C_{\mathrm{sca,L}} = \frac{2\pi}{k^2}\sum_{l=1}(2l+1)\left(|a_{lm}|^2+|b_{lm}|^2+2|c_{lm}|^2\right. \\ \left.-2\,\mathrm{Im}\{(a_{lm}+b_{lm})c_{lm}^*\}\right) \ , \\ C_{\mathrm{sca,R}} = \frac{2\pi}{k^2}\sum_{l=1}(2l+1)\left(|a_{lm}|^2+|b_{lm}|^2+2|c_{lm}|^2\right. \\ \left.+2\,\mathrm{Im}\{(a_{lm}+b_{lm})c_{lm}^*\}\right) \ . \end{aligned} \tag{4.56}$$

When discussing duality and electromagnetic chirality in the course of the next chapter, another quantity characterizing the scatterer is introduced, namely the total interaction cross section defined as [39, Eq. (5)]

$$C_{\mathrm{int}} = \mathrm{Tr}\left(\boldsymbol{T}^\dagger\boldsymbol{T}\right) \ , \tag{4.57}$$

which is independent of the illumination. For an isotropic spherical particle described by its T-matrix, (4.44) the total interaction cross section is equal to the normalized total scattering cross section [39]

$$C_{\mathrm{int}} = \frac{2\pi}{\lambda^2}C_{\mathrm{sca}} \ . \tag{4.58}$$

5 Duality and electromagnetic chirality

In the previous chapter, scattering of electromagnetic waves by a chiral object was described. In this chapter, dual objects, which preserve helicity, and scatterers that are transparent to light of well defined helicity are examined. Therefore, the scattering operator, which defines the object, is used to establish quantitative measures of duality breaking and electromagnetic chirality. This classification and ordering of chiral objects allows for setting guidelines used in the optimization with regard to helicity preservation and transparency. Duality is introduced in section 5.1 and it is shown that objects possessing this symmetry preserve helicity. After proposing a quantitative measure of duality in 5.1.1, helicity preserving media (section 5.1.2) and geometries (section 5.1.3) are examined. In section 5.2 electromagnetic chirality is introduced as an optical property of chiral scatterers. Electromagnetic chirality describes the difference in scattering of light with $+1$ and -1 helicity by the object. Again, a quantitative measure is presented in section 5.2.1 and material properties are found, for which the medium and thus, any scattering object consisting of this medium, is transparent to light of one helicity (section 5.2.2 and 5.2.3).

5.1 Duality and its quantitative measure

In the helicity basis, the solutions of the wave equations in special media, like vacuum, are decoupled and waves with different helicity do not mix upon propagation. Media which do preserve helicity are called dual and show a specific symmetry. Symmetry is a property of a system that is invariant under a linear unitary transformation [48]. From group theory is known that continuous symmetry transformations are determined by a generator $\boldsymbol{G}$ [48, Theorem 6.3]

$$\boldsymbol{T}(b) = e^{-ib\boldsymbol{G}} \ . \tag{5.1}$$

Some physically relevant symmetries and their generators are listed in table 5.1. Every

Symmetry Tranformation $e^{-i\boldsymbol{b}\boldsymbol{G}}$	Generator	Representation
Time translation	energy $\boldsymbol{H}$	$i\frac{\partial}{\partial t}$
Spacial translation	momentum $\boldsymbol{P}$	$i\boldsymbol{\nabla}$
Rotation	angular momentum $\boldsymbol{J}$	$i\boldsymbol{\nabla}\times\boldsymbol{r}-i\varepsilon_{klm}$
Duality	helicity $\boldsymbol{\Lambda}$	$\frac{\boldsymbol{\nabla}\times}{k}$

Table 5.1: Symmetry transformations and their generators, which are the preserved quantities of the invariant system [12, Tab. 2.3]. The operators are given in time and position space representation. ε_{klm} is the Levi-Civita-Symbol, see (2.29). The expression for helicity only holds for monochromatic fields, as discussed in section 2.4.1.

invariance of the system under a transformation results in a conservation law (known as Noether's theorem in classical mechanics) [19, Ch. 17]. A symmetry transformation commutes with the Hamilton operator for invariant systems $\left[\boldsymbol{H}, e^{-i\boldsymbol{b}\boldsymbol{G}}\right]=0$ which results in $\left[\frac{\partial}{\partial t}, e^{-i\boldsymbol{b}\boldsymbol{G}}\right]=0$, using Schrödinger's equation. For the commutator to be zero, $\boldsymbol{G}$ has to commute with the time derivative: $\left[\frac{\partial}{\partial t}, \boldsymbol{G}\right]=0$. Hence, $\boldsymbol{G}$ has to be time independent and is thus a preserved quantity. With that in mind, an object being invariant under the duality transformation

$$\boldsymbol{D}(\Theta)=e^{-i\Theta\boldsymbol{\Lambda}} \tag{5.2}$$

is helicity preserving. Θ is an angle with values between 0 and 2π. The helicity operator is now expressed in the basis of E- and H-field. Using equations (2.25) and (2.34) yields

$$\begin{aligned}\boldsymbol{\Lambda}\boldsymbol{E}&=iZ\boldsymbol{H}\ ,\\ \boldsymbol{\Lambda}\boldsymbol{H}&=-\frac{i}{Z}\boldsymbol{E}\end{aligned} \tag{5.3}$$

and hence,

$$\boldsymbol{\Lambda}=\begin{bmatrix}0 & iZ\boldsymbol{I}_3\\ -\frac{i}{Z}\boldsymbol{I}_3 & 0\end{bmatrix}\ . \tag{5.4}$$

With $\boldsymbol{\Lambda}^2=\boldsymbol{I}_6$ the exponential functional is rewritten:

$$e^{-i\Theta\boldsymbol{\Lambda}}=\boldsymbol{I}_6\cos(\Theta)-i\boldsymbol{\Lambda}\sin(\Theta) \tag{5.5}$$

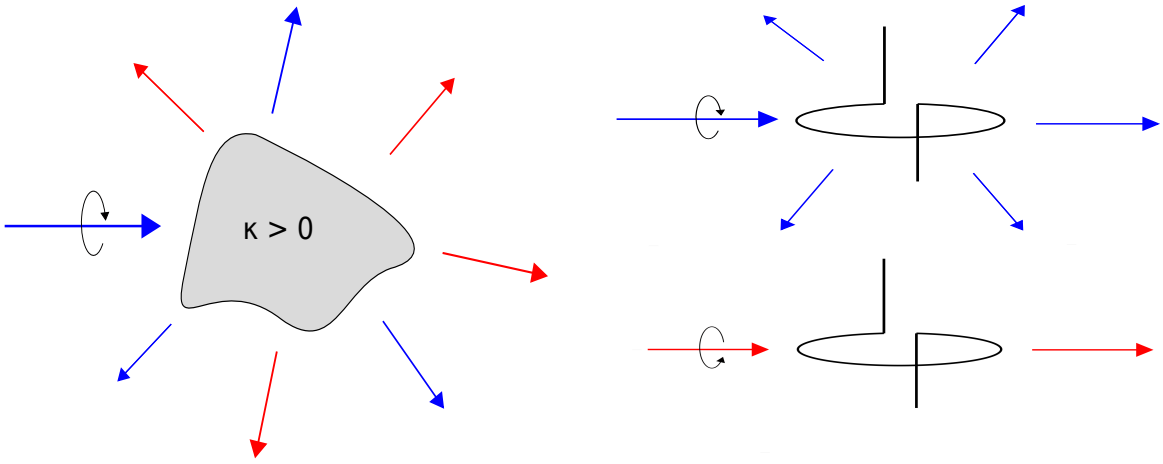

(a) Non-dual chiral scatterer (b) Dual and maximally em-chiral scatterer

Figure 5.1: Scattering of light with well defined helicity (blue corresponds to $+1$ and red to -1 helicity). (a) shows an arbitrary chiral scatterer with $\kappa > 0$, which does not preserve helicity. The scatterer in (b) is dual since light of $+1$ helicity is preserved and additionally maximally em-chiral because light of $\Lambda = -1$ is not scattered.

Thereby, the symmetry transformation takes matrix form

$$\boldsymbol{D}(\Theta) = \begin{bmatrix} \boldsymbol{I}_3 \cos(\Theta) & Z\boldsymbol{I}_3 \sin(\Theta) \\ -\frac{1}{Z}\boldsymbol{I}_3 \sin(\Theta) & \boldsymbol{I}_3 \cos(\Theta) \end{bmatrix} . \tag{5.6}$$

If the system is invariant under duality transformation, the object is called dual and preserves helicity in all scattering directions, as is depicted in Fig. 5.1b. The scattered field is composed solely of modes with the same helicity. The scatterer in Fig. 5.1a flips the helicity of the incident wave for some modes. Thereby, the scatterer does not preserve helicity and is thus not dual.

5.1.1 Quantitative measure of duality breaking

The helicity of light is not changed upon interactions with a dual object. For the scattering matrix $\boldsymbol{S} = \boldsymbol{I} + 2\boldsymbol{T}$, this means that the helicity flipping elements of have to be zero. When $\boldsymbol{T}$ is written in the helicity basis, the helicity-flipping elements

$$T^{\bar{\lambda}\lambda}_{\bar{\boldsymbol{\eta}}\boldsymbol{\eta}} = \left\langle \bar{\boldsymbol{\eta}}\bar{\lambda}\right| \boldsymbol{T} \left|\boldsymbol{\eta}\lambda\right\rangle \tag{5.7}$$

are in the off-diagonal with $\lambda \neq \bar{\lambda}$. The duality breaking $\not{D}$ – or equivalently the helicity change – is measured by the intensity of light, which helicity is flipped in the course of scattering. This corresponds to the sum of the modulus square of the scattering coefficients over all different input $\bar{\boldsymbol{\eta}}$ and output $\boldsymbol{\eta}$ modes for which the sign of the helicity is flipped. The duality breaking is normalized to the total interaction cross section C_{int} [13, Eq. (2)]:

$$\not{D} = \frac{\sum_{\bar{\boldsymbol{\eta}}\boldsymbol{\eta}} \sum_{\lambda_{\pm 1}} |T^{-\lambda\lambda}_{\bar{\boldsymbol{\eta}}\boldsymbol{\eta}}|^2}{\sum_{\bar{\boldsymbol{\eta}}\boldsymbol{\eta}} \sum_{\lambda_{\pm 1}} |T^{-\lambda\lambda}_{\bar{\boldsymbol{\eta}}\boldsymbol{\eta}}|^2 + |T^{\lambda\lambda}_{\bar{\boldsymbol{\eta}}\boldsymbol{\eta}}|^2} \ . \tag{5.8}$$

The duality breaking measure takes values between zero and one. Dual objects introduce no helicity change and thus $\not{D} = 0$. When $\not{D} = 1$ the helicity of light is completely converted into light of opposite helicity in the course of scattering by the object. Using $\boldsymbol{T}$ in the helicity basis together with (4.30), the duality breaking is expressed as a function of the expansion coefficients:

$$\not{D} = \frac{\sum_l (2l+1) 2 |l^{\mathrm{R}}_l|^2}{C_{\mathrm{int}}} \overset{(4.31)}{=} \frac{\sum_l (2l+1) 2 |a_l - b_l|^2}{C_{\mathrm{int}}} \ . \tag{5.9}$$

For dual objects $a_l = b_l$ which indicates that the electric and magnetic response of the scatterer are equal.

5.1.2 Dual objects by means of material properties

It can be shown for specific media that Maxwell's equations are invariant under duality transformation. These media preserve helicity. To derive dual media, Maxwell's equations in the E-, H-basis, c.f. (2.15) are transformed by $\boldsymbol{D}(\Theta)$:

$$\boldsymbol{D}(\Theta) \left\{ \boldsymbol{\nabla} \times \begin{bmatrix} \boldsymbol{E} \\ \boldsymbol{H} \end{bmatrix} \right\} = \boldsymbol{D}(\Theta) \boldsymbol{K} \boldsymbol{D}(\Theta)^{\dagger} \boldsymbol{D}(\Theta) \begin{bmatrix} \boldsymbol{E} \\ \boldsymbol{H} \end{bmatrix} \ . \tag{5.10}$$

Hence, the system is dual if

$$\begin{aligned} &\boldsymbol{D}(\Theta)\boldsymbol{K}\boldsymbol{D}(\Theta)^{\dagger} = \boldsymbol{K} \\ \Leftrightarrow &\begin{bmatrix} -i\sin(\Theta)\cos\Theta\varepsilon(Z^2 - \frac{\mu}{\varepsilon})/Z & i\varepsilon\sin^2(\Theta)(Z^2 - \frac{\mu}{\varepsilon}) \\ i\varepsilon\sin^2(\Theta)(Z^2 - \frac{\mu}{\varepsilon})/Z^2 & i\sin(\Theta)\cos\Theta\varepsilon(Z^2 - \frac{\mu}{\varepsilon})/Z \end{bmatrix} = \boldsymbol{O}\ . \end{aligned} \tag{5.11}$$

Since $Z = \sqrt{\frac{\mu}{\varepsilon}}$, the operators commute $[\boldsymbol{D}(\Theta), \boldsymbol{K}] = 0$ and the electromagnetic field equations are invariant under duality transformation. When dealing with scattering problems, the fields at the boundary where the material parameters are not continuous [16] have to be examined. Therefore, the boundary conditions (4.7) are transformed by

$$\boldsymbol{D}(\Theta)\begin{bmatrix}\boldsymbol{E}\\ \boldsymbol{H}\end{bmatrix}_1 = \boldsymbol{D}(\Theta)\boldsymbol{A}\begin{bmatrix}\boldsymbol{E}\\ \boldsymbol{H}\end{bmatrix}_2 . \tag{5.12}$$

It is sufficient to look at $\boldsymbol{A}_n$ from (4.6) relating the normal components of the fields transformed by the duality transformation

$$\boldsymbol{D}_{\mathrm{n}}(\Theta) = \begin{bmatrix} \cos(\Theta) & -Z\sin(\Theta) \\ -\frac{1}{Z}\sin(\Theta) & \cos(\Theta) \end{bmatrix}, \tag{5.13}$$

since the tangential fields are continuous at the interface. For dual media

$$\boldsymbol{D}_{\mathrm{n}}(\Theta)\boldsymbol{A}_{\mathrm{n}}\boldsymbol{D}_{\mathrm{n}}(\Theta)^{\dagger} = \boldsymbol{A}_{\mathrm{n}} \tag{5.14}$$

must hold. The field is normalized with respect to the outside medium, $Z = Z_2$. The matrix multiplications in (5.14) are executed and the resulting conditions are written element-wise:

$$\underline{\varepsilon_2\mu_1 - \frac{\kappa_1\kappa_2}{c_0^2}} = i\frac{\sin(\Theta)\cos(\Theta)}{c_0}\left(\kappa_1\left(Z_1\varepsilon_2 - \frac{\mu_2}{Z_1}\right) + \kappa_2\left(\frac{\mu_1}{Z_1} - Z_1\varepsilon_1\right)\right) \underline{\varepsilon_1\mu_2 - \frac{\kappa_1\kappa_2}{c_0^2}} + \cos^2(\Theta)\left(\varepsilon_2\mu_1 - \mu_2\varepsilon_1\right) \ , \tag{5.15a}$$

$$\underline{\frac{i}{c_0}\left(\kappa_2\mu_1 - \kappa_1\mu_2\right)} = \underline{-\frac{i}{c_0}Z_1^2\left(\kappa_1\varepsilon_2 - \kappa_2\varepsilon_1\right)} - Z_1\sin(\Theta)\cos(\Theta)\left(\varepsilon_2\mu_1 - \mu_2\varepsilon_1\right) + i\frac{\cos^2(\Theta)}{c_0}\left(\kappa_1(Z_1^2\varepsilon_2 - \mu_2) + \kappa_2(\mu_1 - Z_1^2\varepsilon_1)\right) \ , \tag{5.15b}$$

$$\underline{\frac{i}{c_0}(\kappa_1\varepsilon_2 - \kappa_2\varepsilon_1)} = \underline{-\frac{i}{c_0 Z_1^2}(\kappa_2\mu_1 - \kappa_1\mu_2)} - Z_1\sin(\Theta)\cos(\Theta)(\varepsilon_2\mu_1 - \mu_2\varepsilon_1) + i\frac{\cos^2(\Theta)}{c_0}\left(\kappa_1(Z_1^2\varepsilon_2 - \mu_2) + \kappa_2(\mu_1 - Z_1^2\varepsilon_1)\right) \ , \tag{5.15c}$$

$$\underline{\varepsilon_1\mu_2 - \frac{\kappa_1\kappa_2}{c_0}^2} = -i\frac{\sin(\Theta)\cos(\Theta)}{c_0}\left(\kappa_1\left(Z_1\varepsilon_2 - \frac{\mu_2}{Z_1}\right) + \kappa_2\left(\frac{\mu_1}{Z_1} - Z_1\varepsilon_1\right)\right) \underline{\varepsilon_2\mu_1 - \frac{\kappa_1\kappa_2}{c_0^2}} - \cos^2(\Theta)(\varepsilon_2\mu_1 - \mu_2\varepsilon_1) \ . \tag{5.15d}$$

When solved for arbitrary Θ, all angle dependent terms have to vanish such that only the underlined terms remain. As all angle dependent terms are $\propto (Z_1 - Z_2)$, the object is dual if and only if

$$Z_1 = \sqrt{\frac{\mu_1}{\varepsilon_1}} = \sqrt{\frac{\mu_2}{\varepsilon_2}} = Z_2 \ . \tag{5.16}$$

These findings show that duality symmetry is simply achieved by choosing $Z_1 = Z_2$ independent of the geometry of the scatterer. It becomes apparent that the conditions are independent of the chirality parameters of the media owing to its reciprocity (the electric fields couple to magnetic fields as the magnetic ones do to electric fields). In the optical regime, most dielectrics have a very weak magnetic response compared to the electric one and thus are approximately non-magnetic $\mu_i \approx 1$ forcing $\varepsilon_1 = \varepsilon_2$. Hence, in the case of achiral media a matching of impedances is only possible in the trivial case where the media are identical.

5.1.3 Dual objects by means of geometry

In general, the geometry independent condition $\varepsilon = \mu$ is very hard to achieve with chiral media at optical frequencies. Another degree of freedom is the geometry of the object or in the context of this work the radius of the sphere. A sphere consisting out of a non-dual medium is dual if the duality condition $a_l = b_l$ is simultaneously met for all multipoles, which is not possible by optimizing the radius for ordinary media. However, for small dielectric spheres approximate duality is gained by adjusting the radius such that dipole duality condition $a_1 = b_1$ is met [52]. In [39], the possibility of also approximately meeting the duality condition for the quadrupole and octupole moments $a_2 \approx b_2$, $a_3 \approx b_3$ was presented. Adding a shell to the particle results in additional degrees of freedom, which are chosen to increase the duality breaking of the object compared to a core by minimum one order of magnitude [39, Tab. 1]. These results imply that adding more layers to the sphere will also improve the approximation.

5.2 Electromagnetic chirality and its measure

Chirality is a geometrical property of molecules or building blocks which results in optical effects like circular dichroism and optical activity. There are already several quantitative measures of chirality reviewed in [36]. These approaches are often not applicable to all chiral objects but only to specific classes and do not allow for sorting of the objects in an unambiguous way. Depending on the field of application, it is advantageous to offer a quantitative measure of the optical response of different chiral structures, which makes it possible to order them. This is especially important when it comes to the design of such objects and the evaluation of their performance.

One way to characterize chiral objects is to define them in accordance to how differently these treat light of different helicity. This property is then called electromagnetic chirality (em-chirality)[14]. If all the informations using light of on helicity are obtained by measurements with light of the opposite one, the object is achiral. A definition of em-chirality is provided in section 5.2.1 and it is shown that, if the treatment of different helicities is maximally unequal, these objects are transparent for light of one helicity and called maximally em-chiral. The subsequent section 5.2.2 deals with maximally em-chiral media and general constraints on the material. In section 5.2.3, effective material parameters for which the medium itself becomes maximally em-chiral are derived by means of the general constraints in section 5.2.2.

5.2.1 Measure of electromagnetic chirality

The definition and derivation of em-chirality are taken from [14], where the quantity was first introduced. Electromagnetic chirality is a measure for difference in the treatment of light of differing helicity by the scatterer. This disparity is contained in the non-unit part of the scattering operator $\boldsymbol{S} = \boldsymbol{I} + 2\boldsymbol{T}$ expressed in the helicity basis

$$\boldsymbol{T} = \begin{bmatrix} \boldsymbol{T}_{++} & \boldsymbol{T}_{+-} \\ \boldsymbol{T}_{-+} & \boldsymbol{T}_{--} \end{bmatrix} . \tag{5.17}$$

$\boldsymbol{T}$ is the transfer matrix in the helicity basis. The matrices $\boldsymbol{T}_{\bar{\lambda}\lambda} = \langle\bar{\lambda}| \boldsymbol{S} |\lambda\rangle$ are composed of the scattering coefficients $\langle\bar{\boldsymbol{\eta}}| \boldsymbol{T}_{\bar{\lambda}\lambda} |\boldsymbol{\eta}\rangle$ for incident light of helicity λ and scattered light of helicity $\bar{\lambda}$ for all the modes $\boldsymbol{\eta}, \bar{\boldsymbol{\eta}}$.
An em-achiral object is defined as one for which "[...] all the information which can be obtained from experiments using only one input helicity can also be obtained from experiments using the opposite helicity" [14]. This statement implies constraints on the matrix elements

$$\begin{aligned} \langle\bar{\boldsymbol{\eta}}| \boldsymbol{T}_{++} |\boldsymbol{\eta}\rangle &= \langle\bar{\boldsymbol{\eta}}'| \boldsymbol{T}_{--} |\boldsymbol{\eta}'\rangle \ , \\ \langle\bar{\boldsymbol{\eta}}| \boldsymbol{T}_{-+} |\boldsymbol{\eta}\rangle &= \langle\bar{\boldsymbol{\eta}}''| \boldsymbol{T}_{+-} |\boldsymbol{\eta}''\rangle \ . \end{aligned} \tag{5.18}$$

It is important to note that the measuring basis can change for light of different helicity and the different input/output states are connected by unitary transformations, which do not effect the helicity of the modes $[\boldsymbol{U}_i, \boldsymbol{\Lambda}] = [\boldsymbol{V}_i, \boldsymbol{\Lambda}] = 0$,

$$\begin{aligned} |\boldsymbol{\eta}\rangle &= \boldsymbol{V}_1 |\boldsymbol{\eta}'\rangle \ , & |\boldsymbol{\eta}\rangle &= \boldsymbol{V}_2 |\boldsymbol{\eta}'\rangle \ , \\ |\bar{\boldsymbol{\eta}}\rangle &= \boldsymbol{U}_1 |\bar{\boldsymbol{\eta}}'\rangle \ , & |\bar{\boldsymbol{\eta}}\rangle &= \boldsymbol{U}_2 |\bar{\boldsymbol{\eta}}'\rangle \ . \end{aligned} \tag{5.19}$$

Thus, transforming the right hand side of (5.18) with the above transformations yields

$$\begin{aligned} \boldsymbol{T}_{++} &= \boldsymbol{U_1} \boldsymbol{T}_{--} \boldsymbol{V_1}^\dagger \ , \\ \boldsymbol{T}_{-+} &= \boldsymbol{U_2} \boldsymbol{T}_{-+} \boldsymbol{V_2}^\dagger \ . \end{aligned} \tag{5.20}$$

Some examples to illustrate and validate the definition of em-chirality are given below. For a homogeneous, isotropic, dielectric sphere the results are identical when measuring with light of opposite helicity and the unitary matrices in this case are identity matrices. The

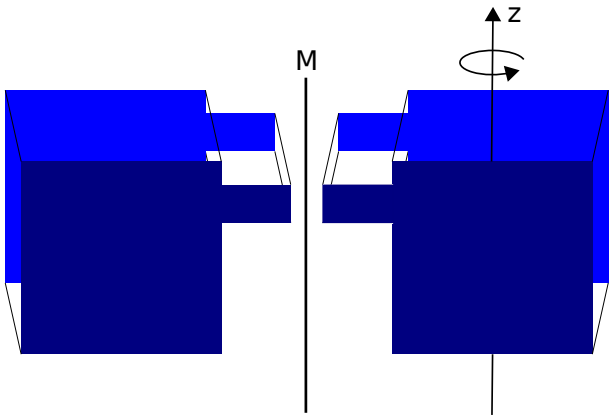

Figure 5.2: 3D achiral object. M is representing the mirror plane. The mirrored object on the right hand side is brought into congruence with the original by rotation around the z-axis (and a translation). The 2D geometry in the plane of projection is a 2D chiral object.

object in Fig. 5.2 has one symmetry plane parallel to the x-z plane (lying in the plane of projection). Objects with at least one mirror plane are 3D achiral in a geometrical sense, because the mirror image can be brought to congruence with the object by rotation and translation. The object will scatter light of plus helicity differently than light of negative helicity. However, if the mirrored object is measured with light of opposite helicity the same measurement results as for the object in the original orientation are obtained. It is possible to obtain from the measurements with one helicity the results of the measurements with the opposite helicity. Thus the unitary transformations in the defintion of em-chirality are rotations and it is shown (more generally in Ref. [14]) that achiral objects are a subset of em-achiral objects. The definition of em-chirality is indeed more general by allowing any unitary transformations commuting with the helicity operator between different input and output states. These include for example boosts, which makes the measure relativistically invariant.

We now proceed with the derivation of a quantitative measure using the definition of em-achiral objects. If an operator $\boldsymbol{B}$ can be transformed into operator $\boldsymbol{A}$ by unitary transformations – as is the case in (5.20) – the singular values of the operators have to be equal [30, p. 193]:

$$\boldsymbol{A} = \boldsymbol{U_i} \boldsymbol{B} \boldsymbol{V_i}^{\dagger} \quad \Rightarrow \quad \sigma(\boldsymbol{A}) = \sigma(\boldsymbol{B}) \; . \tag{5.21}$$

The singular value decomposition of a matrix is given by

$$\boldsymbol{A} = \boldsymbol{U}\boldsymbol{\Sigma}\boldsymbol{V}^{\dagger} \ , \tag{5.22}$$

with the unitary matrices $\boldsymbol{U}, \boldsymbol{V}$ and $\boldsymbol{\Sigma} = \mathrm{diag}(\sigma_1, ..., \sigma_n)$, $\sigma_1 > \sigma_2 > ... > \sigma_n$. The singular values are positive and real valued. For a hermitian square matrix the SVD corresponds to an eigenvalue decomposition. From (5.21) together with (5.20) results

$$\begin{aligned} \sigma(\boldsymbol{T}_{++}) &= \sigma(\boldsymbol{T}_{--}) \ , \\ \sigma(\boldsymbol{T}_{-+}) &= \sigma(\boldsymbol{T}_{+-}) \ . \end{aligned} \tag{5.23}$$

The interaction of light with positive (negative) helicity is summarized in $\boldsymbol{v}_+$ ($\boldsymbol{v}_-$).These vectors contain the singular values for all states of light after scattering in descending order:

$$\boldsymbol{v}_+ = \begin{bmatrix} \sigma(\boldsymbol{T}_{++}) \\ \sigma(\boldsymbol{T}_{-+}) \end{bmatrix} \ , \ \boldsymbol{v}_- = \begin{bmatrix} \sigma(\boldsymbol{T}_{--}) \\ \sigma(\boldsymbol{T}_{+-}) \end{bmatrix} \ . \tag{5.24}$$

From (5.23) follows that for em-achiral objects $\boldsymbol{v}_+ = \boldsymbol{v}_-$ holds. Objects possessing $\boldsymbol{v}_+ \neq \boldsymbol{v}_-$ are thus em-chiral. A measure of em-chirality χ is given by the distance between $\boldsymbol{v}_+$ and $\boldsymbol{v}_-$:

$$\chi = d(\boldsymbol{v}_+, \boldsymbol{v}_-) \ . \tag{5.25}$$

The Euclidean norm is chosen as a distance measure due to physical reasoning: the measurement of intensity corresponds to the Euclidean norm (/absolute value) squared of the fields. Also

$$\begin{aligned} C_{\mathrm{int}} &= \sum_{\bar{\boldsymbol{\eta}}\boldsymbol{\eta}} \sum_{\bar{\lambda}\lambda} |\left\langle \bar{\boldsymbol{\eta}}\bar{\lambda}\right| \boldsymbol{T} \left|\boldsymbol{p}\lambda\right\rangle|^2 = \sum_{\bar{\boldsymbol{\eta}}\boldsymbol{\eta}} \sum_{\bar{\lambda}\lambda} \left\langle \bar{\boldsymbol{\eta}}\bar{\lambda}\right| \boldsymbol{T}^{\dagger}\boldsymbol{T} \left|\boldsymbol{p}\lambda\right\rangle \\ &= \sum_{\bar{\lambda}\lambda} \mathrm{Tr}\Big(\boldsymbol{T}^{\dagger}_{\bar{\lambda}\lambda}\boldsymbol{T}_{\bar{\lambda}\lambda}\Big) = \boldsymbol{v}_+^T\boldsymbol{v}_+ + \boldsymbol{v}_-^T\boldsymbol{v}_- \ , \end{aligned} \tag{5.26}$$

which motivates the choice of the Euclidean norm.
Thereby, a quantitative measure of em-chirality is given by

$$\chi = \sqrt{(\boldsymbol{v}_+ - \boldsymbol{v}_-)^T(\boldsymbol{v}_+ - \boldsymbol{v}_-)} \ . \tag{5.27}$$

χ is found to take an upper bound given by the square root of the total interaction cross section, because recalling that the singular values are real and non-negative

$$\frac{\chi^2}{C_{\text{int}}} \overset{(5.26)}{=} \frac{(\boldsymbol{v}_+ - \boldsymbol{v}_-)^T(\boldsymbol{v}_+ - \boldsymbol{v}_-)}{\boldsymbol{v}_+^T\boldsymbol{v}_+ + \boldsymbol{v}_-^T\boldsymbol{v}_-} = 1 - \frac{2\boldsymbol{v}_+^T\boldsymbol{v}_-}{C_{\text{int}}} \leq 1 \ . \tag{5.28}$$

To make use of the measure in scattering problems featuring spherical particles, χ is expressed as a function of the Mie coefficients. Since the diagonal matrix $\boldsymbol{T}_{\alpha\beta}$ is composed of the Mie coefficients, the entries of $v_\pm$ are $\sqrt{l_l^{\text{L}}(l_l^{\text{L}})^*}$ and $\sqrt{l_l^{\text{R}}(l_l^{\text{R}})^*}$ – each in descending order – or $\sqrt{r_l^{\text{R}}(r_l^{\text{R}})^*}$ and $\sqrt{l_l^{\text{R}}(l_l^{\text{R}})^*}$.
Subsequently, the normalized em-chirality $\frac{\chi}{\sqrt{C_{\text{int}}}} \in [0,1]$ is used. Objects reaching the upper bound are called maximally em-chiral. These objects have to fulfill $v_+^T v_- = 0$ according to (5.28), which corresponds to

$$\sigma(\boldsymbol{T}_{++})^T\sigma(\boldsymbol{T}_{--}) + \sigma(\boldsymbol{T}_{+-})^T\sigma(\boldsymbol{T}_{+-}) = 0 \ . \tag{5.29}$$

Given that all singular values are positive, real and sorted scalars, one of the following four conditions has to hold:

$$\boldsymbol{T}_{++} = \boldsymbol{T}_{-+} = \boldsymbol{O} \ , \ \boldsymbol{T}_{--} = \boldsymbol{T}_{+-} = \boldsymbol{O} \ , \tag{5.30}$$

$$\boldsymbol{T}_{++} = \boldsymbol{T}_{+-} = \boldsymbol{O} \ , \ \boldsymbol{T}_{--} = \boldsymbol{T}_{-+} = \boldsymbol{O} \ . \tag{5.31}$$

The first equations (5.30) represent a medium which is transparent to one of the two helicities. There is no scattering of the field for one helicity and the corresponding matrix elements are zero. For reciprocal objects hold $\boldsymbol{T}_{+-} = \boldsymbol{T}_{-+}$. The second set of solutions is violating reciprocity for $\boldsymbol{T}_{+-} \neq \boldsymbol{O}$. Hence, all maximally em-chiral reciprocal objects are transparent to one helicity and all transparent objects to one helicity are maximally em-chiral. Reciprocity implies $\boldsymbol{T}_{+-} = \boldsymbol{T}_{-+} = \boldsymbol{O}$ and thus $\not{\varnothing} = 0$ with definition (5.8). Maximally em-chiral, reciprocal objects preserve helicity, i.e. they are dual. Note that dual objects are not necessarily em-chiral. These relationships are summarized in diagram 5.3.

5.2.2 Maximally em-chiral objects by means of material properties

It is shown in section 5.1.2 that a scatterer with impedance Z_1 is dual with respect to the outside medium Z_2 if $Z_1 = Z_2$. Below, material constraints on maximally em-chiral and

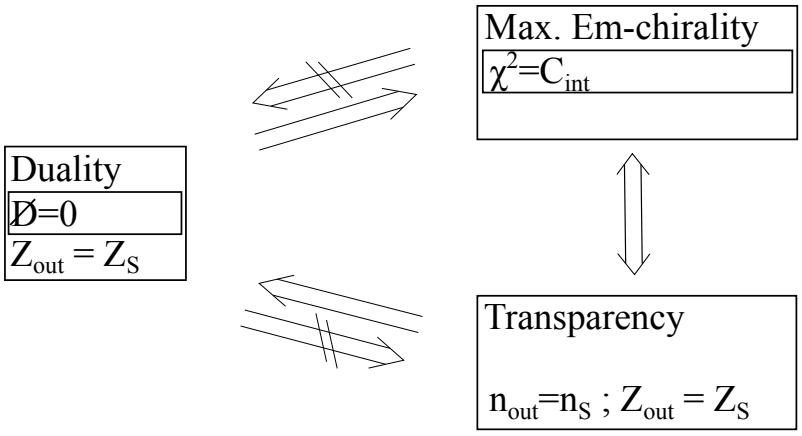

Figure 5.3: Interrelation between em-chirality, transparency for one helicity and duality symmetry for reciprocal objects. The associated material constraints, which are derived in section 5.2.2, are also presented for each property.

reciprocal objects or equivalently for transparency to one helicity are proposed. Therefore, it makes sense to look again at the boundary conditions written in the helicity basis, see (4.12):

$$\begin{bmatrix} \boldsymbol{G}_+ \\ \boldsymbol{G}_- \end{bmatrix}_1 = \begin{bmatrix} \boldsymbol{M}_{++} & \boldsymbol{M}_{+-} \\ \boldsymbol{M}_{-+} & \boldsymbol{M}_{--} \end{bmatrix} \begin{bmatrix} \boldsymbol{G}_+ \\ \boldsymbol{G}_- \end{bmatrix}_2 .$$

The boundary of a medium which is transparent to one helicity is effectively not existent for light of this exact helicity (in terms of transfer matrices represented as unitary matrix), i.e. the field of well defined helicity coming from medium 2 is equal to the field of well defined helicity traveling in medium 1. Hence, transparency of a medium to light of one helicity requires

$$\boldsymbol{G}_{\pm,1} = \boldsymbol{G}_{\pm,2} \tag{5.32}$$

and thus via (4.12)

$$\boldsymbol{M}_{++} = \boldsymbol{I}_3 \text{ and } \boldsymbol{M}_{-+} = \boldsymbol{O} \tag{5.33}$$

$$\text{or } \boldsymbol{M}_{--} = \boldsymbol{I}_3 \text{ and } \boldsymbol{M}_{+-} = \boldsymbol{O} \ . \tag{5.34}$$

The matrix elements of the first constraint (5.33) for transparency to light of $+1$ helicity read (see appendix A)

$$\begin{aligned} \boldsymbol{M}_{++} &= \begin{bmatrix} \frac{Z_1+Z_2}{2Z_2} & 0 & 0 \\ 0 & \frac{Z_1+Z_2}{2Z_2} & 0 \\ 0 & 0 & \frac{n_{+,2}}{n_{+,1}}\frac{Z_1+Z_2}{2Z_2} \end{bmatrix} = \boldsymbol{I}_3 \ , \\ \boldsymbol{M}_{-+} &= \begin{bmatrix} \frac{Z_2-Z1}{2Z_2} & 0 & 0 \\ 0 & \frac{Z_2-Z_1}{2Z_2} & 0 \\ 0 & 0 & \frac{n_{+,2}}{n_{-,1}}\frac{Z_2-Z_1}{2Z_2} \end{bmatrix} = \boldsymbol{O} \ . \end{aligned} \tag{5.35}$$

$$n_{\pm,i}/c_0 = \sqrt{\varepsilon_i \mu_i} \pm \kappa_i/c_0 \qquad , \quad i = 1,2 \tag{5.36}$$

are the refractive indeces for light of either $\Lambda = +1$ or $\Lambda = -1$ of chiral media. From (5.35) transparency conditions are obtained for positive helicity:

$$\begin{aligned} Z_1 &= Z_2 \ , \\ n_{+,1} &= n_{+,2} \ . \end{aligned} \tag{5.37}$$

The same procedure for light of negative helicity yields

$$\begin{aligned} Z_1 &= Z_2 \ , \\ n_{-,1} &= n_{-,2} \ . \end{aligned} \tag{5.38}$$

It is important to note that the above constraints are valid for reciprocal scatterers with arbitrary shape and material both for the near and far field. These relations show, as well, that transparency involves duality at the level of material parameters. As pointed out in section 5.1.2, impedance matching is not (easily) accomplished for optical frequencies since most media are approximately non-magnetic there. Therefore, perfectly transparent media are normally not achievable in this regime.

5.2.3 Effective material parameters for maximally em-chiral media

This section addresses the reasonable choice of chiral material parameters to be considered in the simulations and proposes material parameters for which em-chirality of the medium

takes its maximum value. The discussion is necessary, since an electric and a chiral response requires also the consideration of a magnetic response of the medium. This aspect is often overlooked but needs to be taken into account if reliable predictions shall be made. Firstly, the dependency of the effective magnetic permeability on the permittivity and chirality of the medium and the resulting refractive index and impedance are discussed. Subsequently, the transparency conditions, which have been derived in section 5.2.2, are used to determine effective material parameters of maximally em-chiral media. One has to note the difference between highly em-chiral media and the maximally em-chiral scatterers which we search for primarily. If the medium itself is transparent there is no need to form a scatterer out of it. However, in the course of the parameter studies the following examinations are crucial to understand the simulation results and especially regions of very high em-chirality, which are independent of geometry. These are caused by the sphere's medium being highly em-chiral itself.

Effective material parameters

For simulation purposes, the choice of the investigated parameter space is crucial. Material parameters for achiral media are easily at hand in every frequency range, whereas this is not true for chiral media. Moreover, the different descriptions of chiral media complicate the identification of suitable chirality parameters. In general, these parameters are determined experimentally by means of transmission and reflection measurements from a stack of a chiral medium or a solution of chiral molecules. For naturally available chiral media, the chirality parameter in the visible frequency regime is usually very small, e. g. $\kappa \lesssim 10^{-6}$ for sugar solutions [34]. In recent years, metamaterials have been suggested that sustain much stronger chiral effects [10, 35, 49]. However, for most of these metamaterials an explicit documentation of effective material parameters has rarely been done and, if documented, has often been restricted to specific frequency ranges.

In the following we consider chiral inclusions characterized by their respective polarizabilities inside a host medium. By means of the analytical antenna model in section 3.2, a relationship exists between the electromagnetic cross-coupling terms and the electric and magnetic polarizability of the inclusions. This is fully respected. Afterwards, the inclusions are randomly placed within an achiral, lossless host medium characterized by ε_a and μ_a. In combination, they render after homogenization an effective medium with chiral isotropic properties ε_1, μ_1, κ_1. An illustration of the model and the labeling is given in Fig. 5.4. These relations between the polarizabilities of the inclusions constraint the

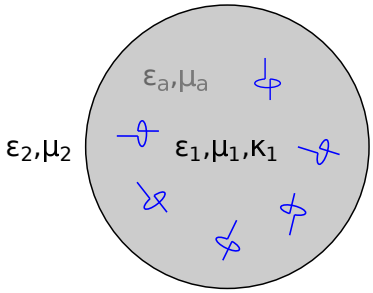

Figure 5.4: Chiral sphere (1) surrounded by an achiral medium (2). The effective material parameters of the chiral sphere ε_1, μ_1 and κ_1 are derived by homogenization of the medium consisting of helical inclusions (*antennas*) in an achiral, lossless host medium ε_a, μ_a. The surrounding medium is assumed to be achiral and material parameters have subscript 2.

effective material parameters of the chiral medium (cf. (3.35)). Moreover, the effective material parameters are interdependent and have to obey the following equations:

$$\begin{aligned}
\varepsilon_1 &= \mathrm{Re}(\varepsilon_1) + i\,\mathrm{Im}(\varepsilon_1)\ , \\
\mu_1 &= \mu_a + \frac{\mathrm{Re}(\kappa_1)^2 \varepsilon_0 \mu_0}{(\mathrm{Re}(\varepsilon_1) - \varepsilon_\mathrm{a})^2} \left(\mathrm{Re}(\varepsilon_1) + i\,\mathrm{Im}(\varepsilon_1) - \varepsilon_\mathrm{a}\right)\ , \\
\kappa_1 &= \mathrm{Re}(\kappa_1) + i\,\mathrm{Re}(\kappa_1) \frac{\mathrm{Im}(\varepsilon_1)}{\mathrm{Re}(\varepsilon_1) - \varepsilon_\mathrm{a}}\ .
\end{aligned} \tag{5.39}$$

Thus, it is possible to restrict the parameter space of μ_1, when the permittivity ε_1 and the chirality parameter κ_1 are chosen for a given host medium with properties $\varepsilon_\mathrm{a}, \mu_\mathrm{a}$. The following examination is restricted to real valued parameters ($\varepsilon_1 = \mathrm{Re}(\varepsilon_1)$, $\mu_1 = \mathrm{Re}(\mu_1)$, $\kappa_1 = \mathrm{Re}(\kappa_1)$), i.e. lossless media, for the sake of simplicity and with respect to the restriction to non-absorbing media in the simulations.

The magnetic response as a function of the effective permittivity and chirality of the medium is illustrated in Fig. 5.5a. There are three physically different parameter regions to distinguish. The singularity at $\varepsilon_1 = \varepsilon_a$ corresponds to an achiral medium with $\kappa_1 = 0$ and is not considered herein. The quadratic dependency of μ_1 on κ_1 (in general on $\mathrm{Re}(\kappa_1)$) is observed in Fig. 5.5a. $\frac{1}{\varepsilon_1 - \varepsilon_a}$ describes the curvature of the function, i. e. for $\varepsilon_1 > \varepsilon_a$ the positive magnetic response decreases with increasing electric permittivity. Thus, the assumption of an approximately non-magnetic chiral medium is valid for a very small

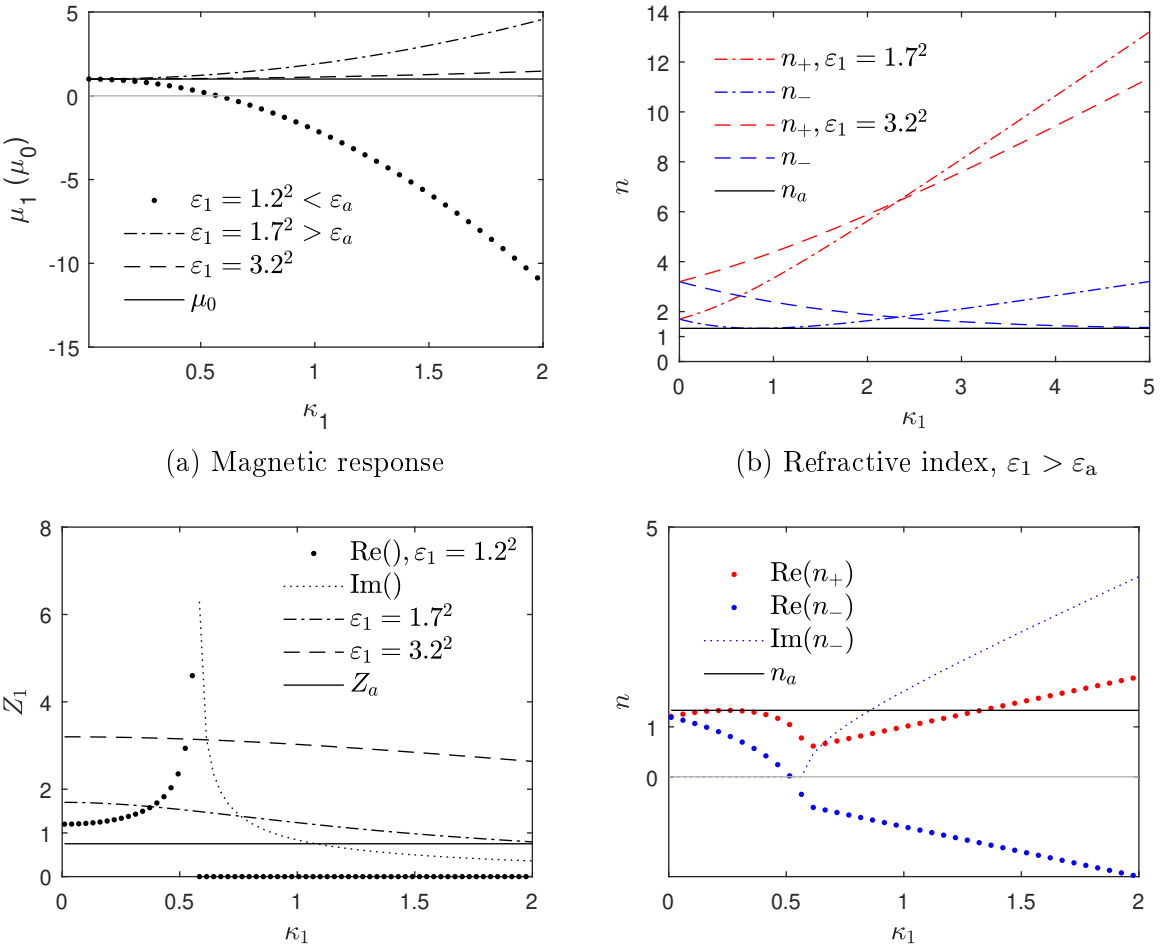

(a) Magnetic response

(b) Refractive index, $\varepsilon_1 > \varepsilon_a$

(c) Impedance

(d) Refractive index, $\varepsilon_1 < \varepsilon_a$

Figure 5.5: Magnetic response, refractive index, impedance depending on the effective electric response ε_1 and the chirality parameter κ_1 for a host medium $\varepsilon_a = 1.33^2$, $\mu_a = 1$. (a) Relative permeability μ_1/μ_0 for different permittivities $\varepsilon_1 < \varepsilon_a$ and $\varepsilon_1 > \varepsilon_a$ as a function of κ_1. (b) and (d) Corresponding refractive indices $n_\pm$ for light of $\Lambda = \pm 1$ as a function of κ_1. n_+ is always real valued. (c) Resulting impedances $Z_1 = \sqrt{\mu_1/\varepsilon_1}$ of the chiral medium. The impedances for $\varepsilon_1 > \varepsilon_a$ are always real valued.

intrinsic chirality and/or very strong electric response of the medium. The resulting refractive indices for light of either helicity are shown in Fig. 5.5b.

In some analyses of lossless chiral media [26, 32], a critical chirality parameter

$$\kappa_{\mathrm{c1}}\sqrt{\varepsilon_0\mu_0} = \sqrt{\varepsilon_1\mu_1} \tag{5.40}$$

is introduced, above which the refractive index of light of negative helicity becomes smaller than zero ($k_- < 0$). Thus, the properties of light propagating in such media change fundamentally above this critical value. However, in [26, 32], where (5.40) is stated, a dependency between the single material parameters is not considered and often the permeability of the medium is set to a constant value bigger than or equal to one. By means of the antenna model utilized in this work, we observe that the refractive index n_- is always bigger than one for $\varepsilon_1 > \varepsilon_{\mathrm{a}}$. Since $\frac{\varepsilon_1}{\varepsilon_1-\varepsilon_a} > 1$, it holds $\forall\varepsilon_1 > \varepsilon_a$

$$\sqrt{\varepsilon_{\mathrm{r},1}\mu_{\mathrm{r},1}} > \sqrt{\frac{\varepsilon_1}{\varepsilon_1-\varepsilon_a}\kappa_1^2} > \kappa_1 \ , \tag{5.41}$$

where $\kappa_1 > 0$ and the parameters with subscript r denote the dimensionless relative permittivity and permeability. Additionally, $n_- = 1$ is achieved when

$$\kappa_1 = (\varepsilon_{\mathrm{r},1} + \sqrt{-\varepsilon_{\mathrm{r},1}^2\varepsilon_{\mathrm{r,a}} + \varepsilon_{\mathrm{r},1}\varepsilon_{\mathrm{r,a}}^2 + \varepsilon_{\mathrm{r},1}^2 - \varepsilon_{\mathrm{r},1}\varepsilon_{\mathrm{r,a}}})/\varepsilon_{\mathrm{r,a}} - 1 \ ,$$

which is only real valued for $\varepsilon_1 < \varepsilon_{\mathrm{a}}$. It follows that

$$n_- > 1, \quad \forall\varepsilon_1 > \varepsilon_a \ . \tag{5.42}$$

The equivalent holds for $\kappa_1 < 0$ and n_+. If the permittivity changes from $\varepsilon_1 > \varepsilon_a$ to $\varepsilon_1 < \varepsilon_a$, the medium changes from a paramagnetic to a diamagnetic state with $\mu_1 < \mu_0$. In this case, μ_1 decreases as a function of κ_1 and assumes negative values above a critical chirality

$$\kappa_{\mathrm{c2}} = \sqrt{|\varepsilon_{\mathrm{r},1} - \varepsilon_{\mathrm{r,a}}|} \ . \tag{5.43}$$

A negative, complex refractive index as depicted in Fig. 5.5d is the result. In summary, the antenna model results in chiral, paramagnetic media if $\varepsilon_1 > \varepsilon_a$ and thus $n_\pm > 1$ is

always given. If $\varepsilon_1 < \varepsilon_a$, effective negative refractive index materials with damping arise for light of $\Lambda = -1$ and media with high intrinsic chirality.

Transparency conditions

In this section, the transparency conditions are analyzed with regard to the effective material parameters. The question whether the antenna model already implies a degree of duality or refractive index matching is addressed. Subsequently, possible parameter choices, which give rise to dual or maximally em-chiral media, are presented.

Transparency implies duality

$$\begin{aligned} Z_2 &= Z_1 \\ \Leftrightarrow \quad \sqrt{\frac{\mu_2}{\varepsilon_2}} &= \sqrt{\frac{\mu_1}{\varepsilon_1}} \ , \end{aligned} \tag{5.44}$$

which is one necessary condition for maximally em-chiral media (section 5.2.2). In addition, the refractive index of a chiral medium, which is transparent to light of one helicity, shall match that of the surrounding medium

$$n_{2,\pm} = n_{1,\pm} \ . \tag{5.45}$$

This equation is brought into a more convenient form after several transformations using relation (3.23): $(\varepsilon_{\mathrm{r},i} - \varepsilon_{\mathrm{r,a},i})(\mu_{\mathrm{r},i} - \mu_{\mathrm{r,a},i}) = \kappa_i^2$ with $i = 1, 2$,

$$\begin{aligned} \sqrt{\varepsilon_{\mathrm{r},2}\mu_{\mathrm{r},2}} + \kappa_2 &= \sqrt{\varepsilon_{\mathrm{r},1}\mu_{\mathrm{r},1}} + \kappa_1 \\ \Rightarrow \sqrt{\varepsilon_{\mathrm{r},2}\mu_{\mathrm{r},2}} \pm \sqrt{(\varepsilon_{\mathrm{r},2} - \varepsilon_{\mathrm{r,a},2})(\mu_{\mathrm{r},2} - \mu_{\mathrm{r,a},2})} &= \sqrt{\varepsilon_{\mathrm{r},1}\mu_{\mathrm{r},1}} \pm \sqrt{(\varepsilon_{\mathrm{r},1} - \varepsilon_{\mathrm{r,a},1})(\mu_{\mathrm{r},1} - \mu_{\mathrm{r,a},1})} \ , \\ \sqrt{\varepsilon_{\mathrm{r},2}\mu_{\mathrm{r},2}} \left(1 \pm \sqrt{\left(1 - \frac{\varepsilon_{\mathrm{r,a},2}}{\varepsilon_{\mathrm{r},2}}\right)\left(1 - \frac{\mu_{\mathrm{r,a},2}}{\mu_{\mathrm{r},2}}\right)}\right) &= \sqrt{\varepsilon_{\mathrm{r},1}\mu_{\mathrm{r},1}} \left(1 \pm \sqrt{\left(1 - \frac{\varepsilon_{\mathrm{r,a},1}}{\varepsilon_{\mathrm{r},1}}\right)\left(1 - \frac{\mu_{\mathrm{r,a},1}}{\mu_{\mathrm{r},1}}\right)}\right) \\ \Leftrightarrow Z_2\varepsilon_{\mathrm{r},2}(1 \pm x_2) &= Z_1\varepsilon_{\mathrm{r},1}(1 \pm x_1) \ , \end{aligned} \tag{5.46}$$

where $Z_i\varepsilon_{\mathrm{r},i} = \sqrt{\varepsilon_{\mathrm{r},i}\mu_{\mathrm{r},i}}$ and x_i are abbreviations for the square roots within the brackets of the penultimate line. Both conditions are only met if $Z_2 = Z_1$ and

$$\varepsilon_{\mathrm{r},2}(1 \pm x_2) = \varepsilon_{\mathrm{r},1}(1 \pm x_1) \ . \tag{5.47}$$

So far, chiral media inside and outside of the scatterer are assumed. Now, an achiral surrounding medium is assumed, which implies $x_2 = 0$ and $\mu_{\mathrm{r,2}} = \mu_{\mathrm{r,a}} = 1$. Thus, the constraint above becomes

$$\begin{aligned}
\frac{\varepsilon_{\mathrm{r,2}}}{\varepsilon_{\mathrm{r,1}}} &= 1 \pm \sqrt{\left(1 - \frac{\varepsilon_{\mathrm{r,a,1}}}{\varepsilon_{\mathrm{r,1}}}\right)\left(1 - \frac{1}{\mu_{\mathrm{r,1}}}\right)} \\
\frac{1}{\mu_{\mathrm{r,1}}} &= 1 \pm \sqrt{\left(1 - \frac{\varepsilon_{\mathrm{r,a,1}}}{\varepsilon_{\mathrm{r,1}}}\right)\left(1 - \frac{1}{\mu_{\mathrm{r,1}}}\right)} \\
1 - \frac{1}{\mu_{\mathrm{r,1}}} &= \mp\sqrt{\left(1 - \frac{\varepsilon_{\mathrm{r,a,1}}}{\varepsilon_{\mathrm{r,1}}}\right)\left(1 - \frac{1}{\mu_{\mathrm{r,1}}}\right)} \\
\sqrt{1 - \frac{1}{\mu_{\mathrm{r,1}}}} &= \mp\sqrt{1 - \frac{\varepsilon_{\mathrm{r,a,1}}}{\varepsilon_{\mathrm{r,1}}}}\ ,
\end{aligned} \tag{5.48}$$

which is met – recalling that $Z_1 = Z_2 \Leftrightarrow \sqrt{\frac{1}{\mu_{\mathrm{r,1}}}} = \sqrt{\frac{\varepsilon_{\mathrm{r,2}}}{\varepsilon_{\mathrm{r,1}}}}$ – by

$$\varepsilon_a = \varepsilon_2\ . \tag{5.49}$$

Hence, a maximally em-chiral medium consists of a host medium that matches in its permittivity that of the surrounding medium. Additionally, for the inclusion on its own (if $\varepsilon_a = \varepsilon_2$) the following statements hold: not only are maximally em-chiral inclusions described by the antenna model dual but also all dual inclusions are maximally em-chiral. An illustration is given by using the polarizabilities of the inclusions. If the inclusions are dual $\alpha_{ee} = \alpha_{mm}/\mu_a$, the cross coupling is equal to the electric and magnetic polarizabilities due to $\alpha_{ee}\alpha_{mm} = \alpha_{em}^2/\mu_a$ in the antenna model. The calculation of the moments induced by light of well defined helicity (see Appendix C) shows that for dual helices of one handedness only light of one helicity leads to the polarization of the material, whereas the other does not contribute.

Transparency requires duality and an additional constraint, which can be formulated as refractive index matching of material parameters. Although a perfectly transparent medium is not achievable within this model, duality is achieved approximately by adjusting the geometry of the sphere. If the refractive index matching condition (5.46) is met, the duality constraint is violated on the level of material properties. In the case of vacuum as surrounding medium, $n_2 = 1$, and assuming lossless media, (5.42) shows

that the refractive index of light of neither helicity is matching the refractive index of the surrounding medium for $\varepsilon_1 > \varepsilon_\mathrm{a}$. For higher refractive index media surrounding the sphere, the matching is generally possible. Refractive index matching in vacuum is only achieved for chiral media with $\varepsilon_1 < \varepsilon_a$. At the same time the impedance of the medium, which is depicted in Fig. 5.5c for $\varepsilon_1 < \varepsilon_a$, strongly deviates from one (vacuum impedance) in the vicinity of the critical chirality parameter. For permittivities close to vacuum and small chirality parameters, the impedance converges to one.

6 Scattering by a single chiral sphere

To start the examination of scattering by chiral media, the most simple case – a single chiral, lossless sphere in vacuum – is considered in this chapter. The influence of intrinsic chirality, represented by κ_1, on em-chirality and duality of the sphere, as well as the interplay with other material parameters and the radius, are investigated via numerical calculations using the extended Mie theory. The chirality parameter of the sphere is found to restrict the overall em-chirality. Small chiral spheres show regions of very low em-chirality for specific combinations of the radius and permittivity of the sphere. With the exception of chiral media which meet the refractive index matching condition, spheres out of weakly chiral media do generally not exhibit high em-chirality. The effects of geometry are only notable for spheres with high intrinsic chirality.

The medium from which the sphere is made consists of chiral inclusions (*antennas*) inside a watery solution ($\varepsilon_{\mathrm{r,a}} = 1.33^2$). All media are assumed to be lossless.
At first, the influence of the chirality parameter κ_1 on the scattering behavior, especially on the electromagnetic chirality χ of the sphere, is examined via parameter studies for κ_1, ε_1 and r. The permeability is adjusted according to effective material parameters (3.21) and their interrelation (3.36), derived by the antenna model, $\mu_{\mathrm{r},1} = \frac{\kappa_1^2}{\varepsilon_{\mathrm{r},1} - \varepsilon_{\mathrm{r,a}}} + 1$. Although em-chirality is not a simple function of κ_1, the overall em-chirality is increased by higher values of the chirality of the inclusions. This intuitive result is depicted in Fig. 6.1 for $\varepsilon_{\mathrm{r},1} = 3.2^2$. The co-domain of $\chi/\sqrt{C_{\mathrm{int}}}$ is generally laying within the magnitude of κ_1 with maximum values up to eight times of κ_1 (for this permittivity). Thus, it is not possible to achieve high em-chirality (bigger than 50 percent of the total interaction cross section) from weakly chiral inclusions and the adjustment of other material parameters and geometry is of limited benefit.

A striking feature in Fig. 6.1 is the strong reduction of em-chirality for a specific radius $r \approx 0.16\lambda$, which is only weakly depending on the chirality parameter. There are no special features/resonances for spheres of this radius shown in the duality breaking (cf. Fig. 6.2b) or interaction cross section of the sphere. The weak κ_1-dependency is indicating

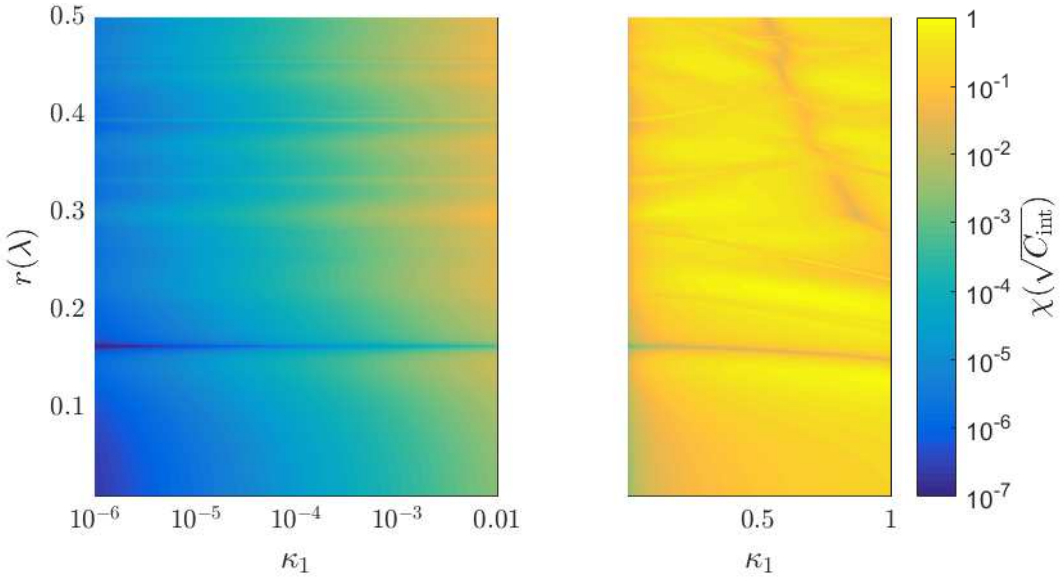

Figure 6.1: Em-chirality χ normalized to the total scattering cross section $\sqrt{C_{\mathrm{int}}}$ as a function of the radius r in units of wavelength λ and the chirality parameter κ_1 for $\varepsilon_{\mathrm{r},1} = 3.2^2$. Em-chirality for high chirality parameters (right hand side) is depicted in Fig. 6.2a with a higher contrast.

that the effect is independent of the chirality of the medium and only depends on the electric and magnetic response $n_1 = \sqrt{\varepsilon_{\mathrm{r},1}\mu_{\mathrm{r},1}} = \frac{1}{2}(n_{1,+} + n_{1,-})$. The weak dependency on the chirality parameter stems from the adjustment of the permeability with respect to the antenna model in the simulation. To further investigate this effect and the dependency on the permittivity and radius, the electromagnetic chirality is depicted as a function of n_1 and the inverse of the radius r^{-1} in Fig. 6.2c. r^{-1} is shown to be a linear function in n_1 with the slope $n_1 r = \frac{1}{2}$ or $(n_{1,+} + n_{1,-})r = 1$ (corresponding to the white dotted line in Fig. 6.2c) and an offset. In this parameter region, em-chirality vanishes in the dipole approximation $\chi_{\mathrm{dipole}} = v_{+,1} - v_{-,1} = |l_1^{\mathrm{L}}| - |r_1^{\mathrm{R}}| = 0$ (see section 5.2.1). For higher radii of the sphere, the region of very low em-chirality fades because higher order multipoles become increasingly relevant. Since meeting the condition for vanishing em-chirality for all multipole expansion coefficient at once is not achievable, such strong reduction of em-chirality is only seen in the case of small spheres compared to the wavelength. The regions of zero em-chirality mark the transition of the particle from scattering mainly light of positive helicity to scattering mainly light of negative as illustrated by Fig. 6.2d.

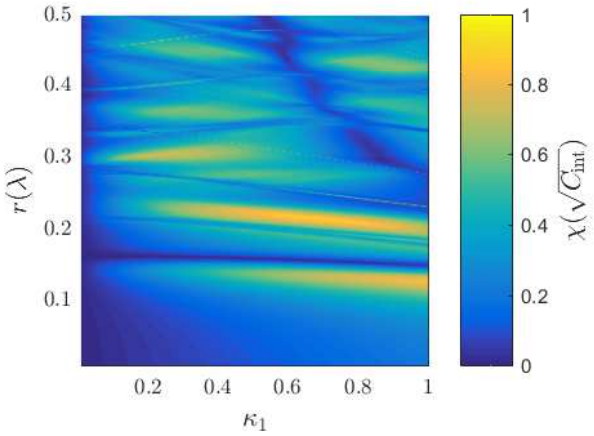

(a) Em-chirality, $\varepsilon_{\mathrm{r},1} = 3.2^2$

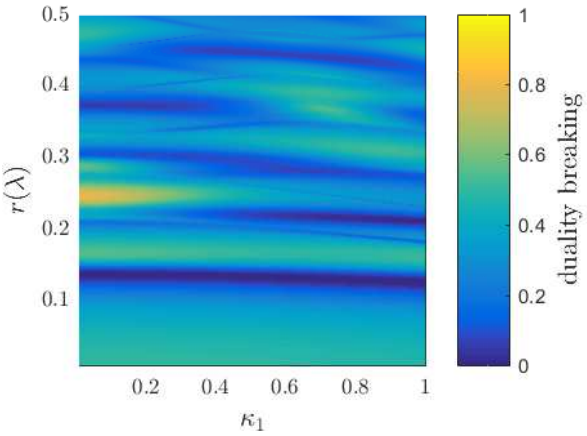

(b) Corresponding duality breaking

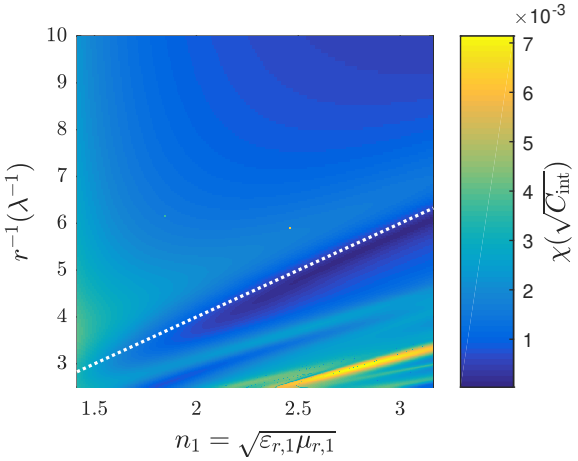

(c) Em-chirality, $\kappa_1 = 10^{-3}$

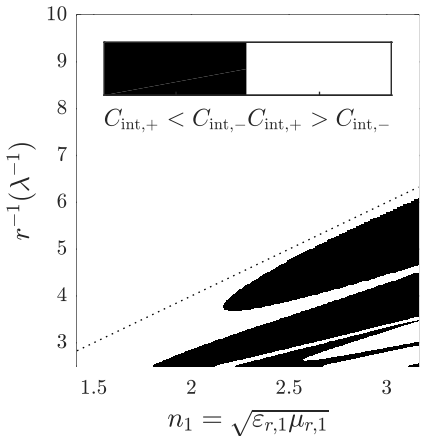

(d) $C_{\mathrm{int},+} - C_{\mathrm{int},-}$, $\kappa_1 = 10^{-3}$

Figure 6.2: (a) Em-chirality and (b) duality breaking as a function of the radius r and the chirality parameter κ_1 of the sphere with the permittivity $\varepsilon_{\mathrm{r},1} = 3.2^2$. (c) Em-chirality for $\kappa_1 = 10^{-3}$ as a function of the inverse radius and the refractive index $n_1 = \frac{1}{2}(n_{1,+} + n_{1,-})$. The white dotted line satisfies $2n_1 r = 1$. (d) Plot of the parameter regions, for which light of negative helicity is scattered more than light of positive helicity $C_{\mathrm{int},+} < C_{\mathrm{int},-}$ (black) and vice versa (white). The black dotted line corresponds to $2n_1 r = 1$.

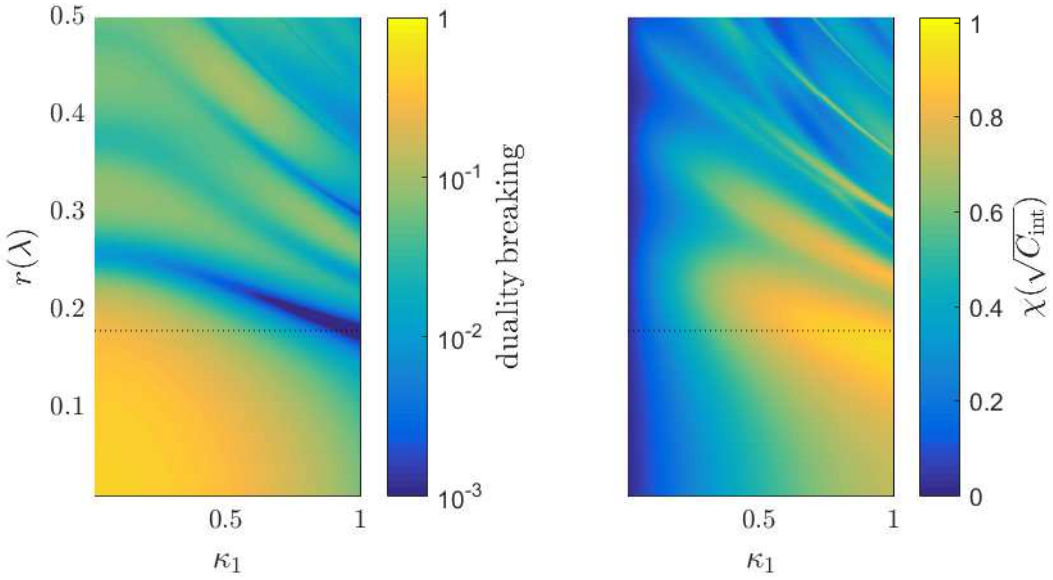

Figure 6.3: Em-chirality and duality breaking as functions of the radius r and the chirality parameter κ_1 for $\varepsilon_{\mathrm{r},1} = 1.7^2$. The dotted black line highlights a radius for which em-chirality is very high and for which low duality breaking results.

Figure 6.3 compares duality breaking to em-chirality for $\varepsilon_{\mathrm{r},1} = 1.7^2$. In accordance with the findings in Fig. 6.2c and the last paragraph, a chirality independent region of very low duality breaking is not obtained for such a small electrical response. In general, highly em-chiral regions imply very low duality breaking. For small κ_1 and radii, the duality breaking is very high and thus, as duality is a necessary condition, em-chirality is also reduced. For very small κ_1, the medium's properties change only slightly and there is a direct correlation between em-chirality and duality: the regions of enhanced em-chirality for specific radii in Fig. 6.1 are due to a decrease in duality breaking for specific geometries. Maximum values of $\chi_{\max} = 0.9265\sqrt{C_{\mathrm{int}}}$ ($r = 0.1575\lambda$ and $\kappa = 1$ for $\varepsilon_{\mathrm{r},1} = 1.7^2$) and $\chi_{\max} = 0.8878\sqrt{C_{\mathrm{int}}}$ ($r = 0.2148\lambda$ and $\kappa = 0.6891$ for $\varepsilon_{\mathrm{r},1} = 3.2^2$) are obtained.

Lastly, the case of $\varepsilon_{\mathrm{r},1} = 1.2^2 < \varepsilon_{\mathrm{r,a}}$ is examined. As is shown in section 5.2.3, the medium changes from being paramagnetic to diamagnetic for $\kappa_1 > \kappa_{\mathrm{c}2}$ with a complex refractive index for $\Lambda = -1$ in the diamagnetic regime. This transition is observed in Fig. 6.4. There is a singularity at $\kappa_1 = \pm\sqrt{\frac{1}{\varepsilon_{\mathrm{r,a}}} - \varepsilon_{\mathrm{r},1}} \approx \pm 0.5735$ due to $\mu_1 = 0$. Em-chirality assumes maximum values of $\chi = 0.9786\sqrt{C_{\mathrm{int}}}$ ($\kappa_1 \approx 0.153$, $r = 0.5\lambda$) in the simulated

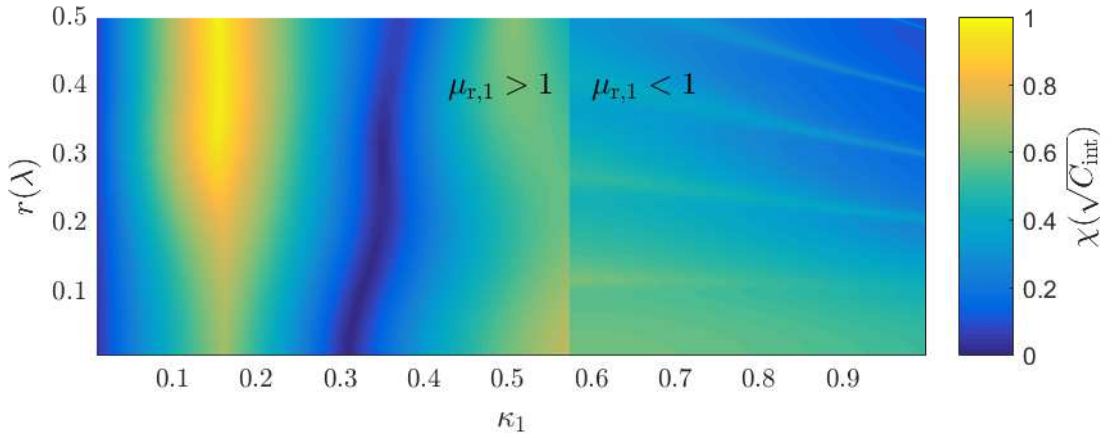

Figure 6.4: Em-chirality as a function of the radius r and the chirality parameter κ_1 for $\varepsilon_{r,1} = 1.2^2$. On the right hand side of the singularity, $\kappa_1 > \kappa_{c2}$, the medium is diamagnetic $\mu_{r,1} < 1$. For smaller κ_1 the medium is paramagnetic $\mu_{r,1} > 1$.

parameter range. This very high em-chirality appears for fixed chirality and for arbitrary radii in Fig. 6.4 and is due to κ_1 fulfilling the refractive index matching condition (5.45) for chiral lossless media in vacuum

$$\begin{aligned} n_{1,-} &= 1 \\ \Leftrightarrow \sqrt{\varepsilon_{r,1}\left(\frac{\kappa^2}{\varepsilon_{r,1}-\varepsilon_{r,a}}+1\right)} &= \kappa \ . \end{aligned}$$

The reduction of em-chirality for smaller radii is due to an increased duality breaking.

Now the dependency of em-chirality on the material parameters, ε_1 and κ_1, is investigated. Therefore, the radius of the sphere is set to $r = 0.2\lambda$ (Fig. 6.5a, 6.5c) and $r = 0.5\lambda$ (Fig. 6.5b). The singularity, where $\varepsilon_1 = \varepsilon_a$, is shifted with the permittivity of the host medium, demonstrated in Fig. 6.5c with $\varepsilon_{r,a} = 1.45^2$ when compared to $\varepsilon_{r,a} = 1.33^2$ in the other figures. Very high values of em-chirality are obtained for rather small permittivities in the vicinity of ε_a for smaller chirality parameters. For these parameter combinations it is possible to match the refractive index to the surrounding medium. These highly em-chiral regions are also observed as bright vertical lines in Fig. 6.4 and Fig. 6.7a or 6.8a. For $\varepsilon_1 > \varepsilon_a$, there are regions with χ up to $0.9\sqrt{C_{int}}$ for very high intrinsic chirality $\kappa > 0.5$. The fine lines of higher em-chirality visible in Fig. 6.5a and more prominent in

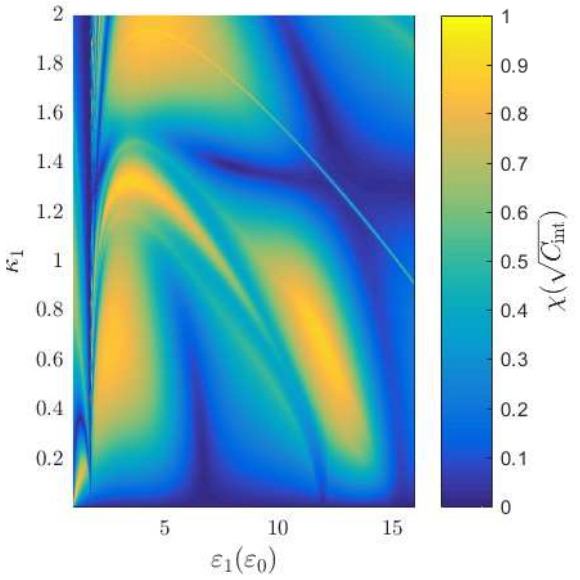

(a) $r = 0.2\lambda$, $\varepsilon_{\mathrm{r,a}} = 1.33^2$

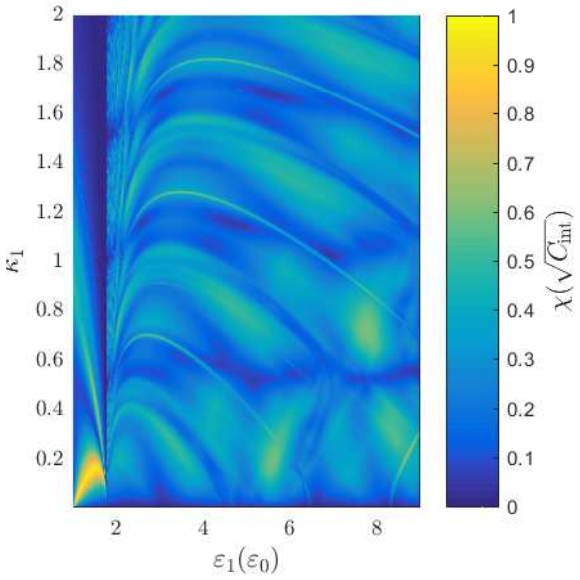

(b) $r = 0.5\lambda$, $\varepsilon_{\mathrm{r,a}} = 1.33^2$

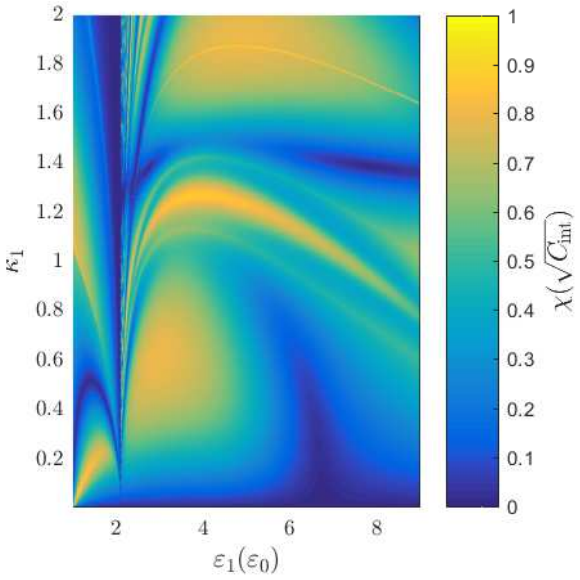

(c) $r = 0.2\lambda$, $\varepsilon_{\mathrm{r,a}} = 1.45^2$

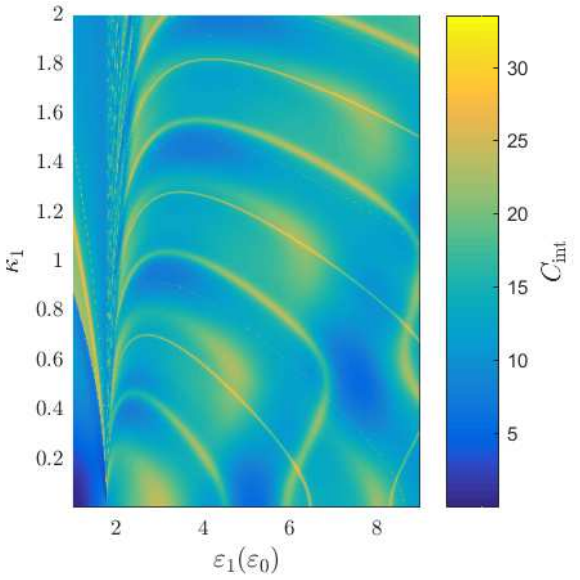

(d) $r = 0.5\lambda$, $\varepsilon_{\mathrm{r,a}} = 1.33^2$

Figure 6.5: Em-chirality as function of chirality parameter κ_1 and permittivity ε_1 for different host media and radii. (d) Total interaction cross section corresponding to (b)

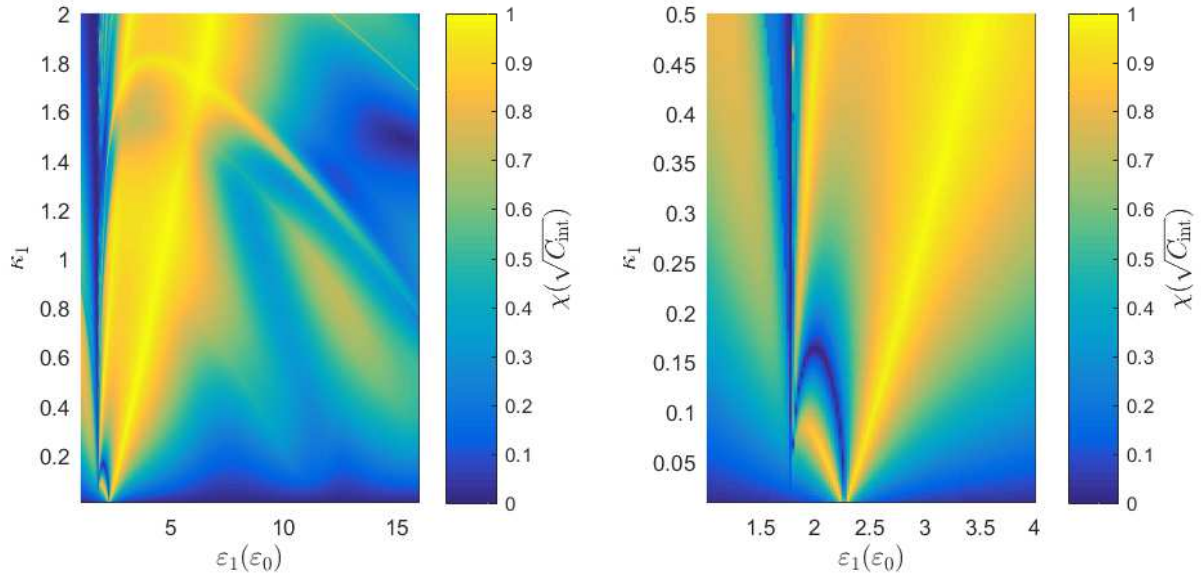

(a) (b)

Figure 6.6: Em-chirality as a function of chirality parameter κ_1 and permittivity ε_1 for a surrounding medium with $n_2 = 1.5$ and radius $r = 0.2\lambda$. (b) Enlarged representation for small parameters of (a)

Fig. 6.5b are due to resonances of the multipoles illustrated by the total interaction cross section in Fig. 6.5d.

So far, the surrounding medium was assumed to be vacuum. The result for glas with $n_2 = 1.5$ as the medium outside of the sphere is displayed in Fig. 6.6. Refractive index matching of the medium with the medium outside is possible for paramagnetic chiral media ($\varepsilon_1 > \varepsilon_\mathrm{a}$). This results in broad parameter regions of em-chirality $\chi > 0.9\,C_\mathrm{int}$. The refractive index matching of light with $\Lambda = -1$ gives rise to the enhanced regions (independent of r). There are two possible parameter combinations to meet the condition for higher κ_1, resulting in two regions, for which em-chirality is very high. For small chirality parameters also the matching of $n_{1,+} = n_2$ is possible.

The ε_1- and r-dependency of em-chirality is depicted for fixed chirality parameters in Fig. 6.7. Starting with very low intrinsic chirality, the general behavior of the chirality parameter, which limits the overall em-chirality, is found: for $\kappa_1 = 10^{-4}$, the maximum em-chirality in the chosen parameter range is about $\chi = 0.0014$ ($\varepsilon_1 = 4.5912$, $r = 1\lambda$) and for $\kappa_1 = 10^{-2}$ $\chi = 0.1207\sqrt{C_\mathrm{int}}$ ($\varepsilon_1 = 2.6806$, $r = 0.9534\lambda$) in Fig. 6.7a and 6.7b. Spheres with a permittivity near vacuum are an exception, because they appear to have very high em-chirality $> 0.9C_\mathrm{int}$ even for small intrinsic chirality, which is shown in Fig. 6.7c. Since $\mu_1 \approx \mu_0$ for small chirality parameters, the refractive index matching is met for $\varepsilon_{\mathrm{r},1} \approx (1 + \kappa_1)^2$ close to the vacuum permittivity. For higher intrinsic chirality, geometry independent effects – as already found in the previous figures – are prominent. One singularity of em-chirality appears at $\varepsilon_{r,1} = \varepsilon_{\mathrm{r,a}}$ and another one in the case of the permittivity corresponding to $\mu_1 = 0$. This permittivity obviously varies with the chirality parameters of the sphere (cf. Fig. 6.8a, 6.8b and 6.8d). In between these singularities, em-chirality is reduced and the duality breaking is enhanced (Fig. 6.8c), which is due to very high permeabilities in this parameter range. Refractive index matching gives rise to very high em-chirality for small permittivities in Fig. 6.8a. This effect is damped by the singularities in Fig. 6.8b and 6.8d, which coincide for these chirality parameters. Disregarding the case of refractive index matching, em-chirality reaches values of $\chi = 0.42\,/\sqrt{C_\mathrm{int}}$ ($r = 0.6559\,\lambda$, $\varepsilon_{\mathrm{r},1} = 4.2091$ and $\kappa = 0.1$) and $\chi = 0.82\,/\sqrt{C_\mathrm{int}}$ ($r = 0.2037\,\lambda$, $\varepsilon_{\mathrm{r},1} = 2.4229$ and $\kappa = 0.5$).

The results in this chapter show that approximately maximally em-chiral media are theoretically feasible. Weakly intrinsically chiral media only all do achieve high em-chirality if they obey the refractive index matching with the surrounding. These regions

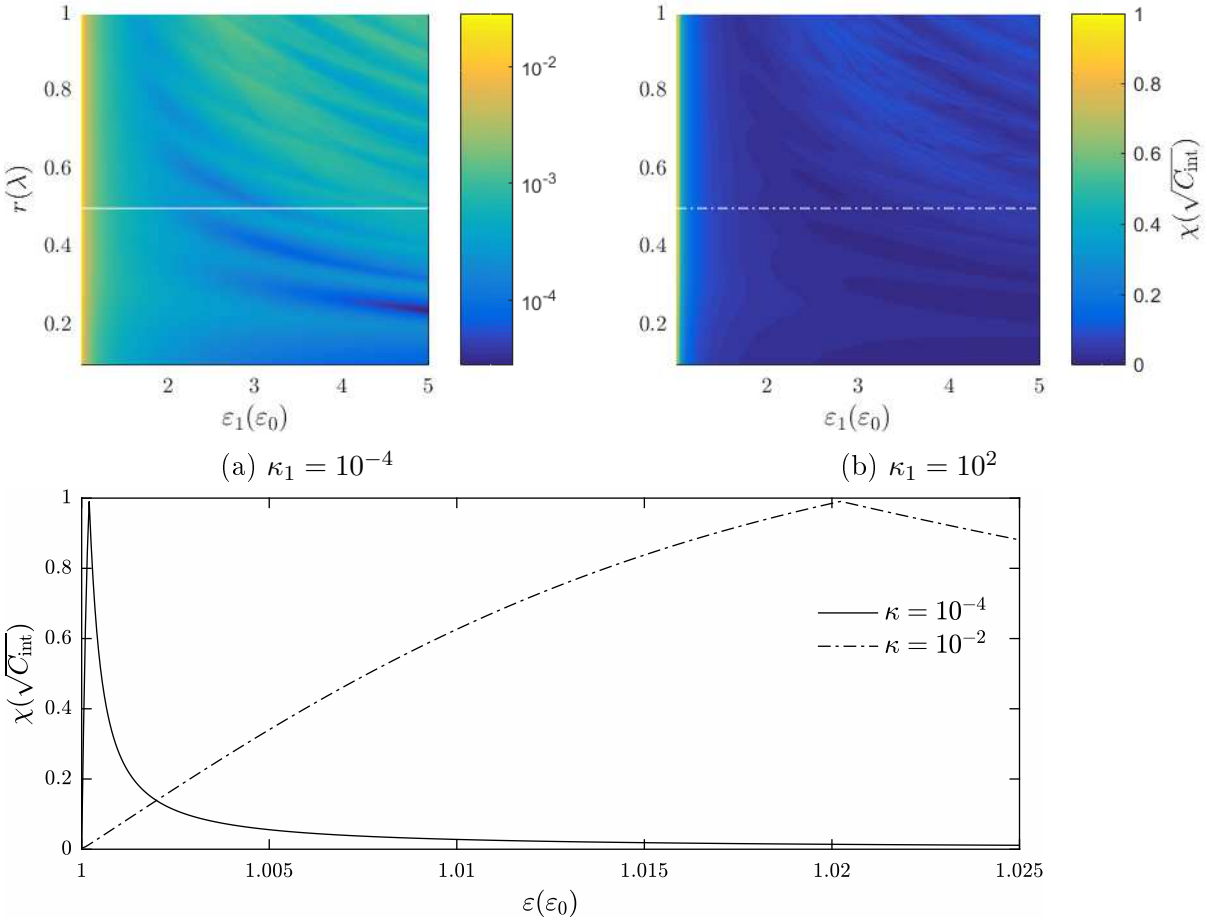

(a) $\kappa_1 = 10^{-4}$ (b) $\kappa_1 = 10^{2}$

(c) $r = 0.5\lambda$

Figure 6.7: (a), (b) Em-chirality as a function of radius r and permittivity ε_1. (c) Em-chirality for samll permittivities and fixed radius $r = 0.5\lambda$, which correspond to the height profile of the horizontal lines in (a) and (b).

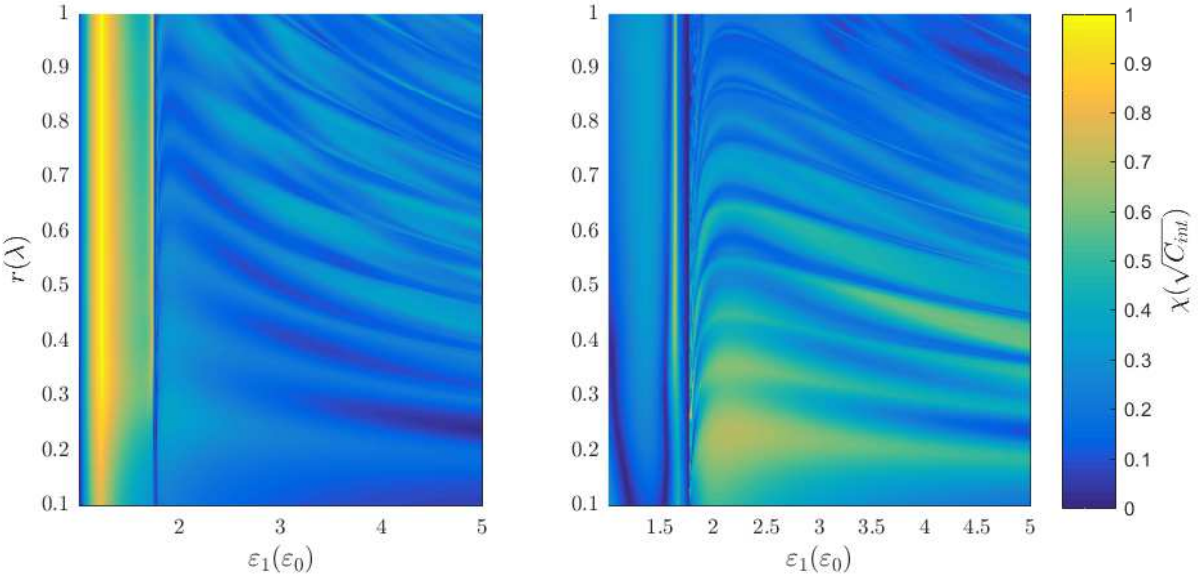

(a) Em-chirality, $\kappa_1 = 0.1$

(b) Em-chirality, $\kappa_1 = 0.3$

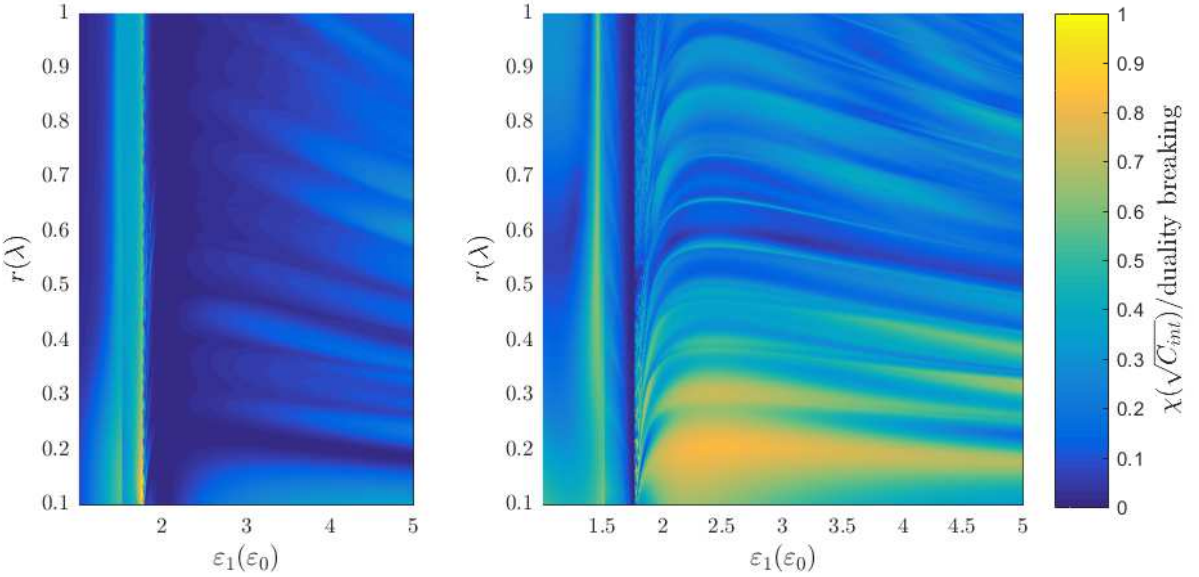

(c) Duality breaking, $\kappa_1 = 0.5$

(d) Em-chirality, $\kappa_1 = 0.5$

Figure 6.8: Em-chirality as a function of the radius r and the permittivity ε_1.

of high em-chirality are narrow and very sensitive to small variations in the material parameters. Refractive index matching for media with higher chirality in vacuum is only possible for diamagnetic scatterers and sometimes not achievable at all due to the kind of model used in this work to describe the chiral inclusions. Generally, high index materials reach high values of em-chirality for small radii and very high chirality parameters $\kappa > 0.5$. The most promising approach appears to be the placement of the sphere inside a higher index medium, which then allows for regions of high em-chirality even for paramagnetic media. These regions are broadened for higher κ.

However, the available materials are very limited in the optical regime. Naturally occurring chiral solutions show only weak chirality and meeting the stated conditions does not seem practical due to the high sensitivity with respect to the geometry and material parameters. Chiral structures, such as metal helices show high em-chirality in the microwave regime but are not easily scaled to optical frequencies. In general, the production of 3D chiral metamaterials poses a challenge with respect to isotropy and homogenization. So far, approaches using collesteric liquid crystals as templates to form radially arranged helical structures within spheres appears to be most useful. These chiral particles achieve $\kappa \approx 0.1$ [9] and thus show high intrinsic chirality. Eventually, the actually achievable parameter space is not clear and the simple model of an effectively isotropic, homogeneous and chiral medium assumed in this work is not at all directly comparable to the liquid crystal structure.

7 Scattering by a chiral core-shell particle

This chapter is motived by the findings of Rahimzadegan *et al.* in [39], where the duality of an achiral spherical particle has been increased by considering additionally a dielectric shell with a specific radius and permittivity surrounding the sphere. Here, we aim to identify possible core-shell-configurations which improve em-chirality. For that purpose we also consider a chiral shell in section 7.1. The core-shells are compared to homogeneous spheres with arbitrary radius out of the shell or core material. Thereby, it becomes apparent that adding a chiral shell to a chiral sphere mostly does not improve em-chirality compared to a homogeneous sphere. Diamagnetic media are the exception. In section 7.2, the case of a thin dielectric coating on a chiral sphere is examined in order to increase the em-chirality especially for weakly chiral spheres. A strong increase in em-chirality is found for thin shells on top of weakly chiral cores when a specific combination of geometry and medium is met.

7.1 Spherical particle with a chiral shell

Firstly, chiral core-shell particles are examined with size and permittivity comparable to to those considered in [39] to reproduce the results presented in there. The material parameters and radius of the core are labeled with subscript '1', such as the ones of a homogeneous sphere. The surrounding medium is labeled by subscript '2' and the shell by 'sh', which is visualized in Fig. 7.1. The host media are assumed to be water for both core and shell. The chirality parameter is chosen equally for both core and shell and sufficiently small, $\kappa_1 = \kappa_{\mathrm{sh}} = 10^{-3}$, such that the influence on the matching of the duality condition in dipole approximation is negligible. In Fig. 7.2, the duality breaking (Fig. 7.2a) and em-chirality (Fig. 7.2b) are shown as a function of the shell radius and the shell permittivity for a fixed core object, i.e. with a radius of $r_1 = 0.105\lambda$ and a permittivity of $\varepsilon_1 = 4^2\varepsilon_0$. The results are in good agreement with the findings of decreased duality breaking in core-shell particles in 7.1: Minimum values of duality breaking are $\not{D} = 5{\cdot}10^{-5}$ for $\varepsilon_{\mathrm{r,sh}} = 2.7^2$, $r_{\mathrm{sh}} = 0.226\lambda$ and $\not{D} = 1.4 \cdot 10^{-4}$ for $r_{\mathrm{sh}} = 0.119\lambda$, cf. Fig. 7.2c. Regions

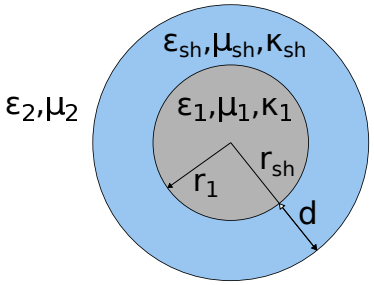

Figure 7.1: Schematic representation of a chiral core-shell particle surrounded by an achiral medium. Material parameters of the core ε_1, μ_1, κ_1 and the shell $\varepsilon_{\mathrm{sh}}$, μ_{sh}, κ_{sh} with thickness $d = r_{\mathrm{sh}} - r_1$

of very low duality breaking for different shell media are depicted in Fig. 7.2a. However, since duality is not a sufficient condition for em-chirality, χ in Fig. 7.2b is not notably enhanced $[\chi/\sqrt{C_{\mathrm{int}}}] \sim [\kappa_1]$ compared to results from a homogeneous sphere with the same chirality parameters, cf. Fig. 6.7. An exception are the regions of very low shell permittivity, which are able to meet the refractive index matching condition with respect to the surrounding medium. This effect dominates over the contributions from the core when the shell becomes bigger. Mie resonances – the absolute values of the Mie coefficients of 4th and 5th order show resonant behavior for bigger radii and are related to the peaks of the total interaction cross section in Fig. 7.2c – are observable for specific radii of the shell. These result in narrow regions of both enhanced em-chirality and duality breaking. While a low duality breaking not always correlates to a large em-chirality, the opposite is true, i.e. a small em-chirality correlates well with high duality breaking. This clearly emphasizes that duality is a necessary but not a sufficient condition for large em-chirality.

High em-chirality for weakly chiral media is also not expected. This is due to $|l_1^{\mathrm{R}}| - |r_1^{\mathrm{R}}|$ being maximally different for maximally em-chiral dipole scatterers. Therefore, one of the scattering coefficients has to be zero while the other one reaches unity. This in turn requires the cross coupling coefficient c_1 to be equal to the Mie coefficients $c_1 = a_1 = b_1$ (also meeting the dipole duality condition), which is not possible for small chirality parameters. This is illustrated in Fig. 7.3, where the electromagnetic chirality and duality breaking are displayed for a core-shell particle with $\kappa_1 = \kappa_{\mathrm{sh}} = 0.5$. Regions of low duality breaking for strong chiral media are slightly shifted compared to media with a lower chirality parameter, since the simulations adjust the permeability of the medium with the chirality parameter and the permittivity. In contrast to the media with small κ,

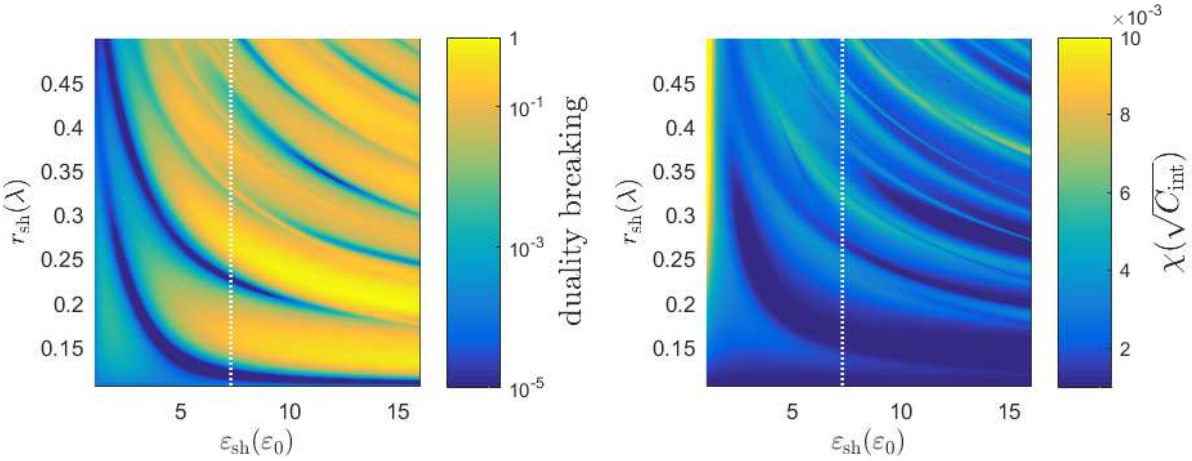

(a) Duality breaking (b) Em-chirality

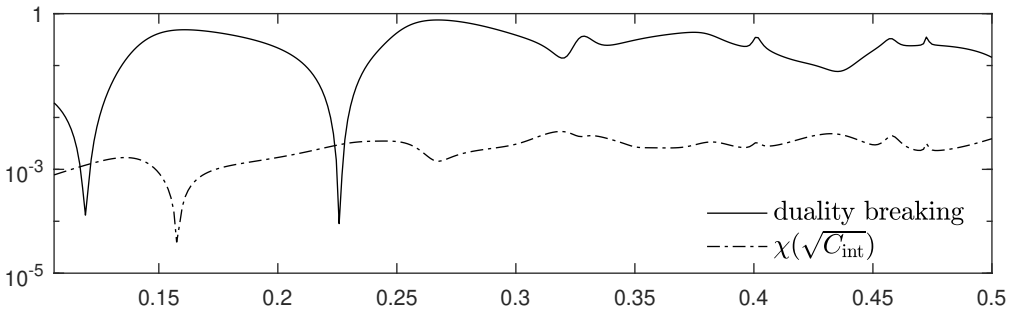

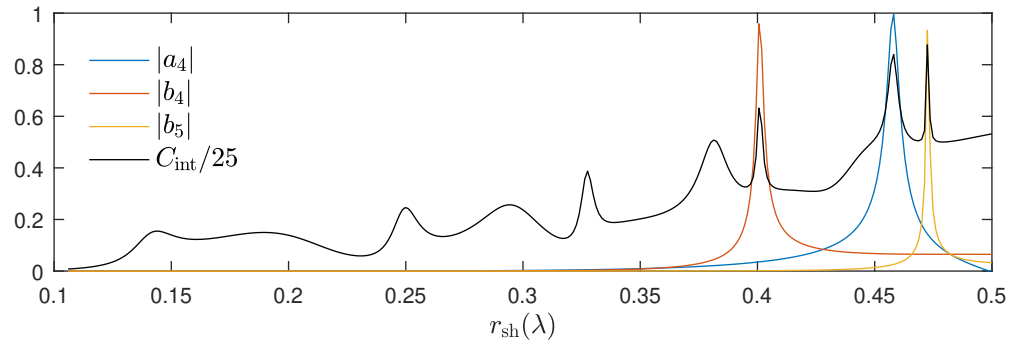

(c) $\varepsilon_{\mathrm{r,sh}} = 2.7^2$

Figure 7.2: (a) Duality breaking and (b) corresponding em-chirality for a core-shell particle with water as the host medium $\varepsilon_{\mathrm{r,a}} = 1.33^2$ (both for core and shell medium). The core has radius $r_1 = 0.105\lambda$, permittivity $\varepsilon_{\mathrm{r},1} = 4^2$ and chirality $\kappa_1 = \kappa_{\mathrm{sh}} = 10^{-3}$. (c) em-chirality, duality breaking and total interaction cross section for $\varepsilon_{\mathrm{r,sh}} = 2.7^2$, corresponding to the white dotted lines in (a), (b).

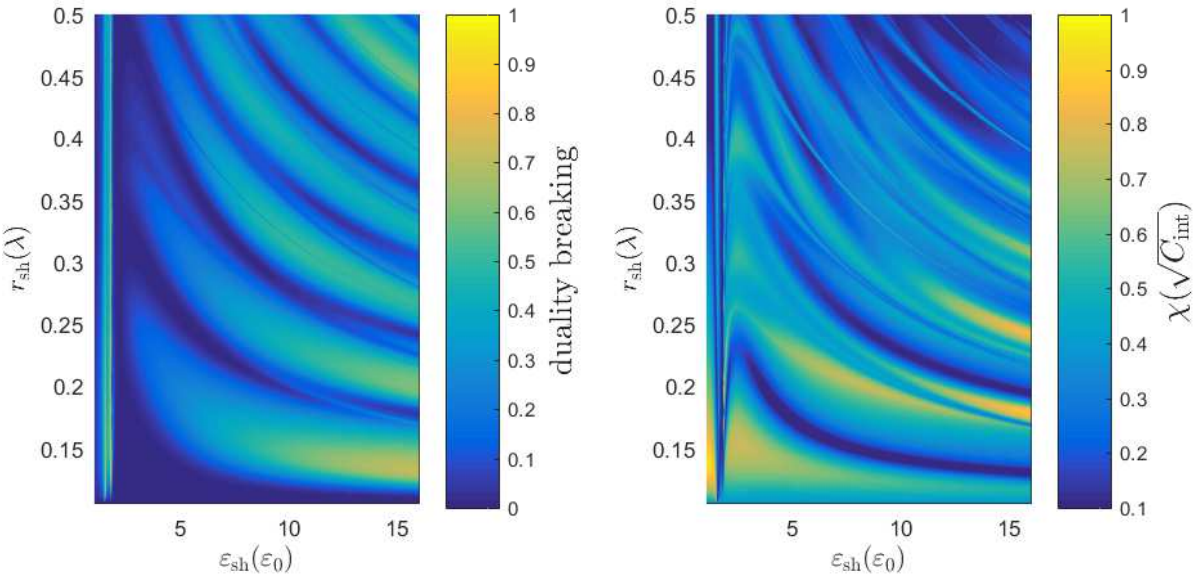

(a) (b)

Figure 7.3: (a) Duality breaking and (b) corresponding em-chirality for water as host medium $\varepsilon_{\mathrm{r,a}} = 1.33^2$, a core with radius $r_1 = 0.105\lambda$, permittivity $\varepsilon_{\mathrm{r},1} = 4^2$ equivalent to the core-shell in Fig. 7.2, except for the increased chirality $\kappa_1 = \kappa_{\mathrm{sh}} = 0.5$.

the chirality parameter together with the change of permittivity and radius allows for very high electromagnetic coupling and thus for approximate matching of the dipole condition for maximally em-chiral objects. Chirality parameters $\chi > 0.8C_{\text{int}}$ are observed for high refractive index media of the shell. In the case of $\varepsilon_{\text{sh}} = 16\varepsilon_0$ the core-shell merges into a homogeneous sphere with the refractive index of the core. Except for a diamagnetic shell, Fig. 7.3b indicates that adding a layer with smaller permittivity to the core does not improve em-chirality, when compared to a homogeneous sphere, since the highest values of em-chirality for the core-shell particle are assumed when the shell medium equals the core.

Furthermore, to evaluate the use of adding a shell to a sphere, the core-shell particle is compared to a homogeneous sphere with the same outer radius and consisting fully out of the shell medium. This is depicted in Fig. 7.4. The homogeneous sphere shows comparable high values of em-chirality. Indeed, for a shell/sphere out of a defined paramagnetic medium, $\varepsilon_{\text{sh}} > \varepsilon_a$, one can always find a sphere with radius r_1, which possess higher em-chirality than the corresponding core-shell particle (though r_1 is assumed of arbitrary size. For a fixed outer radius of the sphere and core-shells there are parameters, in which the core-shell exhibits higher em-chirality). Figure 7.4c and 7.4d present this behavior for shells with $\varepsilon_{\text{sh}} < \varepsilon_{\text{core}}$. The figures also illustrate that for increasing shell radii compared to the core radius (in this case $r = 0.105\lambda$) em-chirality of the core-shell particle is increasingly determined by the shell medium. For a low index contrast between core and shell, the scattering by the core-shell with respect to em-chirality is comparable to the homogeneous sphere, see Fig. 7.4d. In the case of diamagnetic shell media, there are regions of high em-chirality when the shell radius is small compared to the wavelength, illustrated in Fig. 7.5a. These media are interesting because they do not exhibit low duality breaking or resonances at points of high em-chirality. However, dipoles with $\Lambda = -1$ are approximately not scattered, $r_1^{\text{R}} \approx 0$ for specific core-shell configurations (Fig. 7.5b). The Mie coefficients satisfy $|a_1| + |b_1| = 2|c_1|$, but not $a_1 = b_1$, which is depicted in Fig. 7.5c. There is still a mixing of light with different helicities at the interface, which does not allow for perfect transparency, e.g. additional duality. However, the coupling parameter is much smaller than the scattering coefficients for dipoles of $+1$ helicity (in the example in Fig 7.5c: $l_1^{\text{R}} \approx 16\% l_1^{\text{L}}$). The figures in appendix C show further results of em-chirality of a core-shell particle with bigger core and different core material, as well as for shell media with $\varepsilon_{\text{sh}} > \varepsilon_1$ and the comparison to homogeneous spheres of the corresponding medium. These results illustrate that for specific core-shell media, a

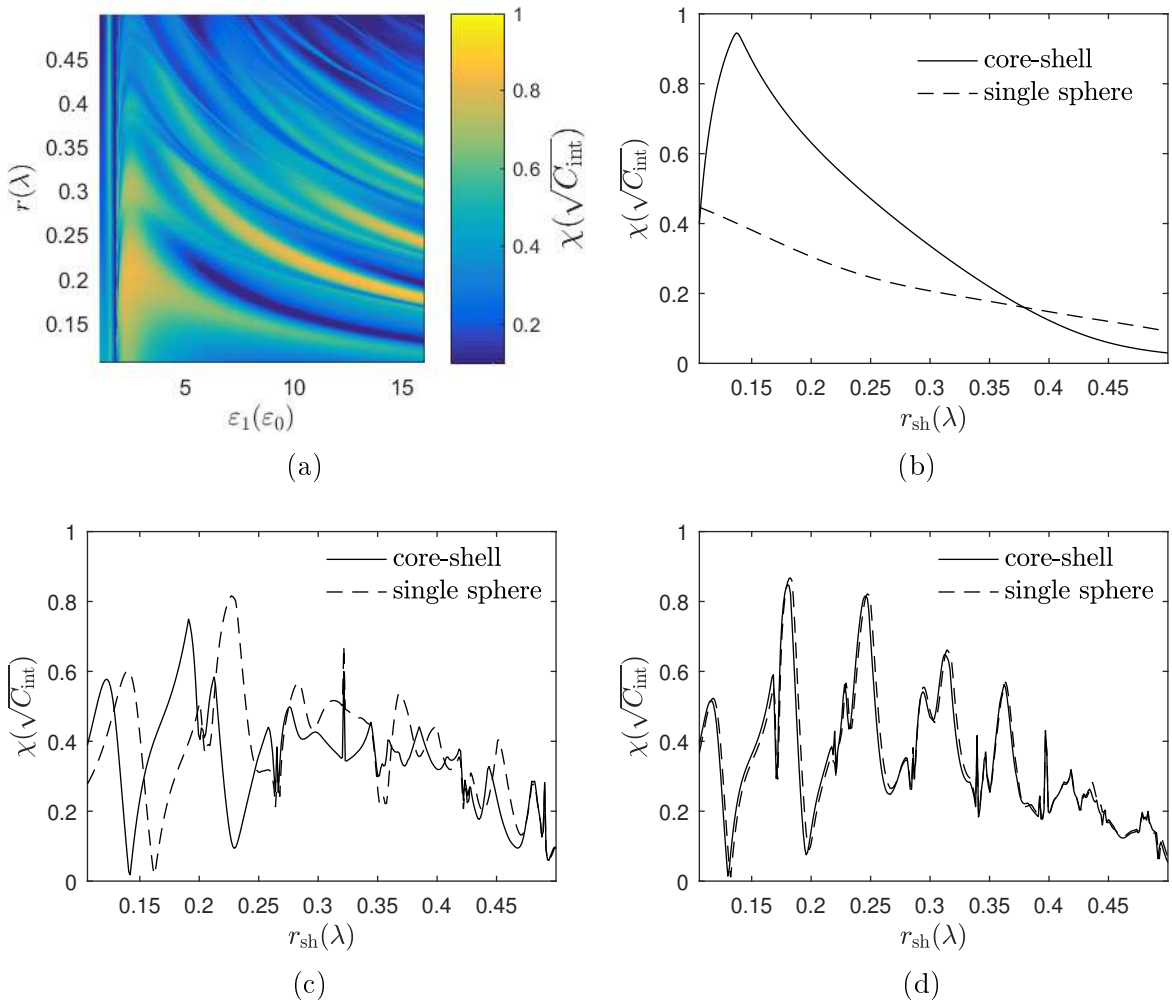

Figure 7.4: (a) Em-chirality for a homogeneous sphere $\kappa_1 = 0.5$. (b)-(d) Comparison to em-chirality for specific shell (core-shell with $\varepsilon_1 = 4^2\varepsilon_0$, $\kappa_{\mathrm{sh}/1} = 0.5$) or sphere (homogeneous sphere) permittivities $\varepsilon_{\mathrm{sh}/1} = 1.16\varepsilon_0$ in (b), $\varepsilon_{\mathrm{sh}/1} = 9,74\varepsilon_0$ in (c) and $\varepsilon_{\mathrm{sh}/1} = 15.25\varepsilon_0$ in (d).

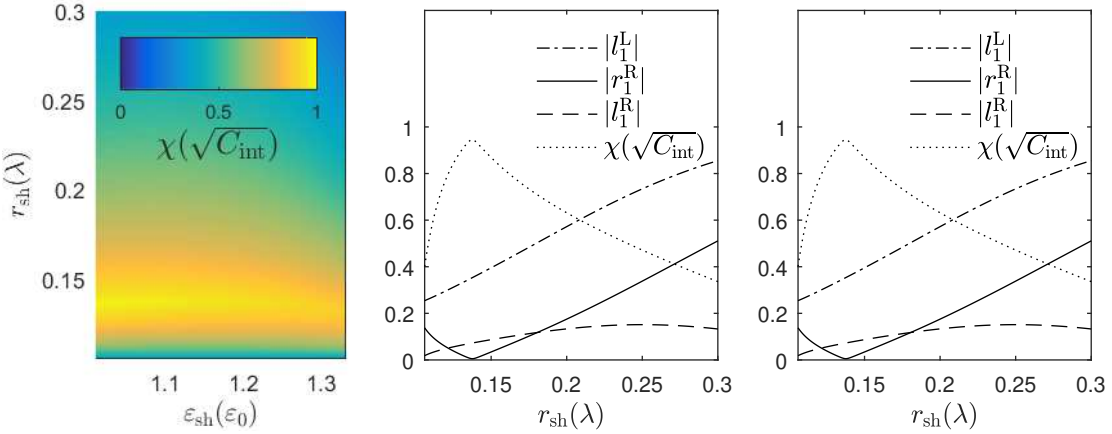

(a) (b) (c)

Figure 7.5: (a) Em-chirality as a function of shell permittivity $\varepsilon_{\mathrm{sh}}$ and shell radius r_{sh} for $\kappa_1 = 0.5$. (b) Expansion coefficents in the helicity basis and (c) Mie coeffients for $\varepsilon_{\mathrm{sh}} = 1.16\varepsilon_0$ as a function of the shell radius. The dotted line represents the normalized em-chirality.

homogeneous sphere of either shell or core medium with a specific radius possess higher em-chirality than the core-shell particle.

A further examination of chirality parameters of core and shell is not shown in the frame of this work, since we obtain similar results as before. Although a strongly chiral shell on top of a weakly chiral core will enhance em-chirality, a homogeneous sphere out of this shell material with comparable size will show a better result. An exception from this general results is found for very thin (dielectric) shells. This is discussed in the following section.

7.2 Particle with thin dielectric coating

A chiral sphere with a thin achiral coating is an interesting case from the perspective of a possible realization of highly em-chiral scatterers with existing and weakly chiral media. It is shown that a dielectric thin layer results in drastically increased em-chirality for specific radius to wavenumber relations between core and shell. For a chiral core with $\kappa_1 = 0.01$, $\varepsilon_1 = 4.5\varepsilon_0$ and $r_1 = 0.3\lambda$ there are shell parameters for which em-chirality is very high, cf. Fig. 7.6a. The shell is a dielectric with refractive index $n_{\mathrm{sh}} = \sqrt{\varepsilon_{\mathrm{sh}}}$.

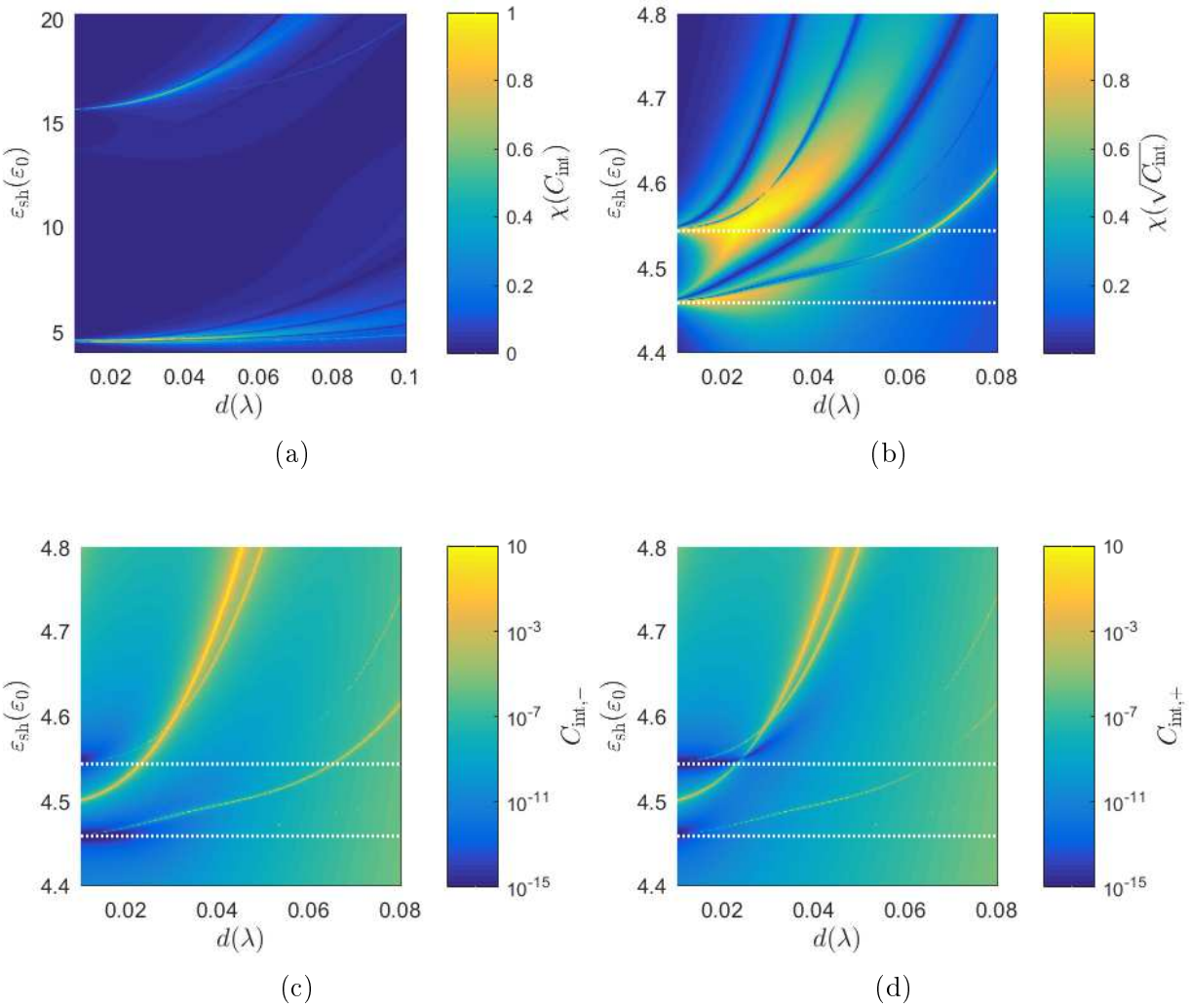

Figure 7.6: (a) Em-chirality as a function of the permittivity $\varepsilon_{\mathrm{sh}}$ and the thickness $d = r_{\mathrm{sh}} - r_1$ of the dielectric shell with and a core with $r = 0.3\lambda$, $\varepsilon_1 = 4.5\varepsilon_0$ and $\kappa_1 = 0.01$. (b) higher resolution of (a) for smaller permittivities. Partial interaction cross sections for light of $\Lambda = -1$ (c) and $\Lambda = +1$ (d), corresponding to (b).

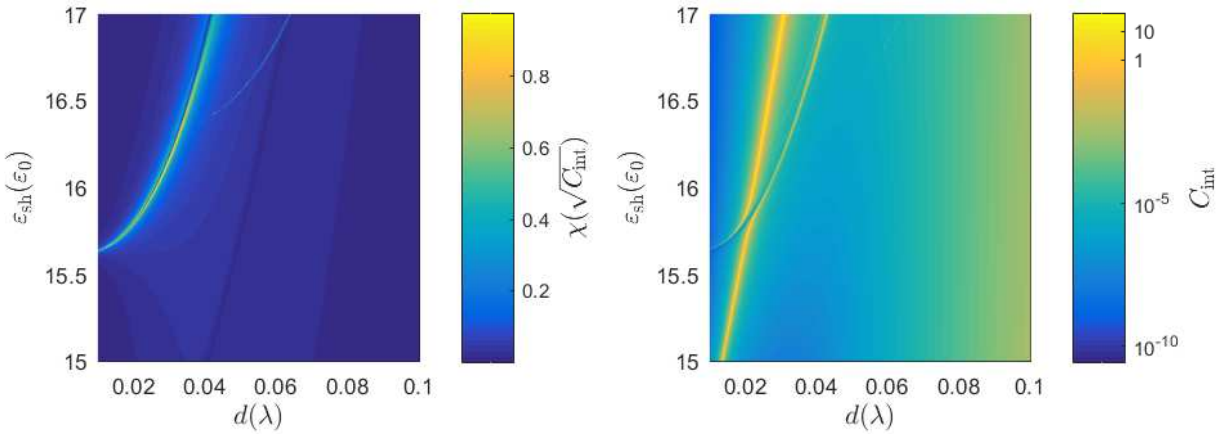

(a) (b)

Figure 7.7: (a) Em-chirality – detail of Fig. 7.6a – as a function of shell thickness and permittivity. (b) Corresponding total interaction cross section.

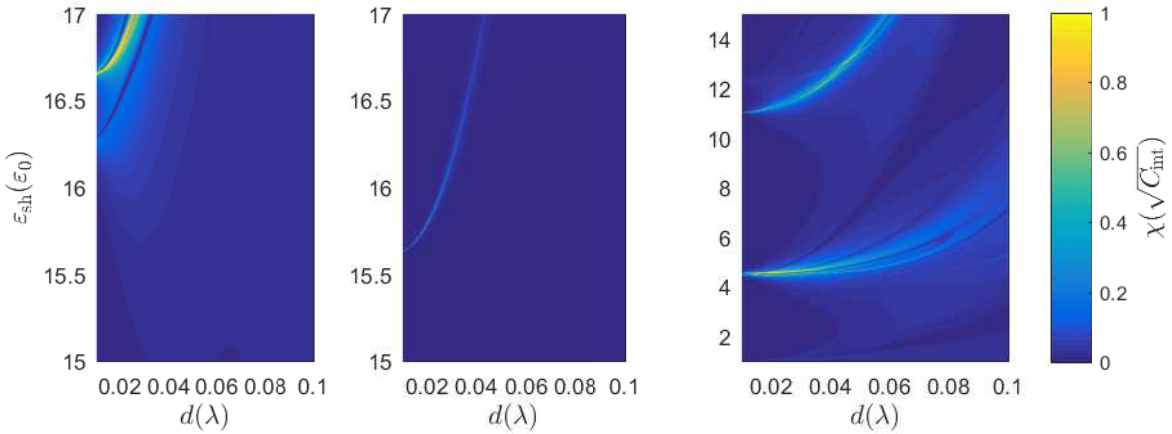

(a) (b) (c)

Figure 7.8: Comparison of em-chirality as a function of high permittivity and thickness d of the shell for different cores. (a) Core with $\varepsilon_1 = 5.5\varepsilon_0$, $r_1 = 0.3\lambda$, $\kappa_1 = 10^{-2}$. (b) Core with $\varepsilon_1 = 4.5\varepsilon_0$, $r_1 = 0.3\lambda$, $\kappa_1 = 10^{-3}$. (c) Core with $\varepsilon_1 = 4.5\varepsilon_0$, $r_1 = 0.4\lambda$, $\kappa_1 = 10^{-2}$.

The parameter region where the refractive index of the shell is comparable to the core is investigated at first. In Fig. 7.6b, a detail of em-chirality as a function of the permittivity and radius of the shell for this parameter region is depicted. There are two regions of very high em-chirality, corresponding to the case of either $n_{\mathrm{sh}} = n_{1,+}$ (upper white dotted line) or $n_{\mathrm{sh}} = n_{1,-}$ (lower line). Light of both helicities is scattered equally at the achiral shell and does not couple electric and magnetic fields. If the refractive index of the shell matches the one of the core for one specific helicity, the core will be approximately (if the duality breaking is low) transparent to this helicity. For a specific thickness of the shell in relation to the medium and radius of the chiral core, light is scattered at the two interfaces such that destructive interference yields very low effective scattering by the core-shell particle. The total interaction cross sections for light of $\Lambda = \pm 1$ are depicted in Fig. 7.6c and 7.6d. High em-chirality implies a very small interaction cross section for one of the two helicities.

Another parameter regime of very high em-chirality is the one for high index media in detail in Fig. 7.7a. There are two resonances crossing each other, one for which the refractive index of the dielectric changes linearly with the thickness of the shell, the other one exhibits a higher order dependency. At the intersection point an anti-crossing is observed in Fig. 7.7b, where the total scattering cross section is much smaller. The very narrow parameter region, for which em-chirality is very high $\chi > 0.99\sqrt{C_{\mathrm{int}}}$, changes for different core media and core radii as illustrated in Fig. 7.8. For smaller chirality of the core em-chirality is reduced but still high compared to values achieved without the shell (Fig. 7.8b). If the core has a higher refractive index, also the refractive index n_{sh} of the highly em-chiral core-shell particle is increased for a constant shell thickness d (Fig. 7.8a). An algebraic expression for the relation between the core and shell medium together with geometry is not deduced in this work. The radius of the core significantly changes the

size parameter of the same, as well as the relative coating thickness d, which leads to a shifting of the parameter region where em-chirality is very high, see Fig. 7.8c.

7.3 Discussion

In this chapter, the basic effects of adding a chiral shell to a chiral sphere have been examined in terms of (further) improvement of em-chirality, because especially weakly chiral spheres are in need of enhancement. However, in most cases weakly chiral media do not allow for strong increase of em-chirality via an additional chiral (!) shell. An exception are diamagnetic shell media. These media imply very high em-chirality for small core-shell particles and approximately meet the transparency condition in the dipole approximation $|a_1|+|b_1| = 2|c_1|$ without being approximately dual $|a_1| \neq |b_1|$, as would be expected. Only chiral media with high intrinsic chirality are found to give rise to very high em-chirality. Since high intrinsically chiral media do already posses high em-chirality for specific geometries and media in homogeneous spheres, the combination of two strongly chiral media does not improve em-chirality in general.

In contrast to chiral shells, thin dielectric coatings on top of a chiral sphere exhibit very high em-chirality for specific core-shell configurations, even for weakly chiral media. The regions of very high em-chirality are quite narrow for high refractive index shells and the effects of the enhancement of em-chirality is not further investigated in this work. For a low index contrast between the core and shell medium, broader regions of high em-chirality are observed, which results in high em-chiral core-shells out of weak intrinsically chiral media.

8 Highly em-chiral spheres in chiral media

Maximally em-chiral spheres scatter light of one helicity, whereas light of the other helicity is not scattered at all. As discussed in chapter 6 and 7, em-chirality of spherical particles depends on geometry and material parameters, but of course also on the surrounding medium. In this last main chapter, the possibility to determine the chirality of the surrounding medium from the change of scattering response of a chiral sphere is shortly investigated. The chiral medium, for example, can be a solution of chiral molecules, whose small chirality parameter is to be determined. This is a preliminary study, which gives the basic idea of detection and points out difficulties, which have to be considered in future work. In other words, we raise the question here to which extent we can use the scattering signal chiral spheres as some sort of sensing device. A good sensor requires rapid change of the scattering behavior for small variations of the chirality parameter of the surrounding medium as well as a different scattering response when immersed in a medium containing differently handed molecules. The magnitude of the interaction cross sections shall be directly related to the chirality parameter – if all other parameters are known the interaction cross section depends solely on the chirality parameter – and in the best case its sign, as well. Thus, the goal is to design spheres that possess a high em-chirality and at the same time a high sensitivity of their em-chirality to changes of the surrounding medium's chirality. Small intrinsically chiral spheres are shown to be very sensitive to a specific parameter range of the surrounding chirality. However, approximations done for the material parameters and the very small total interaction cross section are difficulties of this approach.

High em-chirality of weakly chiral, homogeneous spheres is only achievable when embedding them into a surrounding medium that meets the refractive index matching condition (5.45). Em-chirality is high only in a narrow parameter space for the permittivity of the medium (as was observed in section 6). Thus, the optical response of the sphere is very sensitive to changes of the surrounding medium. Here, we assume weakly chiral spheres with chirality parameters $\kappa_1 = 10^{-6}$ and $\kappa_1 = 10^{-4}$. The refractive index of the chiral sphere for light of negative helicity matches the one of the surrounding medium

($\varepsilon_2 = 1.33^2$) with $\varepsilon_1 = 1.769\varepsilon_0 (\varepsilon_1 = 1.772\varepsilon_0)$ for $\kappa_1 = 10^{-6} (\kappa_1 = 10^{-4})$. The host medium of the sphere with $r = 1\lambda$ is set to be $\varepsilon_{1,\mathrm{a}} = 1.5^2$ (e.g. glas or benzene). When a small amount of chiral scatterers is put into the surrounding medium, the medium outside the sphere is described by means of the mixing theory as an effectively chiral medium with the host medium being water. It is assumed that the solution is so dilute that the effective electric and magnetic response are approximately equal to the medium without the inclusions (i. e. the host medium) $\varepsilon_2 = 1.33^2$, $\mu_2 = 1$ with $\kappa_2 \ll 1$. Figure 8.1 shows the em-chirality as a function of the chirality parameter κ_2 of the surrounding medium and for differently handed spheres, $\kappa_1 = \pm 10^{-6}$ and $\kappa_1 = \pm 10^{-4}$. Changing the sign of κ_1 (changing the handedness of the sphere) has the same effect as changing the sign of κ_2 (changing the handedness of the chiral inclusions in the surrounding medium), because only the relative handedness of both media is important. For a simplified representation we assume a positive sign of κ_2, here, but admit a change in sign of κ_1. In the parameter region where κ_2 is of the same order of magnitude as κ_1, the system is very sensitive to changes of the chirality parameter κ_2. Due to the breaking of the matching condition for sufficiently high chirality of the surrounding medium, em-chirality is heavily reduced for κ_2 approaching κ_1. For chiral spheres, whose chirality parameter has the same sign as the chiral inclusions in the surrounding medium, after passing a point of an achiral behavior, the matching of the refractive indices for light of the opposite helicity becomes possible and em-chirality increases. Without chiral molecules in the surrounding medium, its refractive index matches that of light of negative helicity of the chiral sphere:

$$n_{1,-} = n_2 \ . \tag{8.1}$$

If weakly chiral molecules are placed outside the sphere, the refractive index for light of negative helicity is changed to

$$n_{2,-} = n_2 - \kappa_2 \neq n_{1,-} = n_2 \ , \tag{8.2}$$

and for positive helicity to

$$n_{2,+} = n_2 + \kappa_2 \text{ and } n_{1,+} = n_{1,-} + 2\kappa_1 = n_2 + 2\kappa_1 \ . \tag{8.3}$$

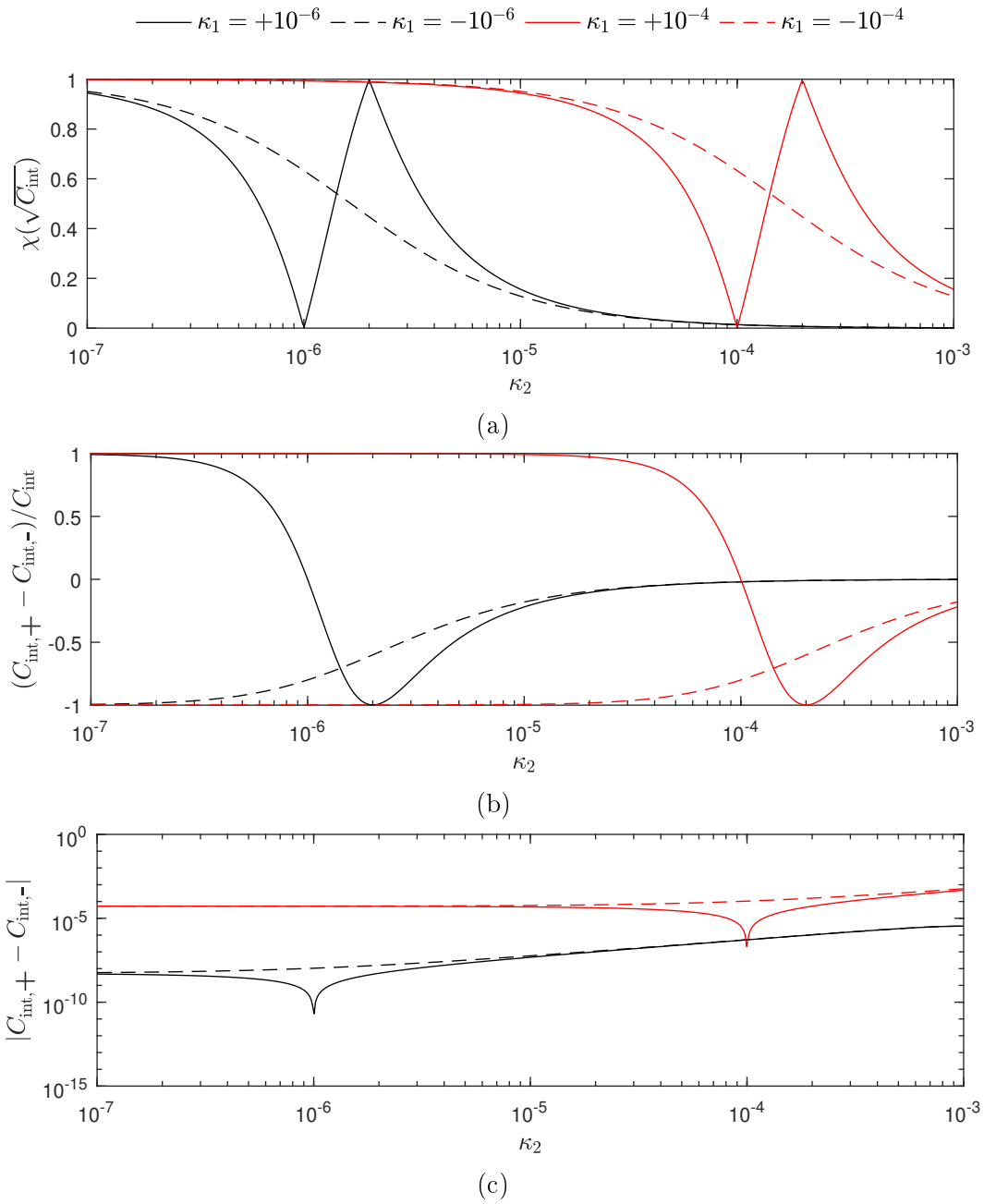

Figure 8.1: (a) Em-chirality of a single sphere as a function of the chirality parameter of the surrounding medium for different spheres with $r = 1\lambda$, $\varepsilon_1 = 1.769\varepsilon_0$ ($\varepsilon_1 = 1.772\varepsilon_0$) and $\kappa_1 = \pm 10^{-6}$ ($\kappa_1 \pm = 10^{-4}$) and host medium $\varepsilon_\mathrm{a} = 1.500^2\varepsilon_0$. (b) Difference between the interaction cross sections of light of $+1$ and -1 helicity as a function of κ_2 normalized to the total interaction cross section. (c) Difference of scattering cross sections not normalized.

Hence, for

$$\kappa_2 = 2\kappa_1 \tag{8.4}$$

the refractive indices for light of positive helicity are matched and em-chirality is very high. If κ_1 and κ_2 have the opposite signs a distinct scattering behavior is observed. For spheres with the opposite handedness the refractive index for positive helicity takes the value of the former refractive index of negative helicity and $n_{1,+} = n_2 + 2\kappa_1 = n_2 - 2|\kappa_1| \neq n_{2,+}$, $\forall \kappa_2 > 0$ (cf. (8.3)). Thus, a matching of the refractive indices for positive helicity is not possible.

In the regions, where em-chirality is changing fast with κ_2, the interaction cross sections of the different helicities change, too. In Fig. 8.1b, the relative difference in relation to the total scattering cross section between the interaction cross sections for the two helicities ($C_{\mathrm{int},+}$,$C_{\mathrm{int},-}$) are depicted as a function of κ_2. Within a restricted parameter region, depending on the chirality of the sphere, κ_2 is detectable by means of the difference between the interaction cross sections. Hence, to enable the detection of chirality of molecules, the properties of the molecule have to be know to some extend. Then, a chiral sphere which is suitable to detect the chirality in this parameter range can be used.

There are two major difficulties in this approach which would deserve some future investigation. Firstly, the small total interaction cross section results in a very small difference between $C_{\mathrm{int},+}$ and $C_{\mathrm{int},-}$ for a single sphere. Figure 8.1c shows the absolute values of $C_{\mathrm{int},+} - C_{\mathrm{int},-}$, which are not above 10^{-7} for $\kappa_1 = 10^{-6}$ and not above 10^{-3} for $\kappa_1 = 10^{-4}$ in the regions of interest. The total interaction cross section can be increased by putting multiple, identical, sensitive spheres in the chiral solution. Since the very small interaction cross section is related to the very small index contrast of the media, higher index media with high em-chirality, e.g. high intrinsically chiral scatterers or weakly chiral spheres with a thin dielectric coating, seem to be an option for improvement. However, in most cases these media are not sensitive to very small changes in the chirality parameter of the surrounding medium. The second restriction of the presented approach is the assumption of a constant electric and magnetic response over the course of small changes in the chirality parameter of the surrounding medium. To which extend these assumptions are valid for real solutions is questionable: The chiral scatterer is very sensitive to changes of κ_2, plus the product of electric and magnetic response are at least of the same order of magnitude as κ_2 (cf. $(\varepsilon_2 - 1.33^2)(\mu_2 - 1) = \kappa_2\sqrt{\varepsilon_0\mu_0}$). Then, even small changes of the permittivity/permeability of the chiral solution will affect the scattering behavior. To

derive the actual relation between the change of κ_2 and the other material parameters, these have to be known or measured during the detection process.

9 Conclusion

The ultimate aim of the present work is to find maximally em-chiral spherical scatterers. In this context, the influence of material and geometry of a spherical scatterer on em-chirality and their interplay are investigated.

A single spherical scatterer is modeled as a homogeneous sphere with or without an additional shell, which is surrounded by a different homogeneous achiral medium. A chiral medium is assumed to consist of a lossless, achiral, homogeneous host medium and chiral inclusions, which are small compared to the wavelength. Interrelations between the polarizabilities of the inclusions and thereby of the effective material parameters are derived by means of a microscopic model. This model for the polarizabilities is used to restrict the parameter space in the parameter studies. The scattering theory for a chiral multi-shell particle in a chiral medium is provided by an extension of the classical Mie theory, which enables the calculation of the T-matrix, the interaction cross section and quantitative measures of electromagnetic duality and electromagnetic chirality. It is shown that dual scatterers can be obtained just by means of material properties if the impedance matches the one of the surrounding medium. This condition is completely independent of the medium's chirality, but hard to achieve in the optical regime. By means of the boundary conditions in the helicity basis, constraints on the material parameters for a transparent medium are derived. Transparency of a medium to one helicity requires duality and refractive index matching, which is only possible if the host medium of the chiral sphere is equal to the surrounding medium. Such media result in maximally em-chiral scatterers independent of their geometry.

An examination of the simplest case, a homogeneous chiral sphere within vacuum, shows that a high effective material chirality of the sphere implies an overall high em-chirality. Highly em-chiral spheres are found for different radii and material combinations. However, highly em-chiral spheres consisting of weakly chiral media are only achievable in few parameter regions. Nearly maximal em-chirality is only achieved if the sphere's medium

matches the outside. High em-chirality by means of geometry is not found in homogeneous spherical scatterers consisting of weakly intrinsically chiral media.

Generally, chiral core-shell particles are found to perform worse than those without shell. In fact building a sphere with arbitrary radius out of the core or shell medium is found to always possess better em-chirality for paramagnetic media. One notable exception are small spheres in vacuum out of diamagnetic media. Thin dielectric coatings with a specific thickness to core ratio constitute another notable exception. For these, very high em-chirality is observed in two parameter regions of the dielectric shell even for weakly chiral spheres. The dielectrics, which possess a comparable refractive index to the chiral medium of the core, are nearly transparent over a broad parameter range. A second very narrow region of high em-chirality is found for high index, thin dielectric shells. This core-shell particles are particularly promising and interesting, as they seem to offer a route to achieve scatterers with a very high em-chirality from a very weakly intrinsically chiral medium. It only requires a thin dielectric shell in a very sensitive parameter space.

This work does not consider and examine the frequency dependency of the scattering behavior and is limited to isotropic, homogeneous and lossless single scatterers. We show an interdependency of the material parameters and use this to restrict the parameter space to media, which conserve energy, instead of assuming arbitrary parameter combinations. Disregarding the regions where the medium itself is highly em-chiral, an interplay of geometry and material parameters does not allow for very high em-chiral spherical scatterers with low intrinsic chirality, which are experimentally more accessible. However, adding a thin dielectric layer to a weakly chiral sphere yields very high em-chirality. Thus, as far as we observed, thin dielectric coatings on top of chiral spheres are a new way of achieving high em-chirality without the need of highly intrinsically chiral media.

Future work should address the validation or adaption of the applied effective material model with respect to actually existing chiral media in the optical regime, Especially, if they are not made of chiral molecules within a solution. This will give more insight into which parameter ranges are achievable, as well as the interdependency between the electric, magnetic and chiral response of the effective medium. Furthermore, investigating and explaining the effects seen in the thin coated chiral spheres enables the application as highly em-chiral scatterers. Proceeding from spherical, highly em-chiral objects, the

arrangement of such scatterers and the interaction among each other or with different chiral structures/molecules is to be exploited next.

A Boundary conditions in Riemann-Silberstein notation

The boundary conditions for an arbitrarily shaped scatterer are given by

$$\begin{bmatrix} \boldsymbol{G}_+ \\ \boldsymbol{G}_- \end{bmatrix}_1 = \begin{bmatrix} \boldsymbol{M}_{++} & \boldsymbol{M}_{+-} \\ \boldsymbol{M}_{-+} & \boldsymbol{M}_{--} \end{bmatrix} \begin{bmatrix} \boldsymbol{G}_+ \\ \boldsymbol{G}_- \end{bmatrix}_2 ,$$

with

$$\boldsymbol{M}_{++} = \begin{bmatrix} \frac{Z_1+Z_2}{2Z_2} & 0 & 0 \\ 0 & \frac{Z_1+Z_2}{2Z_2} & 0 \\ 0 & 0 & *_{++} \end{bmatrix} ,$$

$$\boldsymbol{M}_{+-} = \begin{bmatrix} \frac{Z_2-Z_1}{2Z_2} & 0 & 0 \\ 0 & \frac{Z_2-Z_1}{2Z_2} & 0 \\ 0 & 0 & *_{+-} \end{bmatrix} ,$$

$$\boldsymbol{M}_{-+} = \begin{bmatrix} \frac{Z_2-Z_1}{2Z_2} & 0 & 0 \\ 0 & \frac{Z_2-Z_1}{2Z_2} & 0 \\ 0 & 0 & *_{-+} \end{bmatrix} ,$$

$$\boldsymbol{M}_{--} = \begin{bmatrix} \frac{Z_1+Z_2}{2Z_2} & 0 & 0 \\ 0 & \frac{Z_1+Z_2}{2Z_2} & 0 \\ 0 & 0 & *_{--} \end{bmatrix} .$$

$$
\begin{aligned}
*_{++/--} = & \\
& \frac{\mp\kappa_2(\varepsilon_1 Z_1 Z_2 \pm \kappa_1(Z_1+Z_2)+\mu_1)+\varepsilon_1\mu_2 Z_1 \pm \kappa_1(\varepsilon_2 Z_1 Z_2+\mu_2)+\varepsilon_2\mu_1 Z_2}{2Z_2\left(\varepsilon_1\mu_1-{\kappa_1}^2\right)} \,, \\
*_{+-/-+} = & \\
& \frac{\kappa_2(\mp\varepsilon_1 Z_1 Z_2+\kappa_1(Z_1+Z_2)\pm\mu_1)-\varepsilon_1\mu_2 Z_1 \pm \kappa_1(\varepsilon_2 Z_1 Z_2-\mu_2)+\varepsilon_2\mu_1 Z_2}{2Z_2\left(\varepsilon_1\mu_1-{\kappa_1}^2\right)} \\
& = \frac{\kappa_2 Z_2(\mp n_1-\kappa_1)-\mu_2(\pm\kappa_1+n_1)+\kappa_1 Z_1/(\kappa_2\pm n_2)+\mu_1(\pm\kappa_2+n_2)}{2Z_2\left(\varepsilon_1\mu_1-{\kappa_1}^2\right)} \,,
\end{aligned}
$$

where $n_i = \sqrt{\varepsilon_i\mu_i}$, $i = 1, 2$ and the material parameters are all relative quantities. Using the refractive indices for light of different helicity $n_{i,\pm} = n_i \pm \kappa_i$ yields

$$
\begin{aligned}
*_{+-/-+} &= \frac{n_{1,\pm} Z_2(\mp\kappa_2 - n_2) + n_{2,\pm} Z_1(\pm\kappa_1) + n_1}{2Z_2 n_{1,+} n_{1,-}} \\
&= \frac{n_{1,\pm} n_{2,\pm}(Z_1 - Z_2)}{2Z_2 n_{1,+} n_{1,-}} \\
&= \frac{n_{2,\pm}}{n_{1,\mp}} \frac{Z_1 - Z_2}{2Z_2} \,.
\end{aligned}
\tag{A.1}
$$

And with similar transformations

$$
*_{++/--} = \frac{n_{2,\pm}}{n_{1,\pm}} \frac{Z_1 + Z_2}{2Z_2} \,. \tag{A.2}
$$

B Transparency to one helicity for dual inclusions

For a dual helix the relation between the polarizabilities (3.33) becomes:

$$\begin{aligned} \alpha_{\mathrm{mm}} &= 1/\varepsilon_a \alpha_{\mathrm{ee}} \ , \\ \alpha_{\mathrm{em}} &= \mp i Z_a \alpha_{\mathrm{ee}} \ . \end{aligned} \tag{B.1}$$

The dipole moments induced in the helix are

$$\begin{bmatrix} \boldsymbol{p} \\ \boldsymbol{m} \end{bmatrix} = \alpha_{\mathrm{ee}} \begin{bmatrix} 1 & \pm i Z\mathrm{a} \\ \mp i Z_{\mathrm{a}}/\mu_{\mathrm{a}} & 1/\varepsilon_{\mathrm{a}} \end{bmatrix} \begin{bmatrix} \boldsymbol{E} \\ \boldsymbol{H} \end{bmatrix} \ . \tag{B.2}$$

This equation can be written in the basis of helicity eigenmodes by substituting

$$\begin{bmatrix} \boldsymbol{E} \\ \boldsymbol{H} \end{bmatrix} = \begin{bmatrix} 1 & 1 \\ -i/Z\mathrm{a} & i/Z\mathrm{a} \end{bmatrix} \begin{bmatrix} \boldsymbol{G}_+ \\ \boldsymbol{G}_- \end{bmatrix} \tag{B.3}$$

in (B.2) and the dipole moments are also transformed [12, Sec. 2.7.3]:

$$\boldsymbol{q}_\pm = \frac{1}{\sqrt{2}} (\boldsymbol{p} \pm i\boldsymbol{m}/c_{\mathrm{a}}) \ . \tag{B.4}$$

In matrix notation this is

$$\begin{bmatrix} \boldsymbol{q}_+ \\ \boldsymbol{q}_- \end{bmatrix} = \frac{1}{\sqrt{2}} \begin{bmatrix} 1 & i/c_{\mathrm{a}} \\ 1 & -i/c_{\mathrm{a}} \end{bmatrix} \begin{bmatrix} \boldsymbol{p} \\ \boldsymbol{m} \end{bmatrix} \tag{B.5}$$

The moments $\boldsymbol{q}_\pm$ are a superposition of magnetic and electric dipole moments, which only produce light of either one helicity. The equations are transformed in the basis of helicity eigenstates and the dipole moments are written in the basis of $\boldsymbol{q}_\pm$:

$$\begin{aligned}
\frac{1}{\sqrt{2}}\begin{bmatrix}1 & i/c_\mathrm{a}\\ 1 & -i/c_\mathrm{a}\end{bmatrix}\begin{bmatrix}\boldsymbol{p}\\ \boldsymbol{m}\end{bmatrix} =& \frac{1}{\sqrt{2}}\begin{bmatrix}1 & i/c_\mathrm{a}\\ 1 & -i/c_\mathrm{a}\end{bmatrix}\frac{\alpha_\mathrm{ee}}{\sqrt{2}}\begin{bmatrix}1 & \pm iZ_\mathrm{a}\\ \mp iZ_\mathrm{a}/\mu_\mathrm{a} & 1/\varepsilon_\mathrm{a}\end{bmatrix}\begin{bmatrix}1 & 1\\ -i/Z_\mathrm{a} & i/Z_\mathrm{a}\end{bmatrix}\begin{bmatrix}\boldsymbol{G}_+\\ \boldsymbol{G}_-\end{bmatrix}\\
\Leftrightarrow \begin{bmatrix}\boldsymbol{q}_+\\ \boldsymbol{q}_-\end{bmatrix} =& \frac{\alpha_\mathrm{ee}}{2}\begin{bmatrix}1 & i/c_\mathrm{a}\\ 1 & -i/c_\mathrm{a}\end{bmatrix}\begin{bmatrix}1\pm 1 & 1\mp 1\\ -ic_\mathrm{a}(1\pm 1) & ic_\mathrm{a}(1\mp 1)\end{bmatrix}\begin{bmatrix}\boldsymbol{G}_+\\ \boldsymbol{G}_-\end{bmatrix}\\
\Leftrightarrow \begin{bmatrix}\boldsymbol{q}_+\\ \boldsymbol{q}_-\end{bmatrix} =& \alpha_\mathrm{ee}\begin{bmatrix}1\pm 1 & 0\\ 0 & (1\mp 1)\end{bmatrix}\begin{bmatrix}\boldsymbol{G}_+\\ \boldsymbol{G}_-\end{bmatrix}\,.
\end{aligned}$$

The plus and minus signs stand for the handedness of the helices. For one specific handedness

$$\begin{bmatrix}\boldsymbol{q}_+\\ \boldsymbol{q}_-\end{bmatrix} = \alpha_\mathrm{ee}\begin{bmatrix}2 & 0\\ 0 & 0\end{bmatrix}\begin{bmatrix}\boldsymbol{G}_+\\ \boldsymbol{G}_-\end{bmatrix} \tag{B.6}$$

holds, which implies transparency for light of $\Lambda = -1$.

C Scattering by a chiral core-shell particle

The results shown in Fig. C.1 correspond to a core with $r_1 = 0.2\lambda$, $\varepsilon_1 = 1.7^2\varepsilon_0$ and $\kappa_1 = \kappa_{\rm sh} = 0.5$. Em chirality is very high for very small shell thickness $r_{\rm sh} - r_1 < 0.1$, for some parameter regimes of higher refractive index shell media and in the case of small diamagnetic shells. In the case of $\varepsilon_{sh} < \varepsilon_{\rm a}$, the core-shell particle shows higher em chirality than the single spheres of core or shell medium, cf. Fig. C.1b. For paramagnetic media $\varepsilon_{sh} < \varepsilon_{\rm a}$ – both for $\varepsilon_{\rm sh}$ smaller than the permittivity of the core (Fig C.1c) and bigger than the permittivity of the core (Fig. C.1d) – there is a geometry of a single sphere consisting out of the shell medium, which posses higher em chirality than the core-shell out of this medium.

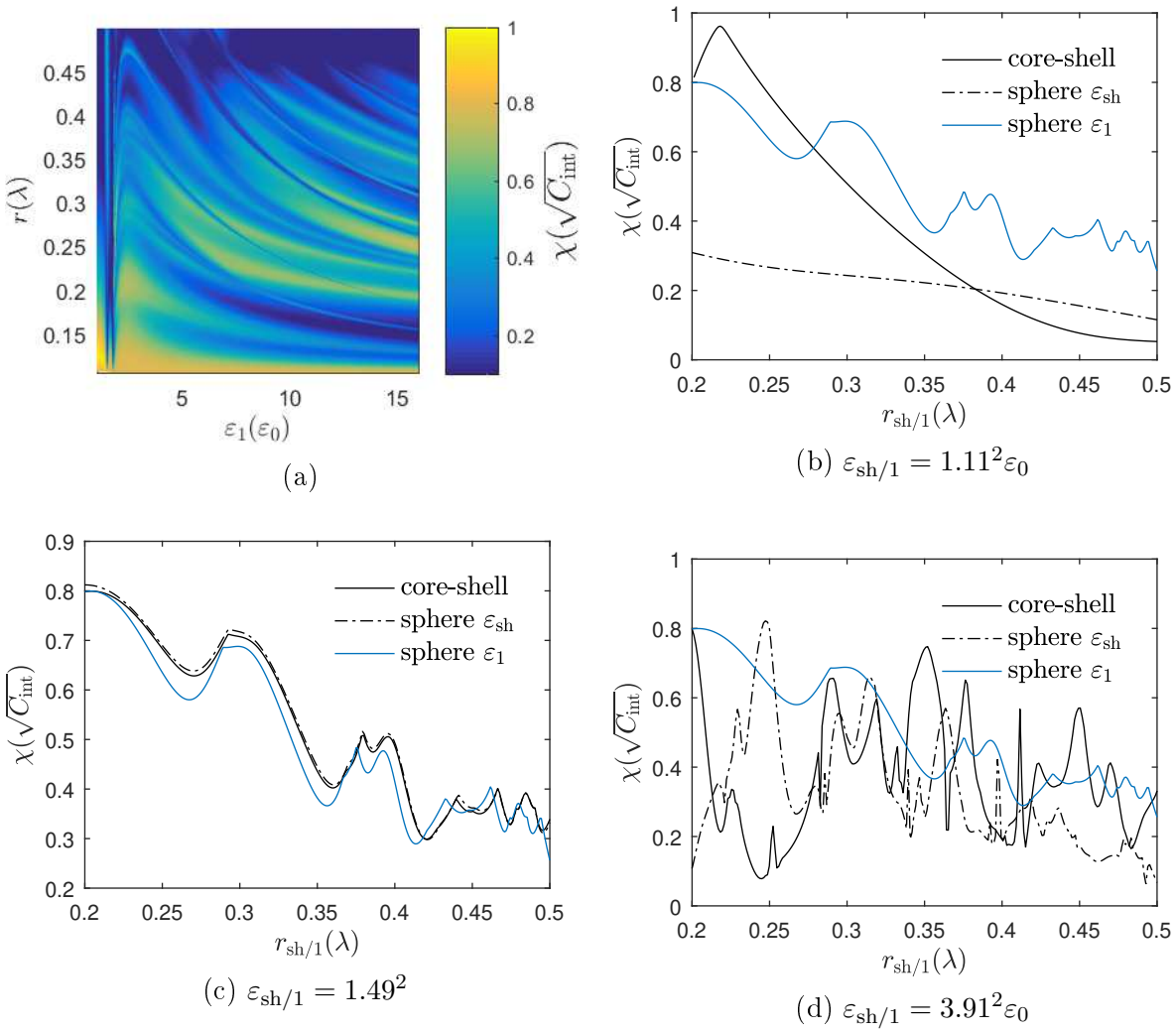

(a)

(b) $\varepsilon_{\text{sh}/1} = 1.11^2\varepsilon_0$

(c) $\varepsilon_{\text{sh}/1} = 1.49^2$

(d) $\varepsilon_{\text{sh}/1} = 3.91^2\varepsilon_0$

Figure C.1: (a) Em chirality of a core shell as a function of the permittivity and radius of the shell and a core with $r_1 = 0.2\lambda$, $\varepsilon_1 = 1.7^2\varepsilon_0$ and $\kappa_1 = \kappa_{\text{sh}} = 0.5$. (b)-(d) Em chirality for different permittivities of the shell as a function of the radius compared to single sphere out of the corresponding (to shell/core) media

Bibliography

[1] Barron, L. D. (2004): *Molecular Light Scattering and Optical Activity*. 2nd ed. Cambridge: Cambridge Univ. Pr. DOI: 10.1017/CBO9780511535468.

[2] Belov, P., S. Maslovski, K. Simovski, and S. Tretyakov (2003): A condition imposed on the electromagnetic polarizability of a bianisotropic lossless scatterer. *Technical Physics Letters* **29**(9), pp. 718–720. DOI: 10.1134/1.1615545.

[3] Benenson, W. and H. Stöcker, eds. (2002): *Handbook of physics*. New York: Springer.

[4] Bilal, M., A. A. Syed, and Q. A. Naqvi (2014): Quasi-static analysis of scattering from a chiral sphere in chiral medium. *Journal of Electromagnetic Waves and Applications* **28**(17), pp. 2169–2187. DOI: 10.1080/09205071.2014.958617.

[5] Bohren, C. F. and D. R. Huffman (2004): *Absorption and scattering of light by small particles*. Weinheim: Wiley-VCH.

[6] Born, M. and E. Wolf (1999): *Principles of optics : electromagnetic theory of propagation, interference and diffraction of light*. 7th ed. Cambridge: Cambridge University Press.

[7] Bose, J. C. (1898): On the rotation of plane of polarisation of electric wave by a twisted structure. *Proceedings of the Royal Society of London* **63**(389-400), pp. 146–152. DOI: 10.1098/rspl.1898.0019.

[8] Cho, K. (2015): Dispersion Relation in Chiral Media: Credibility of Drude-Born-Fedorov Equations. *arXiv preprint arXiv:1501.01078*.

[9] Cipparrone, G., A. Mazzulla, A. Pane, R. J. Hernandez, and R. Bartolino (2011): Chiral self-assembled solid microspheres: a novel multifunctional microphotonic device. *Advanced Materials* **23**(48), pp. 5773–5778. DOI: 10.1002/adma.201102828.

[10] Collins, J. T., C. Kuppe, D. C. Hooper, C. Sibilia, M. Centini, and V. K. Valev (2017): Chirality and chiroptical effects in metal nanostructures: fundamentals and current trends. *Advanced Optical Materials* **5**(16), p. 1700182. DOI: 10.1002/adom.201700182.

[11] Enk, S. V. and G. Nienhuis (1994): Commutation Rules and Eigenvalues of Spin and Orbital Angular Momentum of Radiation Fields. *Journal of Modern Optics* **41**(5), pp. 963–977. DOI: 10.1080/09500349414550911.

[12] Fernandez-Corbaton, I. (2014): *Helicity and Duality Symmetry in Light Matter Interactions: Theory and Applications*. PhD thesis. Department of Physics and Astronomy, Macquarie University.

[13] Fernandez-Corbaton, I., M. Fruhnert, and C. Rockstuhl (2015): Dual and Chiral Objects for Optical Activity in General Scattering Directions. *ACS Photonics* **2**(3), pp. 376–384. DOI: 10.1021/ph500419a.

[14] Fernandez-Corbaton, I., M. Fruhnert, and C. Rockstuhl (2016): Objects of Maximum Electromagnetic Chirality. *Physical Review X* **6** (3), p. 031013. DOI: 10.1103/PhysRevX.6.031013.

[15] Fernandez-Corbaton, I. and C. Rockstuhl (2017): Unified theory to describe and engineer conservation laws in light-matter interactions. *Physical Review A* **95** (5), p. 053829. DOI: 10.1103/PhysRevA.95.053829.

[16] Fernandez-Corbaton, I., X. Zambrana-Puyalto, N. Tischler, X. Vidal, M. L. Juan, and G. Molina-Terriza (2013): Electromagnetic duality symmetry and helicity conservation for the macroscopic Maxwell's equations. *Physical Review Letters* **111**(6), p. 060401. DOI: 10.1103/PhysRevLett.111.060401.

[17] Fisanov, V. V. (2007): The invariants of an isotropic chiral medium. *Journal of Communications Technology and Electronics* **52**(9), pp. 1006–1008. DOI: 10.1134/S1064226907090094.

[18] Flack, H. (2009): Louis Pasteur's discovery of molecular chirality and spontaneous resolution in 1848, together with a complete review of his crystallographic and chemical work. *Acta Crystallographica Section A* **65**(5), pp. 371–389. DOI: 10.1107/S0108767309024088.

[19] Fließbach, T. (2008): *Lehrbuch zur theoretischen Physik*. 5th ed. Vol. 3: Quantenmechanik. Heidelberg: Springer Spektrum.

[20] Gansel, J. K., M. Thiel, M. S. Rill, M. Decker, K. Bade, V. Saile, G. von Freymann, S. Linden, and M. Wegener (2009): Gold helix photonic metamaterial as broadband circular polarizer. *Science* **325**(5947), pp. 1513–1515. DOI: 10.1126/science.1177031.

[21] Hinders, M.K. and B.A. Rhodes (1992): Electromagnetic-wave scattering from chiral spheres in chiral media. *Il Nuovo Cimento D* **14**(6), pp. 575–583. DOI: 10.1007/BF02462344.

[22] Jackson, J.D. (2002): *Klassische Elektrodynamik*. 3rd ed. Berlin: de Gruyter.

[23] Jelinek, L., R. Marqués, F. Mesa, and J. Baena (2008): Periodic arrangements of chiral scatterers providing negative refractive index bi-isotropic media. *Physical Review B* **77**(20), p. 205110. DOI: 10.1103/PhysRevB.77.205110.

[24] Kahr, B. and O. Arteaga (2012): Arago's best paper. *ChemPhysChem* **13**(1), pp. 79–88. DOI: 10.1002/cphc.201100660.

[25] Kelvin, W.T.B. (1904): *Baltimore lectures on molecular dynamics and the wave theory of light*. CJ Clay and Sons. URL: https://ia902604.us.archive.org/6/items/baltimorelecture00kelviala/baltimorelecture00kelviala.pdf.

[26] Klimov, V., I. Zabkov, A. Pavlov, and D. Guzatov (2014): Eigen oscillations of a chiral sphere and their influence on radiation of chiral molecules. *Optics Express* **22**(15), pp. 18564–18578. DOI: 10.1364/OE.22.018564.

[27] Kuwata-Gonokami, M., N. Saito, Y. Ino, M. Kauranen, K. Jefimovs, T. Vallius, J. Turunen, and Y. Svirko (2005): Giant optical activity in quasi-two-dimensional planar nanostructures. *Physical Review Letters* **95**(22), p. 227401. DOI: 10.1103/PhysRevLett.95.227401.

[28] Lakhtakia, A. and W. Weiglhofer (1996): Lorentz covariance, Occam's razor, and a constraint on linear constitutive relations. *Physics Letters A* **213**(3), pp. 107–111. DOI: 10.1016/0375-9601(96)00121-1.

[29] Lakhtakia, A. (1994): *Beltrami fields in chiral media*. Vol. 2. Singapore: World Scientific.

[30] Lancaster, P. and M. Tismenetsky (1985): *The theory of matrices : with applications*. 2nd ed. Computer science and applied mathematics. Orlando: Academic Pr.

[31] Liberal, I. and N. Engheta (2017): Near-zero refractive index photonics. *Nature Photonics* **11**(3), pp. 149–158. DOI: 10.1038/nphoton.2017.13.

[32] Lindell, I.V., ed. (1994): *Electromagnetic waves in chiral and bi-isotropic media*. The Artech House antenna library. Boston: Artech House.

[33] Michel, B., A. Lakhtakia, W.S. Weiglhofer, and T.G. Mackay (2001): Incremental and differential Maxwell Garnett formalisms for bi-anisotropic composites. *Composites Science and Technology* **61**(1), pp. 13–18. DOI: 10.1016/S0266-3538(00)00149-4.

[34] Mohammadi-Baghaee, R. and J. Rashed-Mohassel (2016): The Chirality Parameter for Chiral Chemical Solutions. *Journal of Solution Chemistry* **45**(8), pp. 1171–1181. DOI: 10.1007/s10953-016-0496-4.

[35] Oh, S. S. and O. Hess (2015): Chiral metamaterials: enhancement and control of optical activity and circular dichroism. *Nano Convergence* **2**(1), p. 24. DOI: 10.1186/s40580-015-0058-2.

[36] Petitjean, M. (2003): Chirality and symmetry measures: A transdisciplinary review. *Entropy* **5**(3), pp. 271–312. DOI: 10.3390/e5030271.

[37] Post, E. J. (1997): *Formal structure of electromagnetics: general covariance and electromagnetics*. North Chelmsford: Courier Corporation.

[38] Rafayelyan, M. and E. Brasselet (2016): Bragg-Berry mirrors: reflective broadband q-plates. *Optics Letters* **41**(17), pp. 3972–3975. DOI: 10.1364/OL.41.003972.

[39] Rahimzadegan, A., C. Rockstuhl, and I. Fernandez-Corbaton (2018): Core-Shell Particles as Building Blocks for Systems with High Duality Symmetry. *Physical Review Applied* **9** (5), p. 054051. DOI: 10.1103/PhysRevApplied.9.054051.

[40] Sersic, I., C. Tuambilangana, T. Kampfrath, and A. F. Koenderink (2011): Magnetoelectric point scattering theory for metamaterial scatterers. *Physical Review B* **83**(24), p. 245102. DOI: 10.1103/PhysRevB.83.245102.

[41] Shang, Q.-C., Z.-S. Wu, T. Qu, Z.-J. Li, and L. Bai (2016): Scattering from a multilayered chiral sphere using an iterative method. *Journal of Quantitative Spectroscopy and Radiative Transfer* **173**, pp. 72–82. DOI: 10.1016/j.jqsrt.2015.12.030.

[42] Sihvola, A. (1994): Electromagnetic modeling of bi-isotropic media. *Progress In Electromagnetics Research* **9**, pp. 45–86.

[43] Stratton, J. A. (1941): *Electromagnetic theory*. International series in pure and applied physics. New York: McGraw-Hill.

[44] Thiel, M., M. S. Rill, G. von Freymann, and M. Wegener (2009): Three-dimensional bi-chiral photonic crystals. *Advanced Materials* **21**(46), pp. 4680–4682. DOI: 10.1002/adma.200901601.

[45] Tretyakov, S. A., F. Mariotte, C. R. Simovski, T. G. Kharina, and J. P. Heliot (1996): Analytical antenna model for chiral scatterers: comparison with numerical and experimental data. *IEEE Transactions on Antennas and Propagation* **44**(7), pp. 1006–1014. DOI: 10.1109/8.504309.

[46] Tretyakov, S., A. Sihvola, and L. Jylhä (2005): Backward-wave regime and negative refraction in chiral composites. *Photonics and Nanostructures - Fundamentals and*

Applications **3**(2). The Sixth International Symposium on Photonic and Electromagnetic Crystal Structures (PECS-VI), pp. 107–115. DOI: 10.1016/j.photonics.2005.09.008.

[47] Tretyakov, S. (2003): *Analytical modeling in applied electromagnetics*. Artech House electromagnetic analysis series. Boston, Mass.: Artech House.

[48] Tung, W.-K. (1985): *Group Theory in Physics*. Singapore: WORLD SCIENTIFIC. DOI: 10.1142/0097.

[49] Wang, Z., F. Cheng, T. Winsor, and Y. Liu (2016): Optical chiral metamaterials: a review of the fundamentals, fabrication methods and applications. *Nanotechnology* **27**(41), p. 412001. DOI: 10.1088/0957-4484/27/41/412001.

[50] Waterman, P. C. (1969): New Formulation of Acoustic Scattering. *The Journal of the Acoustical Society of America* **45**(6), pp. 1417–1429. DOI: 10.1121/1.1911619.

[51] Wu, Z.-S., Q.-C. Shang, and Z.-J. Li (2012): Calculation of electromagnetic scattering by a large chiral sphere. *Applied Optics* **51**(27), pp. 6661–6668. DOI: 10.1364/AO.51.006661.

[52] Zambrana-Puyalto, X., X. Vidal, M. L. Juan, and G. Molina-Terriza (2013): Dual and anti-dual modes in dielectric spheres. *Optical Express* **21**(15), pp. 17520–17530. DOI: 10.1364/OE.21.017520.